Nitish Kumar Sinha

Development of an optimizing tool for design of tailored PV modules through Cell To Module (CTM) factor modelling

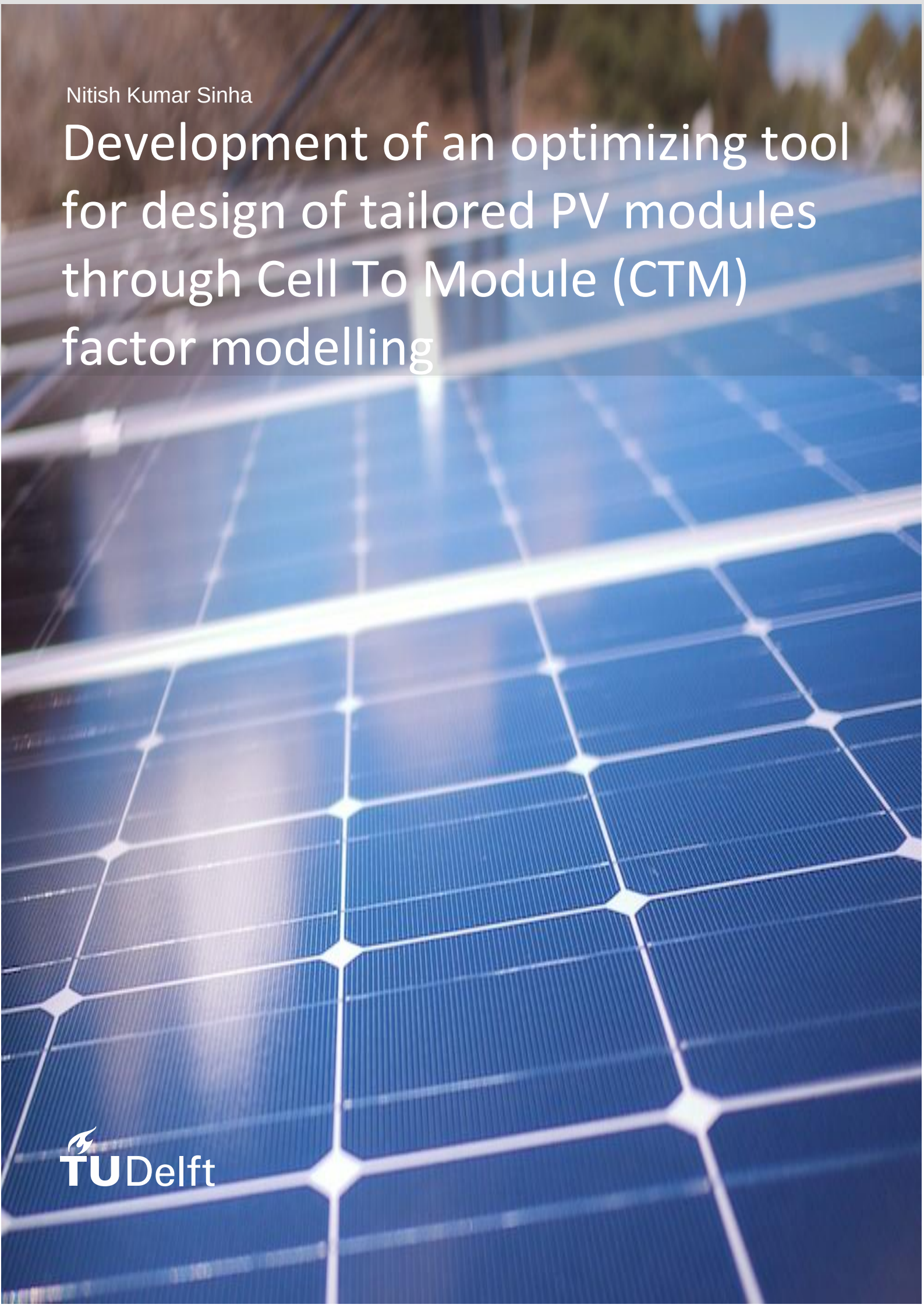

TU Delft

Development of an optimizing tool for design of tailored PV modules through Cell To Module (CTM) factor modelling

By

Nitish Kumar Sinha

in partial fulfilment of the requirements for the degree of

Master of Science
in Electrical Power Engineering

at the Delft University of Technology,
to be defended publicly on Wednesday August 19, 2020 at 10:00 AM.

Thesis committee:	Dr. ir. O. Isabella,	TU Delft, Supervisor, PVMD group
	Ir. J.C. Ortiz Lizcano,	TU Delft, Daily Supervisor, PVMD group
	Dr. ir. Rudi Santbergen	TU Delft, PVMD Group
	Dr. ir. Babak Gholizad	TU Delft, DCE&S Group

This thesis is confidential and cannot be made public until June 30, 2021.

TU Delft

Abstract

The advancement of innovative PV technologies has led to an all-time high integration of the same in the urban environment. Furthermore, development of decentralized power systems complements this rise as it supports in-situ power consumption. Due to space availability constraints in urban environments and a need for appealing aesthetics, tailored PV modules is gaining importance. However, it is desirable to achieve maximum power out of these tailored PV modules to ensure efficiency in space usage.

Literature suggests that one of the most apt performance metric for estimating the goodness of design for PV modules is the CTM ratio. However, various challenges incurred upon implementing the present CTM analysis algorithms on tailored PV modules suggests the need for development of a different approach to estimate the same. The presented work strives towards the development of a tool for the prediction of various performance metrics, including the CTM ratio, of both standard and tailored PV modules to aid its user to make educated design choices to develop optimum modules.

The methodology used for development of the tool encompasses various steps which occur in a pre-programmed flow. Firstly, a developed script automatically creates the module structure based on user inputs. Hereafter, ray tracing is implemented and its results furnishes optical performance of the module. Furthermore, an electrical loss calculation model is developed, using differential element method, which when coupled with the optical performance data enables the estimation of the CTM ratio and other performance metrics. The tool is programmed in Matlab to ensure easy integration of the same with the PVMD toolbox for future research on module designs.

Firstly, an attempt is made to optimize the parameters of the mini-module for maximizing its performance. For a white backsheet test mini-module, optimization through the usage of the tool, leads to a 5.52 % gain from the worst case design. This gain is realized by achieving an optimal tuning between the cell-cell and cell-edge spacing. Moreover, when compared, the white backsheet module's power production capacity outperforms the black backsheet module by around 13.93 %. Additionally, effect of busbars on the performance of the module is investigated.

Furthermore, the tool is able to derive novel empirical formulas which, for different module architectures, predict the effect of cell top metallization on the cell photocurrent density in an encapsulated environment.

Secondly, efficacy of the tool is demonstrated for a comparative study between a 60 cell module and its corresponding 120 half-cut cell module. The tool suggests the half-cut cell module to have a 2.91 % gain in CTM ratio as compared to its full cell counterpart.

Thirdly, the tool demonstrates modelling and simulation of glass-glass modules and achieve optimization. The tool also recommends an increase of the dimension size for the test module to 20×20 cm^2 to achieve the exemplary target transmission of 14 %.

Lastly, the tool efficacy is demonstrated for a triangular PV module. This module with a white backsheet is found to outperform its black backsheet counterpart by 9 % in CTM ratio.

Preface

Coming abroad for my master's was a big decision for me but the quality education and a wide array of personal and professional development opportunities, imparted by TU Delft, has made this decision invaluable. My deepest gratitude to the PVMD group for honing my passion for solar energy. My deepest gratitude to Dr. Olindo for trusting me on this project and guiding me through vital feedbacks that resulted in the completion of this work.

As Donal Sadoway said, "In a battery, I strive to maximize electrical potential. When mentoring, I strive to maximize human potential." , I believe Juan Camilo, my daily supervisor, exemplified this quote. He, through his wise intellect not only guided me through the project but also as a dear friend stood behind and believed in me. Especially, in the unprecedented times of the COVID-19, it was a blessing to receive such support, both from Juan and Dr. Olindo.

I would also like to take this opportunity to thank Dr. Malte and Dr. Rudi for their vital advices which helped me immensely in finding a right direction towards completion of this project. Furthermore, my sincere gratitude to the PhD's in the PVMD group for their support.

And of course I couldn't' have achieved this without the loving support of my parents, back in India. Their unconditional support, not only during my studies in the Netherlands, but also, in taking the big decision to move abroad.

A very special thanks to my elder brother, Dr. Ashish. It was a pleasure to always have him by my side and help me cope up with every facet of life. Discussions with him about various electrical concepts helped me widen my thinking and increase the research acumen in myself.

Lastly, this would not have been possible without my friends who's support has been priceless. To both my friends, here in Netherlands as well as back in India, thank you for all the wonderful memories we have shared.

Nitish Kumar Sinha

August, 2020

Contents

List of figures xv

List of Tables xix

List of abbreviations xxi

List of symbols xxiii

1. Introduction 1

2. Theory 3

2.1. Module architecture 3

2.2. Optical gains and losses 4

2.3. Electrical losses 5

2.4. Cell to Module (CTM) ratio 5

3. Tool building approach 7

3.1. Creation of vertices 8

3.2. Creation of module surfaces 10

3.3. Ray tracing 10

3.4. Optical performance 13

3.5. Electrical loss model 14

3.6. CTM calculation 16

3.7. Approach for custom shape cells and modules 16

4. Demonstration of tool features 19

4.1. PV mini modules 19

4.1.1 Cell-cell and edge-cell spacing 19

4.1.2 Number of Busbars 25

4.1.3 Effect of cell metallization in an embedded environment 31

4.1.4 Optical balance of the module 33

4.2. Full cell vs half cut cell modules 34

4.3. Glass-Glass modules 37
4.3.1 Cell-cell and edge-cell spacing 38
4.3.2 Light transmittance 39
4.4. Triangular (tailored) PV module 41
5. Conclusions and future recommendations 43
6. References 47
Appendix 51
A1 Matlab code for the developed tool for square/rectangular modules 51
A2 Matlab code for the developed tool for triangular modules 73

List of figures

Figure 1 Cross-section of a standard PV module adapted from [3] 3

Figure 2 Cross-section of a PV module with rays indicating the various optical gain and loss mechanisms 4

Figure 3 Flowchart depicting the developed CTM Analysis algorithm 8

Figure 4 Automatic vertex mapping in 3-D space based on user inputs 8

Figure 5 A sample of developed module surfaces by clubbing the vertices 10

Figure 6 Pyramid textures on the cell surface [13] 11

Figure 7 Standard AM 1.5 Spectrum [14] 12

Figure 8 Reflection by a Lambertian scatterer used for modelling backsheet [16] 13

Figure 9 Sample module *R-A-T* response from ray tracing 13

Figure 10 Differential element method for ohmic loss calculation 14

Figure 11 Schematic showing cell interconnection using ribbons adapted from [21] 15

Figure 12 Lasergraaf Laser cutting machine [22] 16

Figure 13 Laser cutting machine operation [23] 17

Figure 14 Tool generated sample model of triangular module 17

Figure 15 (A-Edge spacing, B- Cell spacing) Illustration of cell to cell and edge to cell spacing highlighted in ‘yellow’ [25] 20

Figure 16 CTM Ratio vs Cell spacing for the test PV module with white backsheet 21

Figure 17 Ohmic losses vs Cell spacing for test module with white backsheet 22

Figure 18 Module power vs Cell spacing for test module with a white backsheet 22

Figure 19 CTM ratio vs cell spacing for test module with black backsheet 23

Figure 20 Ohmic losses vs cell spacing for test module with black backsheet 23

Figure 21 Schematic for demonstration of increased light coupling as cell approaches module edges 24

Figure 22 Ray tracing images of module edges for test module with black backsheet 24

Figure 23 Module power vs cell spacing for test module with black backsheet 25

Figure 24 Ohmic losses vs number of busbars for test module with white backsheet 26

Figure 25 CTM ratio vs number of busbars for test module with white backsheet....26
Figure 26 Module power vs number of busbars for test module with white backsheet....27
Figure 27 Active area ratio vs number of busbars for test module with white backsheet....27
Figure 28 Active area ratio vs number of busbars for test module with white backsheet....28
Figure 29 Ohmic losses vs number of busbars for the test module with white backsheet....28
Figure 30 Module power vs number of busbars for the test module with white backsheet....29
Figure 31 (A-D) Summary of varying performance trends with increasing number of busbars (reducing active area ratio) for test module with black backsheet....30
Figure 32 (A-D) Summary of varying performance trends with increasing number of busbars (increasing active area ratio) for test module with black backsheet....31
Figure 33 comparison of active area ratio and ratio of module photocurrent with vs without metallization for test module with white backsheet....32
Figure 34 Difference between the ratios (‘orange’ and ‘blue’) vs the active area ratio....32
Figure 35 optical balance (%) for the test module with white backsheet....33
Figure 36 Optical balance (%) fort the test module with black backsheet....34
Figure 37 Schematic of half cut cells modules vs full cell modules [32]....34
Figure 38 Module power comparison for full cell and half cut cell modules....35
Figure 39 Ohmic losses comparison for full cell and half cut cell modules....35
Figure 40 Photocurrent density comparison for full cell and half cut cell modules....36
Figure 41 CTM ratio comparison for full cell and half cut cell modules....36
Figure 42 Rotterdam central station equipped with glass-glass modules [36]....37
Figure 43 Module with glass vs backsheet as bottom layer [37]....37
Figure 44 CTM ratio v s cell spacing for the test glass-glass module....38
Figure 45 Module power vs cell spacing for test glass-glass module....38
Figure 46 Transmission (%) of light for the test glass-glass module....39
Figure 47 Transmitted light (%) vs module size for the test glass-glass module....40
Figure 48 CTM ratio vs module size for the test glass-glass module....40

Figure 49 Complex shapes made using triangular blocks [39] 41

Figure 50 Comparison of performance (CTM Ratio) of triangular module with white and black backsheets 42

Figure 51 Comparison of performance (Module Power) of triangular module with white and black backsheets 42

Figure 52 Optimized test mini module with white backsheet 43

Figure 53 Optimized test mini module with black backsheet 44

List of Tables

Table 1 Different module geometry inputs 9

Table 2 Additional input parameters for triangular modules 18

Table 3 Specification of test PV mini module 20

Table 4 Reducing dimensions of busbars..... 28

Table 5 Triangular module parameters 41

List of abbreviations

PV	Photovoltaic
PVMD	Photovoltaic Materials and Devices
CTM	Cell To Module
EVA	Ethyl Vinyl Acetate
STC	Standard Test Conditions
AM	Air Mass
SRR	Spectral Response Range
MEMS	Micro Electro-Mechanical Systems
BoM	Bill of Materials
BIPV	Building Integrated Photovoltaics

List of symbols

X_M	Performance parameter for module
X_C	Identical performance parameter for cell
N	Number of cells
E	Energy
P	Power
n	refractive index
R	Reflectivity
T	Transmittivity
k	Extinction coefficient
$R\text{-}A\text{-}T$	Reflectance-Absorptance-Transmittance
V_{OC}	Open circuit voltage
I	Current flowing through conductor
L	Length of conductor
x	Position of the differential element
dx	Length of the differential element
W	Width of the conductor
D	Thickness of the conductor
dR	Resistance of the differential element
ρ	Resistivity
$P1$	Slope of the 1^{st} order polynomial
$P2$	Ordinate of the 1^{st} order polynomial
$f(x)$	1^{st} order polynomial function
R_P	Ratio of photocurrent with to without metallization in an embedded environment
A_C	Ratio of cell active area to the cell total area

1. Introduction

With the advancement of power systems towards decentralized power generation, photovoltaic (PV) technology has become a promising option for production of energy at various usage points in urban environment. Furthermore, the declining prices of PV based electricity and development of innovative PV modules for better integration make PV technology one of the most promising choices for power generation in urban environment [1].

While considering urban PV applications, it is not just the power output but also the aesthetics that are important contemplations. In most urban integrated PV applications space availability is a limiting factor. Therefore, it becomes one of the most important design considerations so as to get maximum power out of a given limited space. Moreover, ensuring the visual appeal of the PV modules certifies smooth integration into a specific urban environment.

In view of the above, tailored PV modules can be a promising choice for implementation of PV in urban environment.

Tailored PV modules are non-standard PV modules which are characterized by their custom-made properties for specific applications. These properties may include module size, cell size, form factor, shape, etc. However, the design of such tailored PV modules have certain challenges associated with it. Numerous design considerations need reassessment to ensure optimization of these modules for diverse applications. Various parameters of these modules are utilized for design considerations. These include active area ratio, cell size and shape, cell and edge spacing, choice and thickness of encapsulant, glass and backsheet, etc.

The objectives of this thesis can be classified as follows-

1. Development of a tool for automatic modelling of PV modules with desired characteristics.

2. Simulation of the modelled PV module, in the developed tool, for quantifying its optical and electrical behaviour.

3. Ensuring the tool's efficacy to deliver a quantifiable metric for performance measurement of diverse module types, thereby enabling the user to undertake educated design decisions.

4. Demonstration of the tool's ability to analyse the effect of different module parameters on the performance in various module architectures.

5. Optimization of the aforementioned parameters to enhance the performance and suitability of the modules for specific applications.

6. Ensuring the integrability of the developed tool into the already existing Photovoltaic Materials and Devices (PVMD) toolbox.

In the present work, section 2 encompasses a summary of the theory applicable in the development of the tool wherein the module's architecture, gains and losses involved when making it out of cells are discussed. Thereafter, the concept of Cell To Module (CTM) ratio is discussed. Furthermore, chapter 3 deals with a detailed explanation regarding the methodology developed for building the required tool. Chapter 4 focusses

on the demonstration of the tool features, wherein the applicability of the tool for various module architectures is presented. Sections 4.1 to 4.4 explain the results obtained using the tool for mini-modules, half cut-cell modules, glass-glass modules and triangular modules respectively, as test subjects.
Finally chapter 5 concludes the present work with enlistment of the detailed discussions of the previous chapters along with viable future recommendations as prospective adaptations for improvement of the tool.

2. Theory

The present chapter illustrates various concepts that have been utilized in the development of the tool. The effects of building a module out of the cells is highlighted and thereafter the definition of CTM ratio has been discussed.

2.1. Module architecture

Figure 1, shown hereunder, illustrates a standard PV module along with its layers of formation. The study done in [2] discusses the functions of various layers and the production processes involved for the same. The cells are first interconnected by tabbing and soldering. Furthermore the interconnected cells are embedded in an encapsulant and other module layers are adhered on it. One of the most widely used encapsulant is Ethyl Vinyl Acetate (EVA). This encapsulation is commonly done using vacuum lamination process. On top of the encapsulant layer, as shown in Figure 1, a layer of glass is used. The glass provides mechanical support, high transparency in the spectral response range of the cells and protection against harsh environmental conditions.

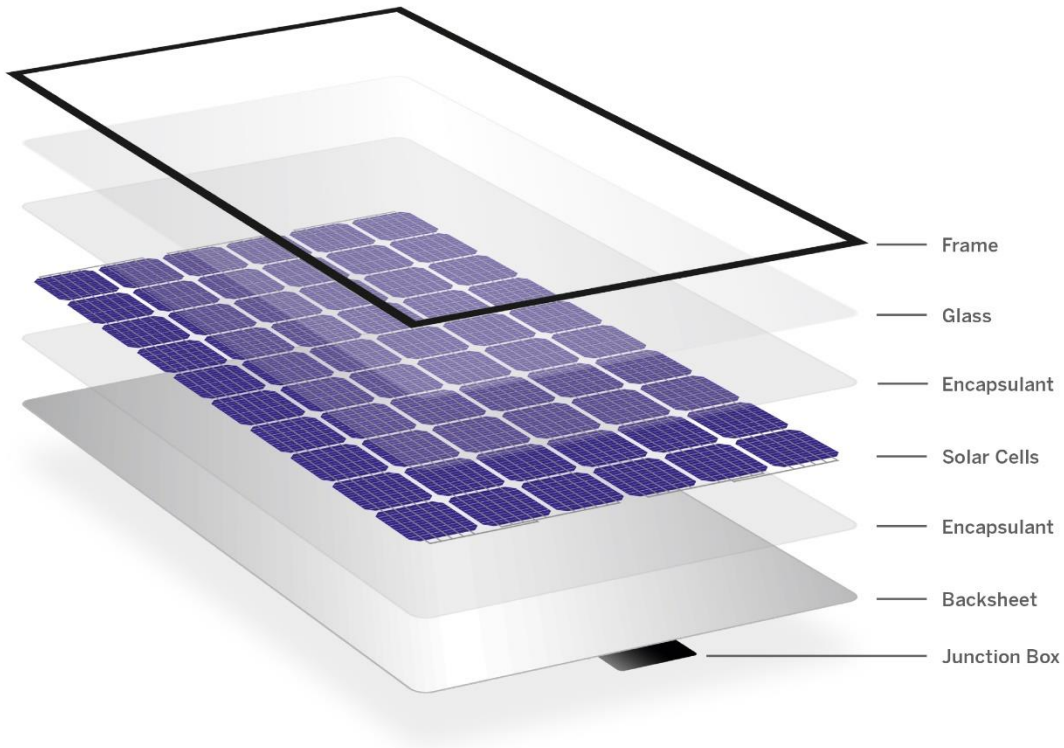

Figure 1 Cross-section of a standard PV module adapted from [3]

At the backside of the encapsulant, a layer called the backsheet is placed. It provides protection and insulation features to the cells and furthermore helps in enhancing the optical behaviour within the module. Finally, a frame is used to encompass all the layers thereby providing mechanical rigidity and protection. The various electrical interconnections are terminated at the junction box, where external insulated connectors are installed.

2.2. Optical gains and losses

When a cell is interconnected and encapsulated into a module there are certain optical gains and losses associated with the same. According to the work documented by the authors of [4], a 10 to 15 percent loss in efficiency can be observed owing to the loss and gain mechanisms. These mechanisms can be further sub-divided into direct and indirect optical gains and losses. Furthermore, it should be noted that the gains and losses mentioned herein are with reference to a single non encapsulated cell placed in air, i.e. in a medium with refractive index of 1.

- *Direct optical gain*- This gain arises due to the fact that the cell had initially been placed in an environment having refractive index of 1. However, by making a module out of the cell, each cell is now embedded in an environment with several layers whose refractive index are different. Typically a cell has a refractive index of around 3. The anti-reflective coating provides an intermediate refractive index of around 2.2. Further reduction in refractive index gapping is achieved by placing a glass layer in front of the module. Due to the reduced refractive index gapping between the layers, the amount of reflection of light out of the module reduces and hence a gain is observed.

- *Direct optical losses*- These losses are accounted to the reflection and absorption of the light rays in the different module layers. Light rays can either get absorbed in the layers of the module before reaching the active area or can be reflected away from it by the intermediate layers. This loss mechanism shall not be present for the reference un-encapsulated cell in air and therefore accounts as a loss when compared to the reference case. The thickness and the complex refractive index of the intermediate layers play a vital role in determining this optical loss mechanism.

- *Indirect optical gains*- Light rays incident on the cell active area, backsheet, cell, fingers, busbars or ribbons may be redirected to the active area by internal reflections caused by the module layers. In comparison to the reference case of an un-encapsulated cell placed in air, these light rays would have been lost, hence a gain is achieved.

In Figure 2, the various optical loss and gain mechanisms in a PV module are highlighted. The red region showcases the active area with the cell busbars placed both on top and bottom. Moreover, the cell is encapsulated in an encapsulant with a glass layer and backsheet at the top and bottom surfaces respectively.

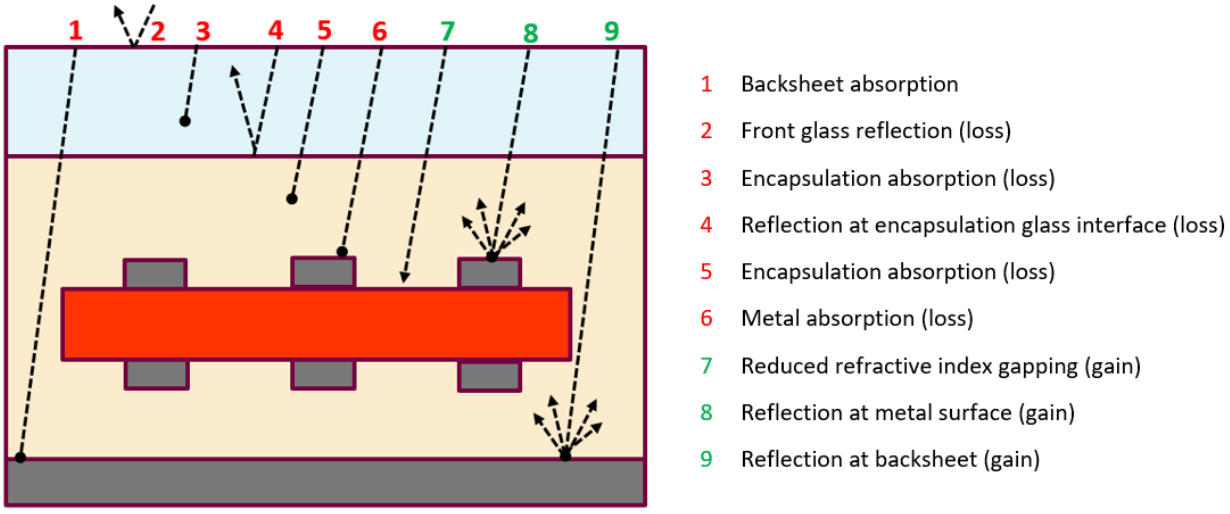

Figure 2 Cross-section of a PV module with rays indicating the various optical gain and loss mechanisms

Rays marked 1-6 in Figure 2 depict the mechanism of direct optical losses as explained earlier in this section. Furthermore, ray 7 highlights a case for a direct optical gain as the light ray is coming through intermediate layers with reduced refractive index gaping before being incident on the active layer. Finally, rays 8-9 depict indirect optical gains as these rays are getting another chance to be redirected to the active area by internal reflection within the module layers.

2.3. Electrical losses

Apart from the optical gains and losses mentioned in the previous section, there are coexisting electrical losses within a module. As explained in the study done in [5], these losses are the resistive losses owing to the current which flows in the various conductors that are used in the module. These conductors may include, cell fingers, busbars, string connectors, tabs, etc. Furthermore, joints and soldering also contribute to extra resistance and therefore increase the electrical losses.

$$Electrical\ losses\ = Current^{\,2} \times Resistance \tag{1}$$

Equation 1 describes the electrical losses incurred in a conductor of a given resistance when a certain amount of current flows through it.

$$Resistance = Resistivity \times \frac{Length\ of\ the\ conductor}{Area\ of\ cross\ section\ of\ the\ conductor} \tag{2}$$

Furthermore, the resistance is described by equation 2 as shown above. As is evident from the above equations, reduction of conductor length is essential for minimizing the electrical losses. Moreover, the area of the cross-section varies inversely as compared to the length of conductor for corresponding reduction in the aforementioned electrical losses.

2.4. Cell to Module (CTM) ratio

CTM ratio provides a quantitative metric to estimate the goodness of design for a PV module. It indicates how well the performance of a single cell can be replicated when a module is formed from the cell. The CTM ratio incorporates, in itself, the optical gains and losses arising due to module embedding of the cell and the electrical losses within the module. These electrical losses are caused due to the resistive losses that occur when current flows in the busbars, ribbons, fingers, and other used conductors within the module. There are various ways of defining the CTM ratio but in general the CTM ratio can be defined by equation 3 as-

$$CTM\ ratio = \frac{Performance\ parameter\ of\ the\ module\ (X_M)}{Performance\ parameter\ of\ a\ single\ cell\ (X_C) \times\ number\ of\ cells\ (N)} \tag{3}$$

As showed in [6], the performance parameter (X_M, X_C) used to define the CTM ratio is energy yield (E). This way of defining the CTM ratio helps compare the performance of the cell with the module for a given period of time. Furthermore, effect of field exposure can be better observed using this approach. Another approach for defining the CTM ratio, as depicted by the study done in [7], compares the power (P) of the module and the cell. Therefore, the performance parameter is the generated power.

In the present work, the employed performance parameter for the cell and module is power (P in Watts). Furthermore, the power output for both the cell and module is simulated under Standard Test Conditions (STC) with Air Mass (AM) 1.5 spectrum.

The CTM algorithms, as shown in the existing literatures [6] and [8], have higher degree of complexity. This infers a certain level of disadvantages to be associated with them. Apart from the complexity issue, there are certain other disadvantages which are listed below-

1. Large number of experimental and/or simulation based inputs are required.
2. Owing to the higher input requirements, the overall process of estimation with regards to CTM ratio is time consuming.
3. These algorithms are more suited for conventional module designs and taking into consideration the effects of tailored designs of PV modules is challenging.
4. Most of the current CTM algorithms suffer from symmetry induced error. In these algorithms the CTM analysis is done for a single cell placed in a module environment and the results are extended for the entire module. This induces error in the CTM estimation as the coupling of light varies from cell to cell within a module [9].

The CTM analysis algorithm used in the present work aims to overcome the above mentioned limitations.

3. Tool building approach

The ongoing chapter discusses the approach utilized for development of the tool to fulfil the objectives as already mentioned in chapter 1 and the challenges introduced in chapter 2.

There are various methods which have been discussed in the available literature to analyse the CTM ratio of a module, which in turn, provides the means to quantify the goodness of design of the module. In the study accomplished by the authors of [6], the methodology for analysing the CTM of a module under field exposure is discussed. The performance parameter used to define CTM in this approach is energy yield. Provided the fact that the intended tool's aim is to help make design choices prior to module production, analysing CTM using STC, amounts to a simpler and adequate approach. Furthermore, as per the approach in [8], STC conditions are used for studying the CTM of the module. As concluded in this work, the power production may be effectively used as a performance parameter for defining CTM. However, as per Arturo's work [10], where a similar approach has been utilized to calculate the CTM, wherein it has been specified that such an approach may not be accurate for tailored PV modules and is more suitable for full scale standard PV modules. This is because such approaches are based on assumptions that are valid only for square shape cells and modules. Another underlying assumption in these approaches is the uniform distribution of light rays throughout the module. For tailored PV modules this can offset the results significantly. Furthermore, in the previous chapter, additional disadvantages of the existing CTM algorithms is also provided.

Moreover, since the objective of the tool development is to use it primarily for optimized design of tailored PV modules, a different approach needs to be developed. This serves as the motivation for the design and development of a new approach which overcomes the existing drawbacks.

Furthermore, with the objective to integrate the proposed tool in the already existing PVMD toolbox, the entire coding has been done in MATLAB. In the proposed tool, the following development methodology has been used-

1. Automatic creation of vertices in three dimensional (3-D) space for all the different surfaces in the module structure as per the inputs provided.
2. Using the vertices to form the module surfaces.
3. Performing ray tracing on the built module structure and estimate its optical performance.
4. Similar analysis for a single cell.
5. Developing a model to estimate the electrical losses for both the cell and the module.
6. Finally, estimation of power production for both cell and module and assessing the CTM using the same.
7. Parameter sweeping to arrive at the most optimised module design.

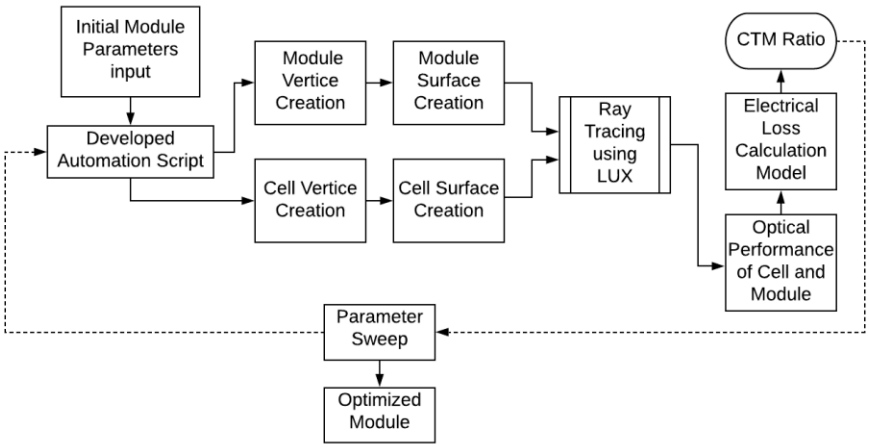

Figure 3 Flowchart depicting the developed CTM Analysis algorithm

Figure 3, represents the flowchart of the implemented CTM analysis algorithm. In the following sections the methodology, as depicted in Figure 3, will be explained in detail.

3.1. Creation of vertices

With the help of user inputs about the geometry of the module, the various vertices are automatically plotted in 3-D space using the developed MATLAB script shown in the appendix. These inputs include information about the module geometry like the cell size, cell spacing, module size, number of cell rows and columns in the module, cell metallization grid structure, thickness of various layers like glass and encapsulation, and other such geometry related parameters. Upon receiving these inputs, the developed code automatically maps them in 3-D space.

Figure 4, as shown hereunder, exemplifies the process of vertex creation by the developed code. The figure shows the result of vertex creation using a sample input of module geometry by the user. The vertex points are represented in ‘red’ whereas the respective vertex numbers are highlighted in ‘blue’.

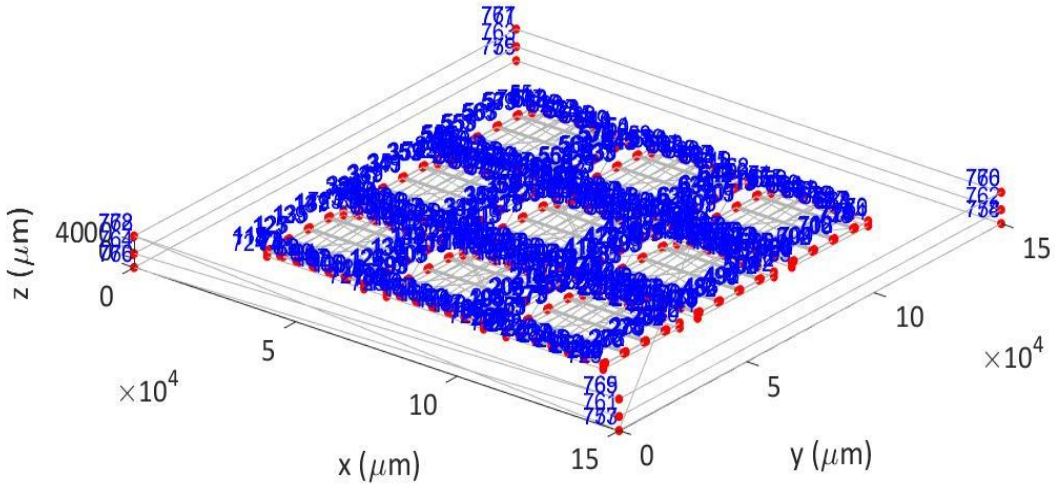

Figure 4 Automatic vertex mapping in 3-D space based on user inputs

The developed code, depending on the module geometry inputs, automatically centres the cells in a symmetrical way inside the module. The different module geometry parameters which the user may enter and vary is shown in Table 1.

It must be noted that the reference point in the 3-D space used for plotting is the origin i.e. x=y=z=0. The vertices are stored in a matrix [V] which contains information for the x, y and z coordinates for the respective vertex points.

Furthermore, in addition to the parameters shown in Table 1, other parameters have also been used to define the geometry of tailored PV modules. These parameters will be discussed in the corresponding sections.

Sl. No.	Parameter	Variable name used in the code
1	Length of the module	l_m
2	Breadth of the module	b_m
3	Length of the cell	l
4	Breadth of the cell	b
5	Rows of cells in the module	r_m
6	Columns of cells in the module	c_m
7	Thickness of the cells	t_c
8	Thickness of the back contact	t_bc
9	Thickness of the encapsulant above cell surface	t_eva_ac
10	Thickness of the encapsulant below the back contact	t_eva_bc
11	Thickness of the front glass	t_fg
12	Thickness of the backsheet	t_bs
13	Cell ending edge to cell starting edge spacing	s_c
14	Number of busbars on the top metallization	n_bb
15	Width of the busbar	w_bb
16	Thickness of the busbars	t_bb
17	Distance between the busbars	d_bb
18	Distance of the first busbar from the edge of the cell	d_s_bb
19	Distance between the fingers	d_fi
20	Thickness of the fingers	t_fi
21	Width of the fingers	w_fi
22	Open circuit voltage of the cell	v_oc
23	Resistivity of fingers	res_fi
24	Resistivity of busbars	res_bb
25	Resistivity of back contact	res_bc
26	Resistivity of interconnecting ribbons	res_int
27	Number of cells in series in a string	n_c_ser
28	Number of strings in parallel	n_s_par
29	Thickness of the metal carrying parallel current	t_par
30	Width of the metal carrying parallel current	w_par
31	Thickness of the interconnecting ribbon	t_bb_t

Table 1 Different module geometry inputs

3.2. Creation of module surfaces

Once the vertices are created and stored in a matrix [V], as explained in the previous sub-section, they are used to define the various facets which form the solar module. This section illustrates the methodology used for the creation of such facets.

For the creation of these facets a minimum of three and a maximum of four vertices can be joined. The developed code automatically clubs the respective vertices to form the module surfaces as described by the module geometry inputs.

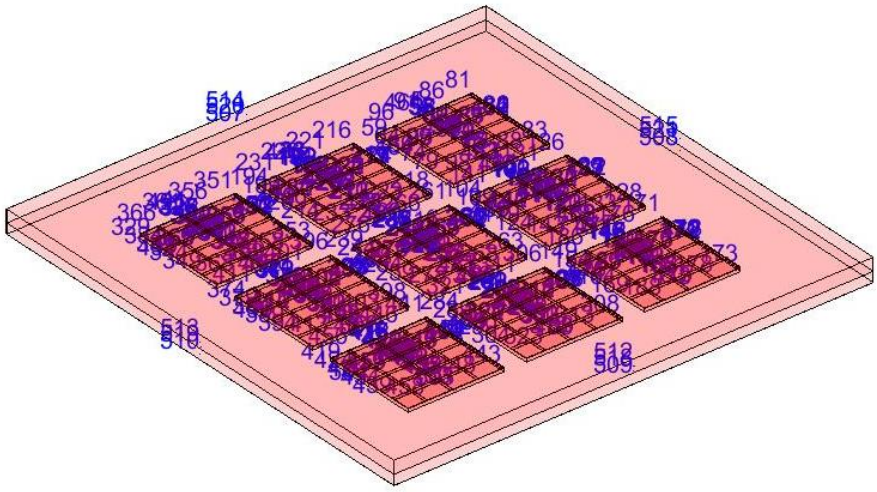

Figure 5 A sample of developed module surfaces by clubbing the vertices

The module surfaces are numbered and represented in 'blue' as shown in Figure 5. The information of the vertices used for the creation of a particular module surface is stored in a matrix [F].

Depending on the module geometry inputs, the flow of the code automatically prepares the vertices and the facets for the module elements shown below-

1. Creation of vertex and facet matrix for solar cells
2. Creation of vertex and facet matrix for front metallization grid
3. Creation of vertex and facet matrix for back contacts
4. Creation of vertex and facet matrix for encapsulation
5. Creation of vertex and facet matrix for front glass
6. Creation of vertex and facet matrix for backsheet

Thus, with the [V] and [F] matrices ready, the module modelling is complete. Hereafter, it is now required to simulate its electrical and optical behaviour.

3.3. Ray tracing

To evaluate the optical and electrical behaviour of the developed solar module model, we use LUX [11]. LUX enables ray tracing on the developed solar module model and its results can be further used to estimate the optical and electrical behaviour of the module. The manual enclosed with LUX package can be used to provide a detailed knowledge on its usage.

In order to use LUX, one must specify the optical properties of the module surfaces built using the [V] and [F] matrices, as discussed in the previous sections. These optical properties can be defined by using a

complex refractive index which comprises of the refractive index (n) and the extinction coefficient (k) [12] as the real and imaginary parts respectively. Alternatively, the reflectivity (R) and the transmittivity (T) can also be specified for the module surfaces.

In this work, perfect absorbers are used for the solar cells i.e. $R=T=0$. This approach has been used to mitigate the problem of practically non usable computation times for the creation of the vertices and facets of the solar cell texturing structures.

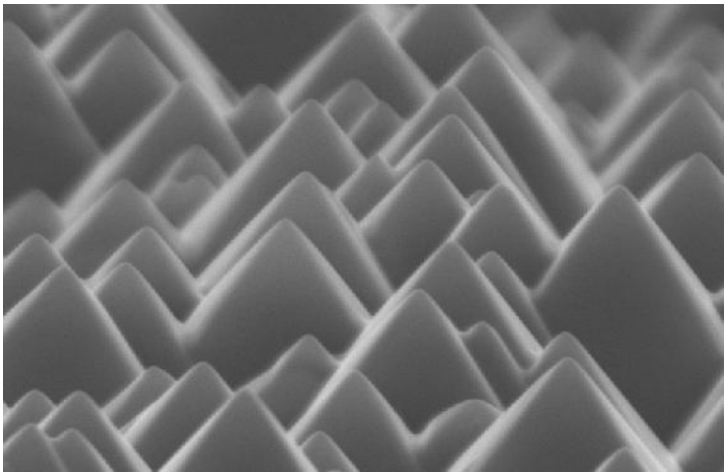

Figure 6 Pyramid textures on the cell surface [13]

This delay is primarily caused due to the extremely high number of vertices required to build the pyramid textures, as shown in Figure 6, on the cell surfaces. Furthermore, ray tracing on these structures induces a greater delay with respect to the computational times.

Using the perfect absorbers as a replacement for the solar cells enables the estimation for the maximum potential of the module design, irrespective of the choice of the cell. This is desirable owing to the fact that the main objective of the proposed tool is to optimize module design. It should be noted that the front and back contacts of the cells are still included in the model as it is required to incorporate the shadow effect on the cells and also due to the indirect optical gains to which it may contribute.

A brief enlistment of the advantages of using perfect absorbers as a replacement of actual solar cells is presented below-

1. Enables faster calculation.
2. Gives the estimate of the maximum potential performance of a proposed module design.
3. Absorption occurs only in the Spectral Response Range (SRR) of the cell to avoid overestimation of maximum potential performance.
4. Module design efficiency can be estimated irrespective of cell technology.

In LUX we use the standard AM 1.5 spectrum for ray tracing as the intended study of the module is under STC.

In Figure 7 the AM 1.5 spectrum is illustrated by the ‘orange’ curve. The ‘blue’ curves show the extra-terrestrial irradiance whereas the ‘grey’ curve shows the direct and circumsolar irradiance. Furthermore, in LUX an additional surface is needed which acts as an emitter for the AM 1.5 irradiation. To accomplish this we create additional enclosure surfaces for the entire module structure. The top surface of his enclosure acts as the emitter whereas the other surfaces of the enclosure are absorbers which indicate the irradiation which escapes the module structure.

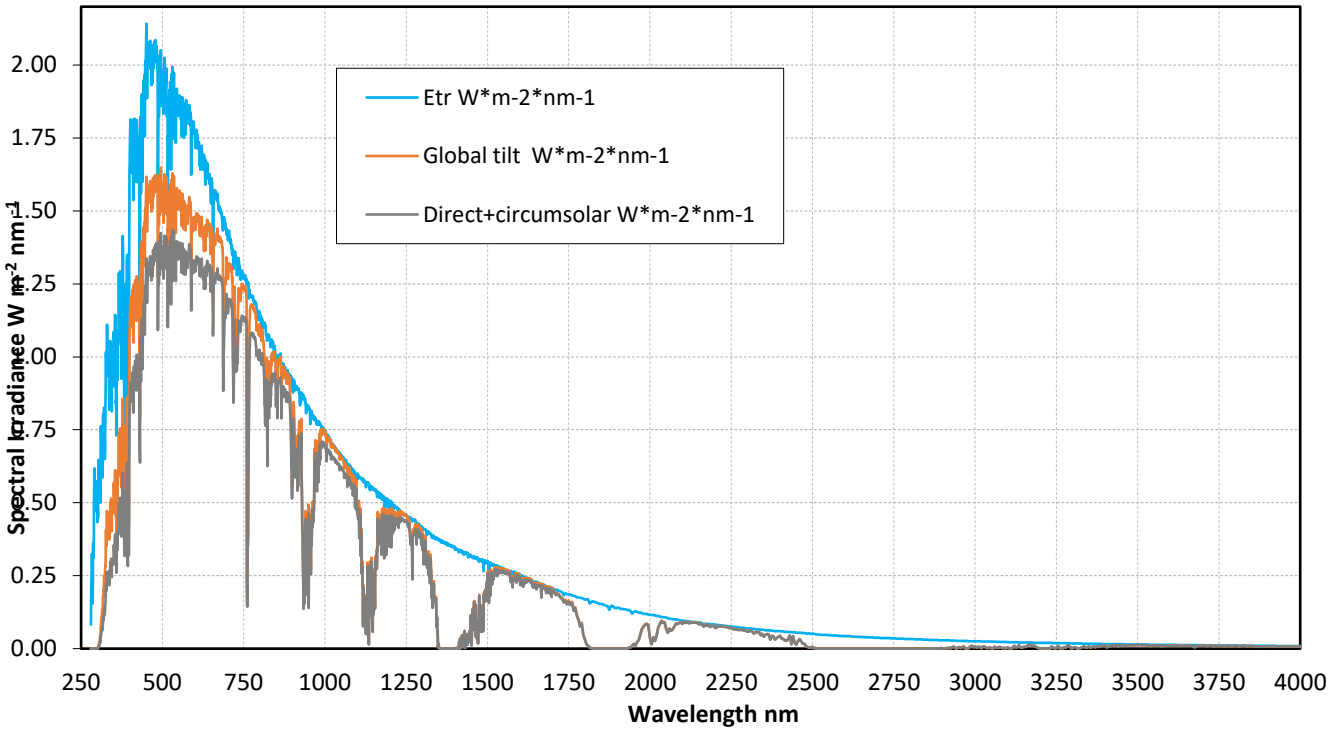

Figure 7 Standard AM 1.5 Spectrum [14]

It must be noted that the boundaries for the module surfaces are defined as interface between the respective module surface and air. Furthermore, the number of rays emitted from the emitter surface of the enclosure affects the accuracy of simulation. Variation in the accuracy of simulation is in direct proportion to the number of rays. However, with a higher number of rays the simulation time also increases. Therefore a trade-off is to be made between the intended accuracy and the computational time.

LUX also requires the wavelength range to be specified in order to perform analysis of the photocurrent produced and generating the reflectance (*R*), absorptance (*A*), and the transmittance (*T*) analysis of the various surfaces. Therefore, the wavelength range of 300 nm to 1200 nm is used as an input to LUX, as this range has optimal coherence with the spectral response of crystalline silicon [15]. Furthermore, the steps in the wavelength need specification in order to postulate the range of the wavelengths. Larger steps result in faster simulation but reduced accuracy whereas smaller steps results in a more accurate result at the cost of increased computational time.

An important consideration in defining the optical properties of the module surfaces is the optical properties of the backsheet. Backsheet could not be simply modelled by specifying the *n-k* or *R-T* values owing to the scattering behaviour of the backsheet.

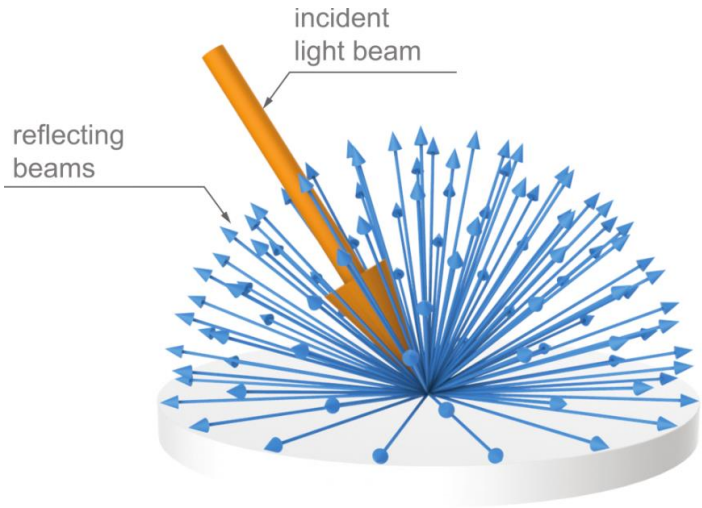

Figure 8 Reflection by a Lambertian scatterer used for modelling backsheet [16]

In the work done by the authors of [9], it is stated that the backsheet can be effectively modelled as a Lambertian scatterer, as shown in Figure 8, without any significant overestimation of the re-reflected light within the module. Furthermore, in software such as the SUNSOLVE by PVLighthouse [17], it is seen that for modelling the backsheet , perfect Lambertian scatterer is indeed used. An overview of the Lambertian scattering and the Phong model is presented in [18].

3.4. Optical performance

Once the ray tracing is performed on the built structure, we get the Reflectance- Absorptance-Transmittance (*R-A-T*) profile of the structure. An example of the *R-A-T* response of a sample module is shown in Figure 9 for exemplification.

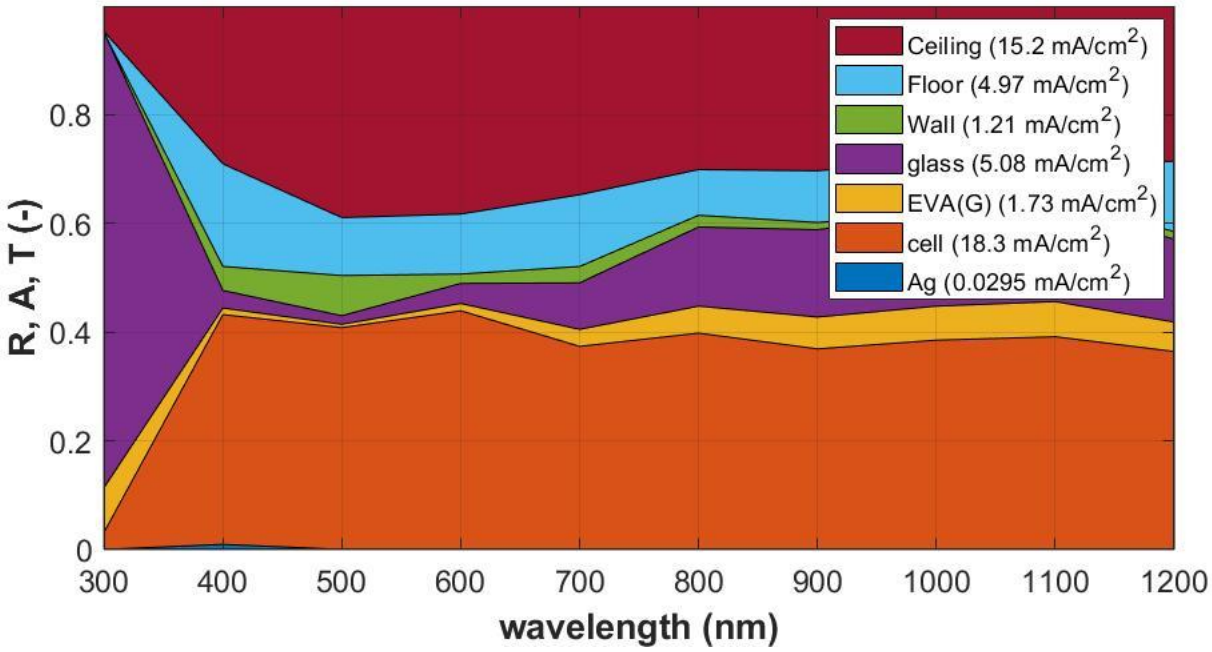

Figure 9 Sample module *R-A-T* response from ray tracing

The *R-A-T* response of the modules is spectrally resolved and also presents the photocurrent density of the used materials in the module structure. It is worth noting that the photocurrent density of materials presented, after ray tracing, is with respect to area of the ray emitting surface. The developed script then automatically

converts the photocurrent density for the cell material with respect to the top surface area of the cells. This is shown by the equation 4.

$$Photocurrent\ Density = \left(\frac{emitter\ surface\ photocurrent\ density}{Area\ of\ top\ surface\ of\ cells}\right) \times Area\ of\ emitter\ surface \quad (4)$$

With the knowledge of the area of the cells and the open circuit voltage (V_{oc}) of the cells, the short circuit power of the module is estimated.

During the development of the tool, as already stated, in the previous section, perfect absorbers are used and an estimation of the maximum potential performance of a particular module design, irrespective of the cell choice, is made. Therefore, to include the fill factor or recombination effects, which predominantly is dependent on cell material properties, would defy the purpose of module potential performance estimation irrespective of the cell choice. Furthermore, the performance estimation is based on the short circuit power.

Using ray tracing the power generated for a single cell is also quantified. However, it must be noted that these module and cell powers are the powers generated and the same amount would not be delivered due to resistive losses. Therefore, it is required to create a model which can estimate the electrical losses and calculate the deliverable powers of both the cell and the module.

3.5. Electrical loss model

In the previous section, it has been demonstrated how the short circuit power can be estimated. However, this power is not available due to the various resistive losses in the metallization used within the module [19]. In this section, a model for the estimation of resistive losses in the cells and module is elaborated.

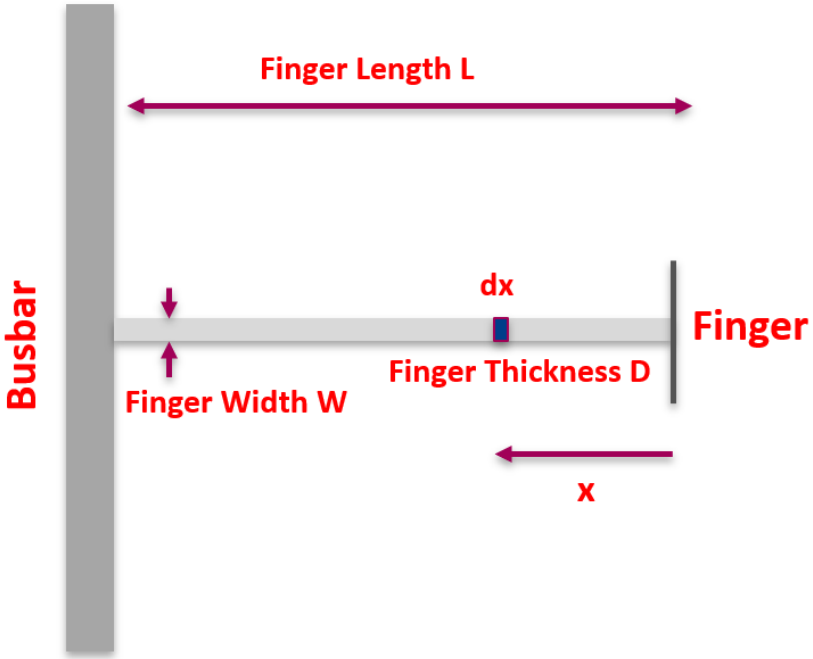

Figure 10 Differential element method for ohmic loss calculation

In this work, differential element method is implemented to calculate the resistive losses [20]. In Figure 10, a cell finger and a busbar is seen. The first step is to find the current flowing through the differential element at a position '*x*' from the reference. In the tool, this is done by first calculating the current output of each busbar. The tool finds this by distributing the total generated current by the cell, among the busbars with reference to the area of influence under each busbar. Thereafter, this current is uniformly distributed over the cell fingers on each side of the busbar depending on the area of influence on each side of the busbar.

Therefore, the current contribution of each cell finger to the busbar is obtained. Assuming that this current, say '*I*' is uniformly distributed over the length of the cell finger, the following equations ((5)-(9)) are defined-

$$I(x) = \frac{I}{L} \times x \tag{5}$$

where, '*L*' is the length of the cell finger under the influence of the busbar as shown in Figure 10.

The next step is to compute the differential power loss in the small finger element '*dx*'. Therefore, the differential resistance '*dR*' of the element '*dx*' is defined as-

$$dR = \rho \times \frac{dx}{W \times D} \tag{6}$$

where '*W*' and '*D*' are the width and the thickness of the cell fingers as shown in figure 10.

'ρ' in the above equation represents the resistivity of the metallization material. Now the power loss '*dP*' in the small differential element 'dx' is given as-

$$dP = I(x)^2 \times \rho \times \frac{dx}{W \times D} \tag{7}$$

Now, having estimated the power loss in the differential element, the power loss '*P*' in the entire cell finger can be estimated by integrating the power loss across the length of the cell finger.

$$P = \int_0^L I(x)^2 \times \rho \times \frac{dx}{W \times D} \tag{8}$$

The above equation can be simplified and rewritten as-

$$P = \frac{I^2 \rho\, L}{3WD} \tag{9}$$

Thus, by equation 9, the resistive losses in the cell fingers is estimated. For calculating the resistive losses in the busbars, a similar approach is followed. For busbars, the direction of the current or the '*x*' vector is assumed to be downwards with reference to Figure 10.

Apart from the cell fingers, ohmic losses also occur in the interconnecting ribbons shown in Figure 11-

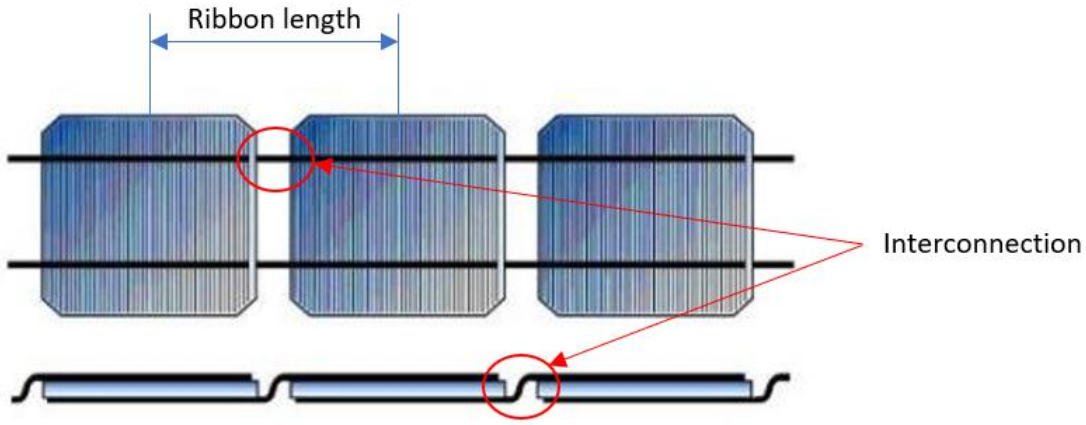

Figure 11 Schematic showing cell interconnection using ribbons adapted from [21]

Since the current flowing through each busbar is known, the ohmic losses in these interconnecting ribbons can be directly estimated using equation 1. It must be noted that the resistive losses due to soldering the ribbons to the busbars is neglected in the present analysis. Furthermore, the sheet resistance faced by the charge carriers when moving towards the fingers and busbars are also neglected.

These interconnecting ribbons carry the current as a result of series connection of the cells. Furthermore, the tool also takes into consideration the resistive losses due to the parallel interconnection of strings. The tool can estimate the losses automatically for maximum up to four busbars. However, if the application requires to use more busbars, the coding methodology, as shown in the Appendix, can be adopted to predict the ohmic losses for busbars beyond four in number.

The tool automatically performs computation for the total ohmic losses for both the cells and the module. This enables to make prediction about the CTM ratio for the particular module as explained in the next section.

3.6. CTM calculation

Having estimated the potential power delivered by both the cell and module, the CTM ratio can be estimated which provides a metric for analysing the goodness of design of the module. The estimation of CTM ratio can be done using equation 10 as-

$$CTM\ Ratio = \frac{Power\ of\ the\ Module}{Power\ of\ the\ cell\ \times Number\ of\ cells} \quad (10)$$

The effect of varying different input parameters on the CTM ratio can be studied to observe various trends and optimize the module design to suit a particular application. This would be explained in detail in the following chapter.

3.7. Approach for custom shape cells and modules

As explained earlier, a key element of consideration for the development of the tool is to ensure that the tool is able to quantify the goodness of design of not just standard modules but also of tailored PV modules. The tailored PV modules can have several distinct features as compared to a standard PV modules like, cell size, shape, module size and shape. The input parameters shown in Table 1, gives the user of the tool the flexibility to automatically model and simulate only square or rectangular cell or module designs. Arturo's work suggests less performance degradation of triangular cut cells as compared to other custom shapes [10]. These custom shapes can be generated using standard cell and laser cutting. A typical laser cutting machine, from Lasergraaf, is shown in Figure 12.

Figure 12 Lasergraaf Laser cutting machine [22]

These fibre laser cutters use optic fibre cables to transport light beams, typically in the range of 1070 nm [22]. The light beams then reach the substrate as shown in Figure 13. However, several mirrors are used to direct the light beam towards a θ-lens. This lens evenly distributes the focus of the beam on the entire plane as compared to a single point [23]. In Figure 13, the operation of the laser cutting machine is illustrated.

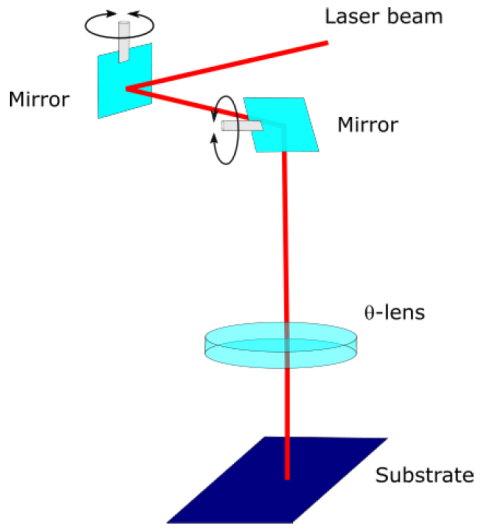

Figure 13 Laser cutting machine operation [23]

A triangular cell can be joined with other triangular cell pieces to build a variety of other shapes. Therefore, a separate coding methodology is implemented for modelling and simulating triangular modules to show the tools efficacy in modelling and simulating tailored PV modules. A model developed of such a sample module using the tool is shown in Figure 14.

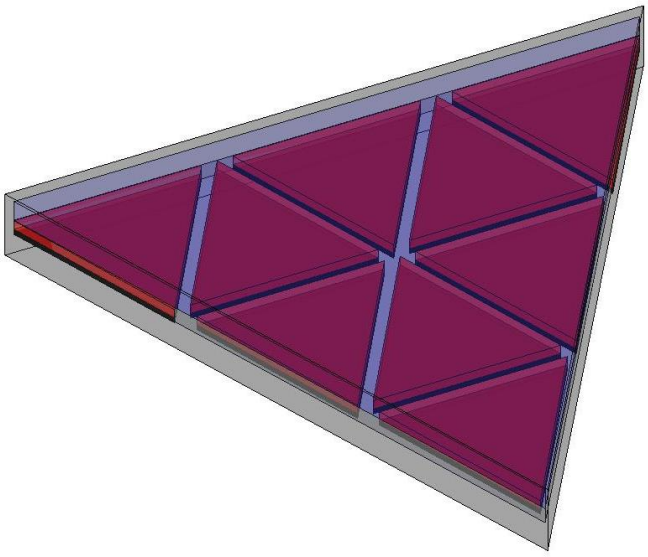

Figure 14 Tool generated sample model of triangular module

The tool performs ray tracing on the above built model and furnishes its optical performance. As is evident from Figure 14, the cells are placed in an alternate inverted arrangement to achieve a higher packing density.

However, when such tailored shapes of cells are modelled using the tool, incorporating the metallization on cell structures becomes challenging owing to the fact that only a maximum of four vertices can be defined for a surface in LUX. To mitigate this challenge, in this work, an empirical formula is developed which can

estimate the optical impact of the metallization in an encapsulated environment rather than actually including the metallization structure of the cell in the modelling. In the following chapter, the derivation of this empirical formula is discussed in detail.

Another challenge for simulation of such tailored modules is estimation of the electrical losses as the metallization is not actually incorporated in the modelling. To mitigate this, a comparative approach is used. In this approach, the electrical losses for a square cell of equal area as that of the triangular cell is used. However, it must be noted that the current used for calculation of these losses is that of the triangular cell and only the geometry of an equivalent square cell is used.

The above approach of using the developed empirical formula and comparative estimation must only be used for simulating custom shapes, when creation of the metallization structure on the cell top surface is not feasible, to ensure higher accuracy. For the triangular module discussed here, the input parameters in contrast to the one mentioned in Table 1 is shown hereunder-

Serial Number	Parameter	Variable name used in the code
1	Length of the equilateral module edge	m_e
2	Number of cells in the base row of the module	c_m_b
3	Length of the equilateral triangle cell edge	c_e

Table 2 Additional input parameters for triangular modules

As is evident from Table 2, the tool only requires the number of cells in the bottom row of the module and automatically places the cells for maximum packing density. For building an equilateral triangular module it must be ensured that the input for number of cells in the bottom row of the module should be an odd number.

The tool exemplifies its use for tailored PV modules by modelling and simulating triangular modules. The coding structure used to do so can also be adopted for building other custom shapes depending on the application.

4. Demonstration of tool features

The present chapter discusses a variety of scenarios that are used to depict the usage of the tool. Furthermore, this chapter aims to illustrate the use of the tool to identify various trends in the performance with respect to varying parameters which help to make better design decisions for the particular scenario. The scenarios discussed in this chapter are as follows-

1. Performance evaluation and optimization of PV mini modules
2. Performance evaluation and comparison of standard PV modules vs half cut cell modules
3. Performance evaluation and optimization of glass-glass modules
4. Performance evaluation of triangular modules

The ongoing chapter aims to not only exemplify the efficacy of the tool for various scenarios but also highlight interesting results obtained from the simulation.

4.1. PV mini modules

In recent times PV mini modules, characterized by their use of small area cells, have seen widespread applications like for instance in low power electronics, building integrated solutions or autonomous power supply in the field of Micro Electro Mechanical Devices (MEMS) [24].

When manufacturing such modules, several design choices are available with the manufacturer. However, a quantified analysis is desirable to make an educated design choice. The various design questions that might arise are summarised as-

1. Is there an optimum tuning between the cell-cell and cell-edge spacing for maximum power output ?
2. How would inclusion of more busbars during cell cutting affect the performance?
3. What is the optical balance of the system?

Furthermore, it will be worthwhile to see the effect of backsheet in the above mentioned design questions. An attempt has thus been made to investigate the solution to these questions using the developed tool.

4.1.1 Cell-cell and edge-cell spacing

As illustrated in Figure 15, the cell to cell spacing refers to the uniform spacing between the adjacent edges of the cells placed within the module. The edge to cell spacing on the other hand refers to the spacing between the edge of the module and the cell edge.

It has been proven that, when cell to cell spacing is increased, the recoupling of light from the backsheet increases leading to indirect optical gains [9], [26]. However, in these findings, when one increases the cell to cell spacing, the module size marginally increases to accommodate the increased inactive area. In this section an investigation is carried out to find an optimal tuning between the cell to cell spacing and the edge to cell spacing keeping the module dimensions as constant. An exemplification is done to demonstrate the tools efficacy in finding such optimality.

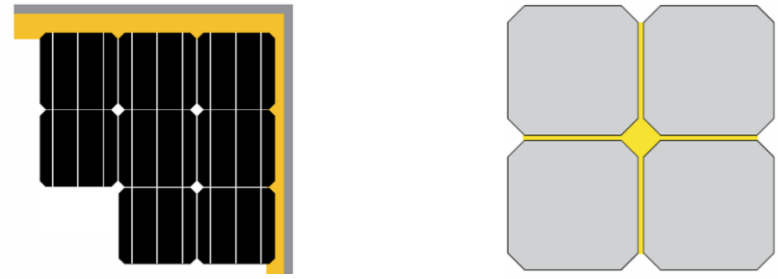

(A) (B)

Figure 15 (A-Edge spacing, B- Cell spacing) Illustration of cell to cell and edge to cell spacing highlighted in 'yellow' [25]

A test PV mini module modelled with specification tabulated in Table 3 is used for performing simulations. A 3 × 3 module is specifically used as a test mini module as this module encompasses all the possible cell positions in a module i.e. centre, edge and intermediate positions.

Sl. No.	Parameter	Value
1	Length of the module	12 cm
2	Breadth of the module	12 cm
3	Length of the cell	3 cm
4	Breadth of the cell	3 cm
5	Rows of cells in the module	3
6	Columns of cells in the module	3
7	Thickness of the cells	180 µm
8	Thickness of the back contact	1 mm
9	Thickness of the encapsulant above cell surface	1 mm
10	Thickness of the encapsulant below the back contact	1 mm
11	Thickness of the front glass	4 mm
12	Thickness of the backsheet	0 (single layer)
13	Cell ending edge to cell starting edge spacing	0.5 cm
14	Number of busbars on the top metallization	1
15	Width of the busbar	1 mm
16	Thickness of the busbars	15 µm
17	Distance between the busbars	0 (Single Busbar)
18	Distance of the first busbar from the edge of the cell	1.5 cm
19	Distance between the fingers	1.568 mm
20	Thickness of the fingers	15 µm
21	Width of the fingers	45 µm
22	Open circuit voltage of the cell	0.65 V
23	Resistivity of fingers	1.638495×10^{-2} Ω µm
24	Resistivity of busbars	1.638495×10^{-2} Ω µm
25	Resistivity of back contact	1.638495×10^{-2} Ω µm
26	Resistivity of interconnecting ribbons	1.638495×10^{-2} Ω µm
27	Number of cells in series in a string	3
28	Number of strings in parallel	3
29	Thickness of the metal carrying parallel current	0.8 mm
30	Width of the metal carrying parallel current	5 mm
31	Thickness of the interconnecting ribbon	0.8 mm

Table 3 Specification of test PV mini module

The backsheet used for the above specified PV mini module is a perfect white and a perfect black backsheet. Thereby reflecting and absorbing all the incident wavelengths respectively. An analysis is performed on both the backsheets to identify the performance difference for two extreme backsheet choices. The number of rays used for ray tracing in the simulation is 100000 for white backsheet modules, whereas, for black backsheet, 500000 rays are used. This is done to keep the simulation time relatively low, as for white backsheet due to the high number of reflections, the simulation time can be much larger for higher number of rays.

Furthermore, it is assumed that for each pair of cells, the interconnecting ribbons have total length which is equal to the summation of cell spacing and the cell's length as shown in Figure 11 of chapter 3. The width of these ribbons is assumed to be equal to that of the busbar's width. Furthermore, the metal carrying the parallel current from the strings is assumed to be of length equal to the thickness of the module.

The wavelength range used is from 300 nm to 1200 nm to ensure absorption in the spectral response range of crystalline silicon. The steps used for the wavelength is 100 nm to speed up the simulation.

The entire module structure is embedded within an enclosure to facilitate ray tracing. This enclosure maintains a 10 μm distance from the module structure within it.

It should be noted that these parameter values are chosen for the test PV mini module and can be easily changed in the tool to suit application specific modules.

Herein, the effect of changing cell to cell and edge spacing on the module performance is presented. It must be noted that the cell spacing is varied from 0 to the maximum available space in the module structure. When the cell to cell spacing is 0, all the cells are clubbed together and the edge spacing is maximum. An increase in the cell spacing would result in the decrease of edge spacing until it finally reaches 0 value.

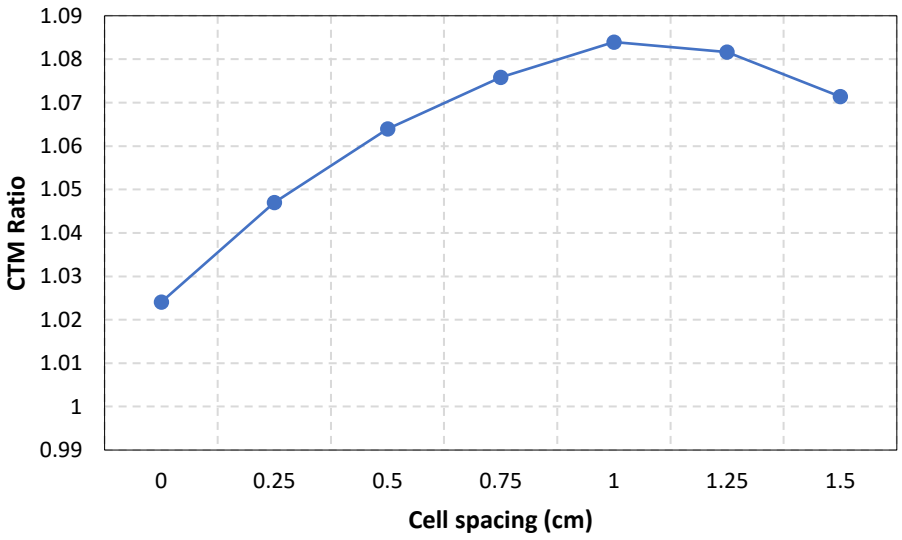

Figure 16 CTM Ratio vs Cell spacing for the test PV module with white backsheet

As is evident from Figure 16, initially, when the cell spacing starts to increase, more light rays, which are redirected from the backsheet, are able to recouple with solar cells. Though the contribution of light rays coming from the edge spacing decreases, it is, however, overcompensated by the light rays coming from the cell to cell spacing. This is due to the fact that the probability of light reaching the active area from the cell to cell spacing is higher than that of light coming from the edge spacing. The light coming from the cell to cell spacing can influence a larger number and area of cells as compared to the light coming from the edge spacing which can largely influence only the edge cells.

Hence, a relatively linear increase in the CTM ratio is observed with the increase of cell spacing until a saturation point is reached. This saturation point is reached because of the fact that the effect of increased light coupling due to increasing cell spacing is neutralized by the effect of decreased light coupling due to the decreasing edge spacing. This saturation point is the most optimum point for determining values of cell and edge spacing.

Beyond the saturation point, the effect of decreasing light coupling due to reduced edge spacing is dominant and therefore a decrease in the CTM ratio is noticed.

It must be noted that apart from the optical contributions of increasing cell spacing and decreasing edge spacing, another factor which contributes to the CTM ratio, are the ohmic losses. With increasing cell spacing the length of the interconnecting ribbon between the cells also increases which leads to higher ohmic losses. This is represented graphically in Figure 17.

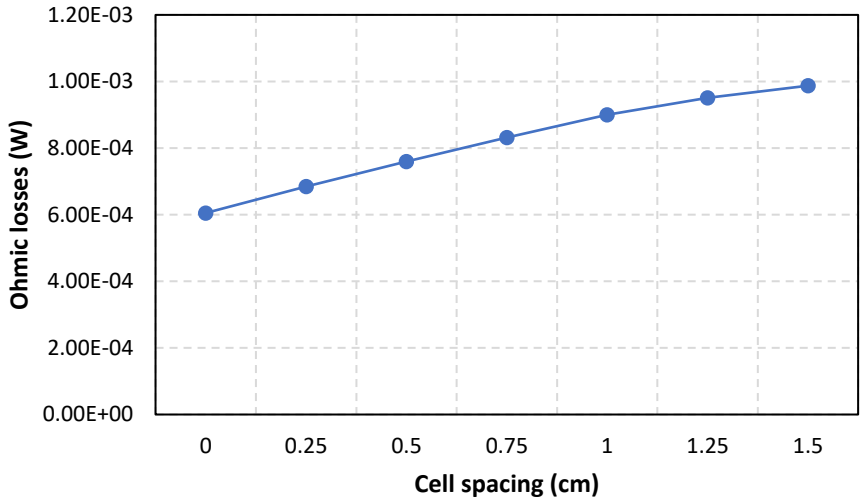

Figure 17 Ohmic losses vs Cell spacing for test module with white backsheet

However, as per Figure 16, the effect of increasing ohmic losses is less as compared to the gain in light coupling due to the increased cell to cell spacing and therefore a gain in CTM ratio is observed.

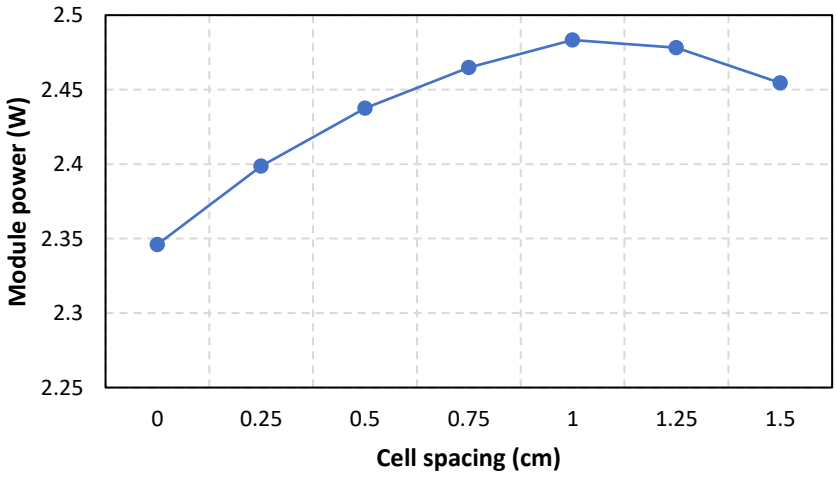

Figure 18 Module power vs Cell spacing for test module with a white backsheet

The tool is also able to estimate the module power for each of the varying cell spacing values, as shown in Figure 18. The trend for the module power follows the CTM ratio trend and therefore, the maximum power

out of the module is attained at the saturation point. This also shows that power optimization for the test module is driven by optical gains/losses rather than electrical losses. Therefore, the tool provides with an optimal tuning between the cell to cell spacing and the edge spacing for the test module. In this case, the simulation result suggests that the optimal cell spacing is 1 cm for a corresponding edge spacing of 0.5 cm.

With an increasing application of black backsheet modules [27], the tool is also able to provide optimization points for such modules. Herein, the simulation results for the same test module, however, with a black backsheet, is presented.

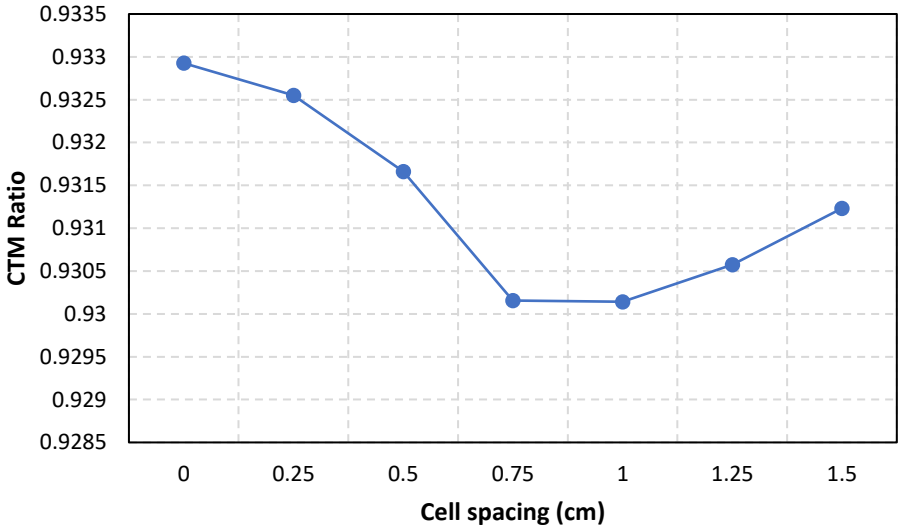

Figure 19 CTM ratio vs cell spacing for test module with black backsheet

Figure 19, shows the variation of CTM ratio with the cell spacing. It is contrastingly different with respect to the trend observed in Figure 16 for the white backsheet test module. It is also observed that the changes in the CTM ratio is very less compared to its white backsheet counterpart. This is due to the fact that there is very little contribution of light rays from the black backsheet as it behaves as a perfect absorber.

As the cell spacing increases, the CTM ratio decreases owing to the increase in the ohmic losses due to increased interconnecting ribbon length as shown in Figure 20.

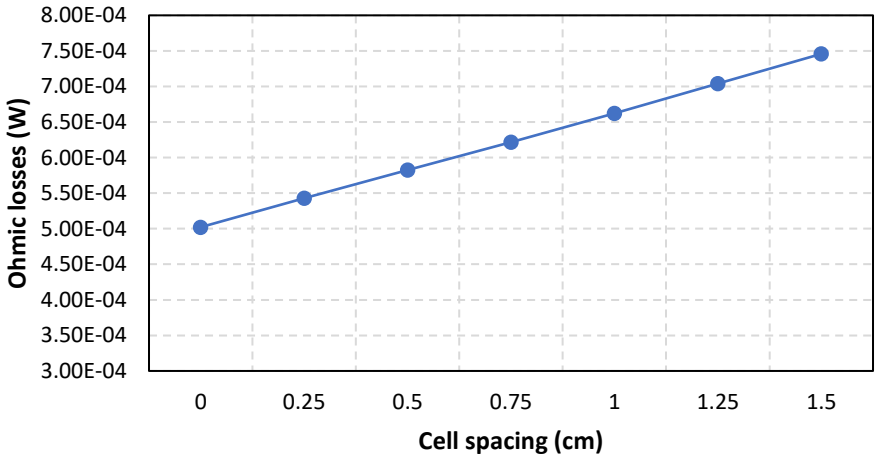

Figure 20 Ohmic losses vs cell spacing for test module with black backsheet

Furthermore, it again observed that a saturation point is being reached in the range of 0.75 cm to 1 cm. Beyond 1 cm, a small increase in the CTM ratio with respect to the cell spacing is observed. The simulation results suggest that there is an increased light coupling (0.12 %) with the active area when the cells are

approaching the module edges. This results in the initial saturation region and thereafter a gain in CTM ratio. This slight gain can be explained with reference to Figure 21 as shown hereunder.

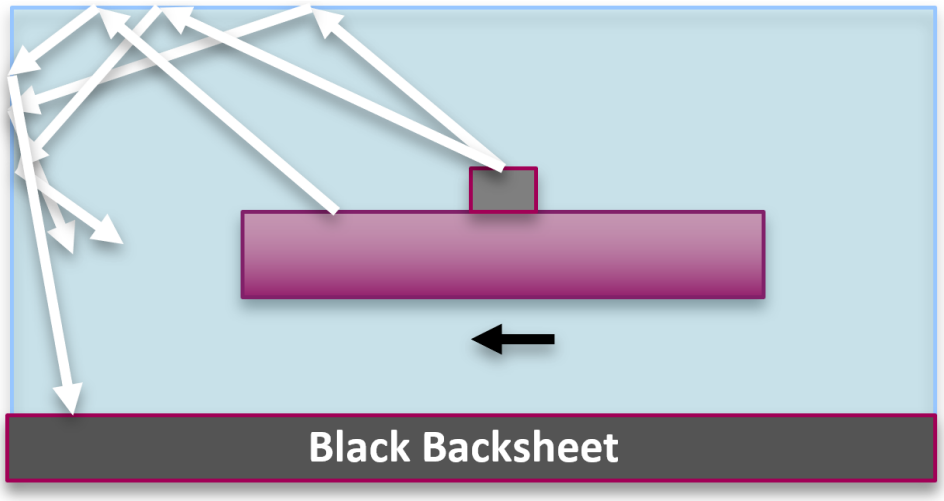

Figure 21 Schematic for demonstration of increased light coupling as cell approaches module edges

As depicted in the Figure 21, the simulation results show that the density of light rays along the edges of the module is slightly larger compared to the light ray density in the rest of the module due to internal reflection within the module geometry. When cells approach the edges, these light rays can then be coupled with the active area and thereby result in an increased photocurrent density.

Figure 22 Ray tracing images of module edges for test module with black backsheet

Figure 22, as shown above, illustrates the ray tracing results for the test module with black backsheet. As is evident from the figure, the ray density along the module edges is indeed larger owing to internal reflections.

The tool further informatively furnishes the module power generation for selecting the optimum point for design. Figure 23, shows the variation of module power with the cell spacing.

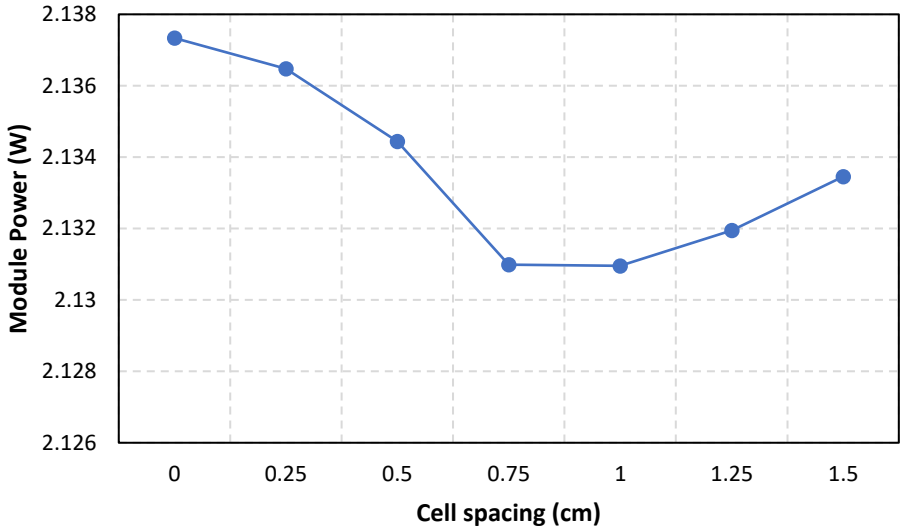

Figure 23 Module power vs cell spacing for test module with black backsheet

As is evident from the above figure, that the module power follows the trend of the CTM ratio. However, a minimal variation in the CTM ratio with respect to cell spacing infers to a nominal module power variation as well (around 0.3 %).

The simulation results promote design of the test module with black backsheet with theoretical cell spacing of 0 cm which is, however, practically not feasible, depending on the module technology. Therefore, minimal cell distances should be ensured for mini-modules.
Furthermore, it is seen from Figure 19 that when the cells are close to the module edges an extra gain in CTM ratio is derived. Therefore, it must be ensured that the cells are as close as possible to the module edges. Owing to insulation needs and prevention of shading due to dirt coverage on module edges [28], the edge distances cannot be made very small. However, it should be as minimal as possible. To imply these findings to the present test module, it is beneficial to reduce the size of the module to ensure minimal cell and edge spacing to yield maximum performance results.

4.1.2 Number of Busbars

During the manufacturing of mini modules, as already mentioned, laser cutter is used to obtain cells of desired shape. During the laser cutting process, it is often possible to include one or more busbars in the cell of desired size. Higher number of busbars help in lowering the ohmic losses due to increased metallization in which the charge carriers can flow. However, at the same time, higher number of busbars also reduce the active area of the module and cause shading and reflective losses [29]. The tool enables the study of the effect of these factors on the module performance and thereby implement quantified design decisions.

In the current section, firstly a study of the effect of increasing the number of busbars in the same test module for both white and black backsheets is accomplished. It must be noted that, as explained in the previous chapter, the effect of reduced recombination losses and sheet resistance with increasing busbars have not been considered.

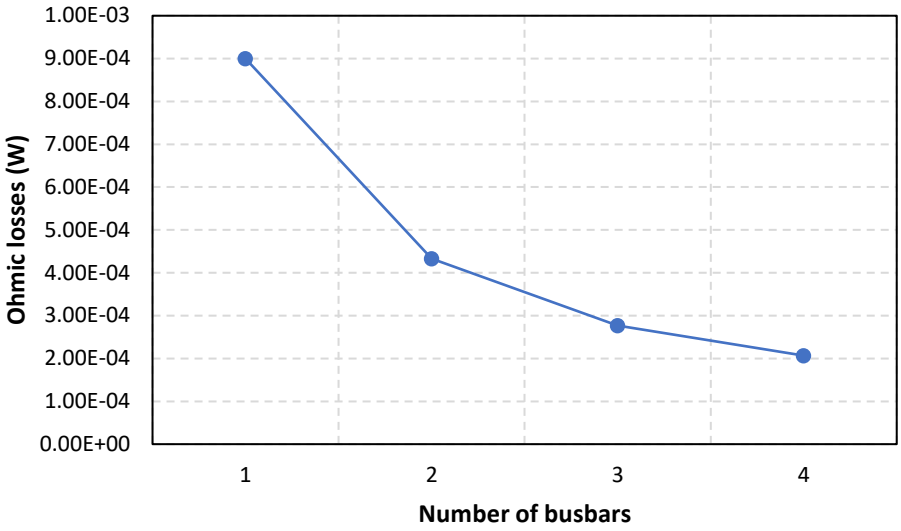

Figure 24 Ohmic losses vs number of busbars for test module with white backsheet

As is evident from Figure 24, the ohmic losses within the module decreases as the number of busbars is increased. This decrease is most substantial when busbar is increased from 1 to 2. Thereafter, the decrease in ohmic losses is less steep. This decreasing trend is attributed to the increased metallization available for the flow of charge carriers with increasing busbars.

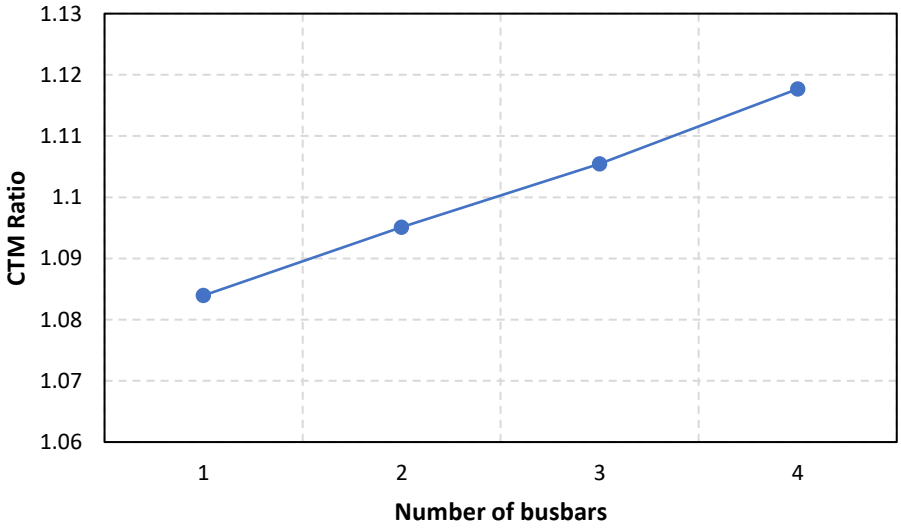

Figure 25 CTM ratio vs number of busbars for test module with white backsheet

Due to the reduced ohmic losses, as shown in Figure 25, the CTM ratio increases with an increase in the number of busbars. However, as shown in Figure 26, a contrasting trend is observed in module power despite the improved CTM ratio.

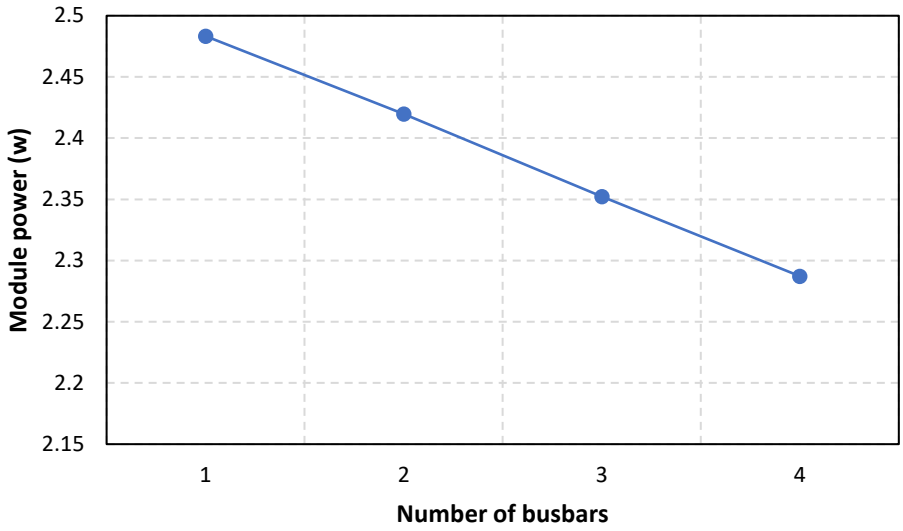

Figure 26 Module power vs number of busbars for test module with white backsheet

This contrasting trend can be attributed to the increased shading and reflection losses due to the higher number of busbars. With the increase in the number of busbars, the active area ratio of the module reduces, thereby reducing the power generating capacity of the module. The active area ratio of the module is defined hereby using equation 11 as -

$$Active\ area\ ratio = \frac{total\ surface\ area\ of\ cells - total\ surface\ area\ of\ top\ metallization}{Total\ surface\ area\ of\ the\ cells} \quad \textbf{(11)}$$

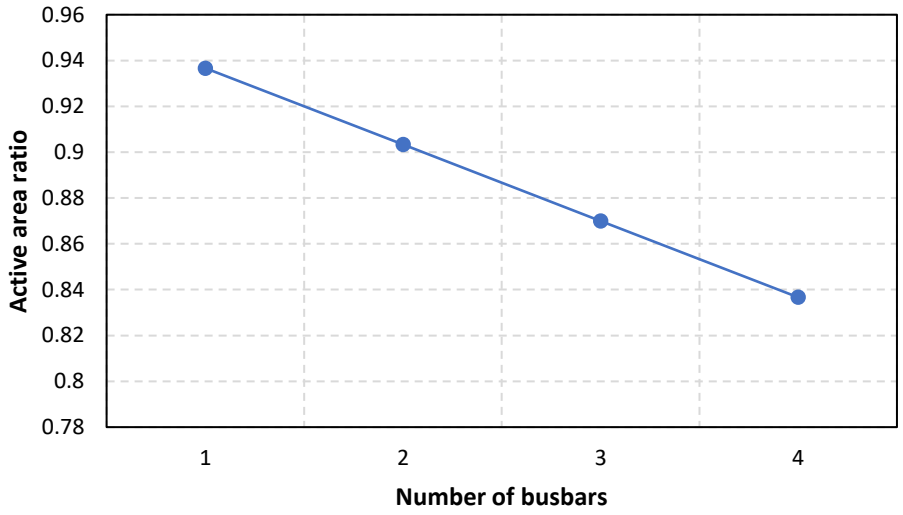

Figure 27 Active area ratio vs number of busbars for test module with white backsheet

Therefore, from the simulation results it can be observed that the effect of decreasing active area ratio by increasing the number of busbars is more dominant than the resulting reduction in ohmic losses. Hence, even though the CTM ratio improves the module power decreases with an increasing number of busbars.

In these results, the underlying assumption is that the active area ratio decreases when including more busbars in the cells. This is true for mini modules whose cells are produced by laser cutting process. However, certain manufacturing facilities can produce cells of desired size for use in mini modules by direct fabrication, thereby bypassing the laser cutting process. In such cases it is possible to implement multibusbar design philosophy without decreasing the active area ratio and sometimes even increasing the same as well [30].

This is achieved by reducing the dimensions of the busbars for an increasing number of the same. This is shown in Table 4.

Number of Busbars	Singe busbar width (µm)
1	1000
2	450
3	280
4	200

Table 4 Reducing dimensions of busbars

It is evident from Table 4 that with an increase in the number of busbars the active area ratio increases from the predecessor case. This is verified with the trend shown in Figure 28.

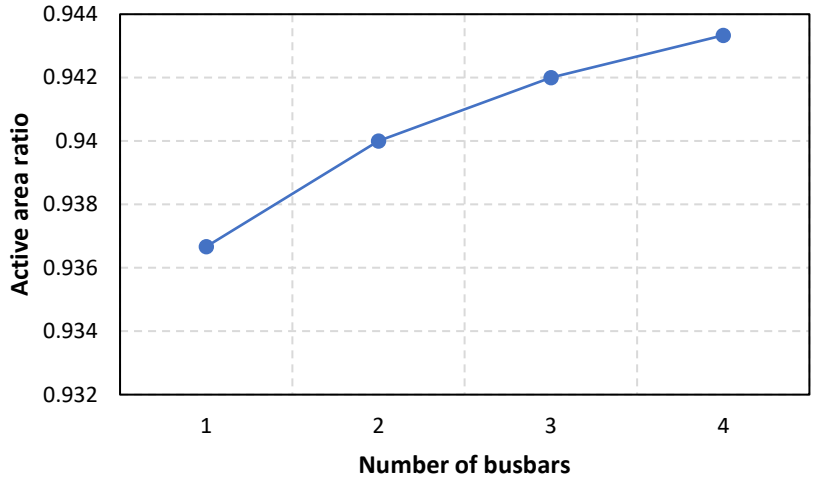

Figure 28 Active area ratio vs number of busbars for test module with white backsheet

As is evident from Figure 29, the ohmic losses increases marginally with an increasing number of busbars.

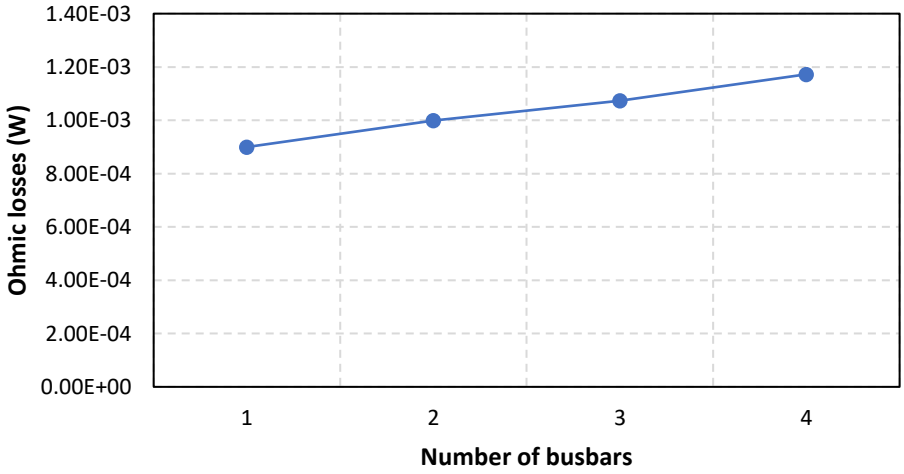

Figure 29 Ohmic losses vs number of busbars for the test module with white backsheet

The effect of an increasing active area ratio is dominant and therefore, an increasing trend in the module power output is observed as shown in Figure 30.

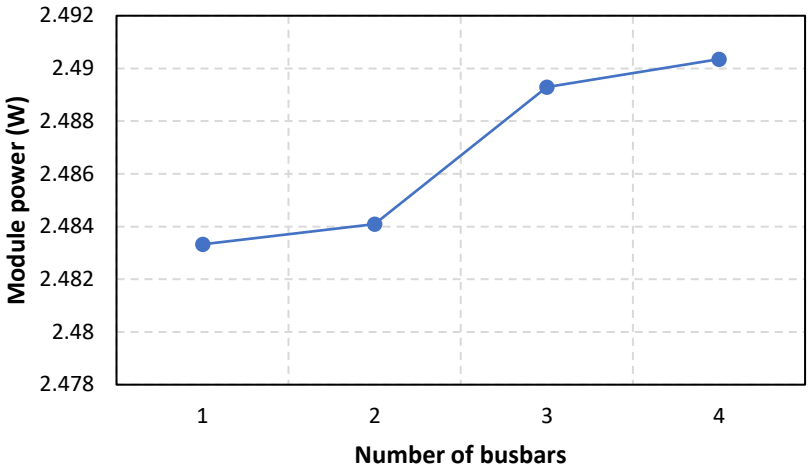

Figure 30 Module power vs number of busbars for the test module with white backsheet

All of the above observations (Figure 24 - Figure 30) listed in this section is for the test module with a white backsheet. Similar trends have been observed for the same test module but with a black backsheet. A summary of the same is shown below.

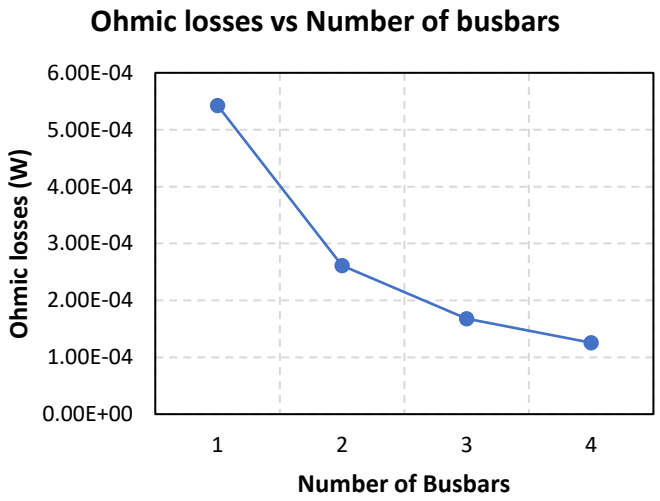

(A)

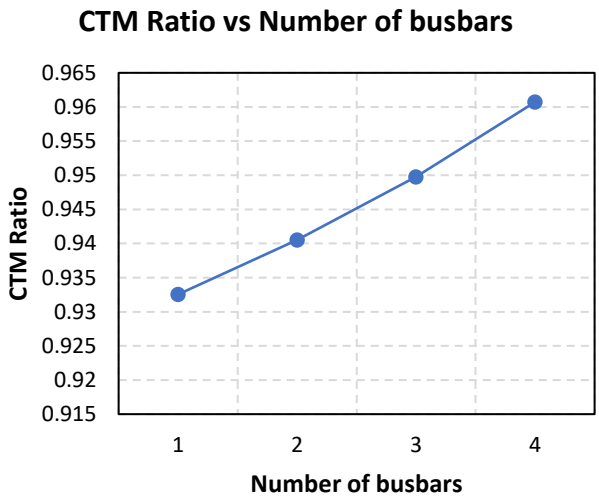

(B)

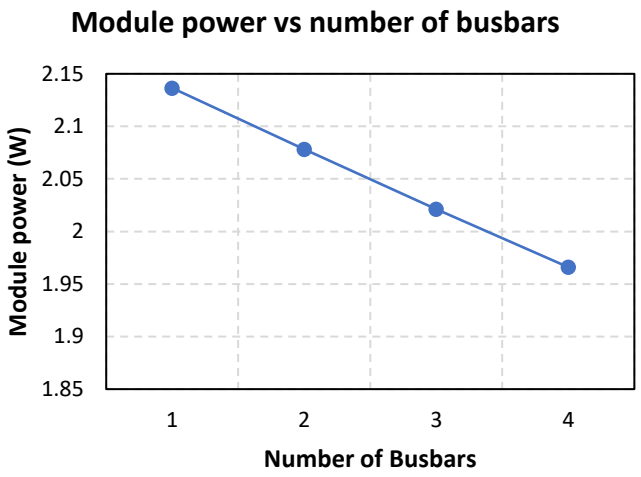

(C)

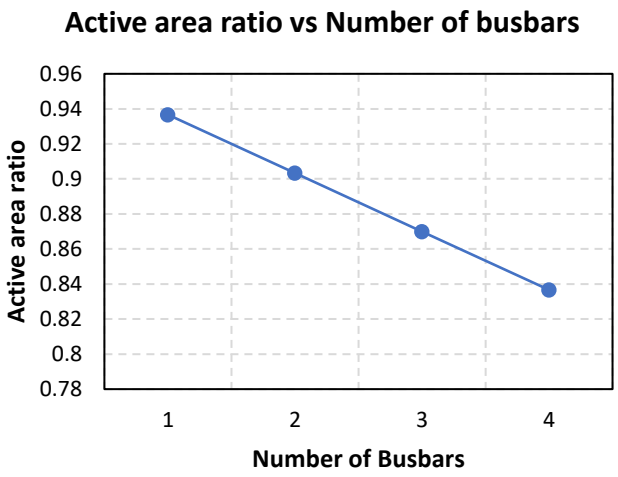

(D)

Figure 31 (A-D) Summary of varying performance trends with increasing number of busbars (reducing active area ratio) for test module with black backsheet

A similar summary is presented for the black backsheet test module for performance trends with increasing number of busbars wherein the active area ratio is increased.

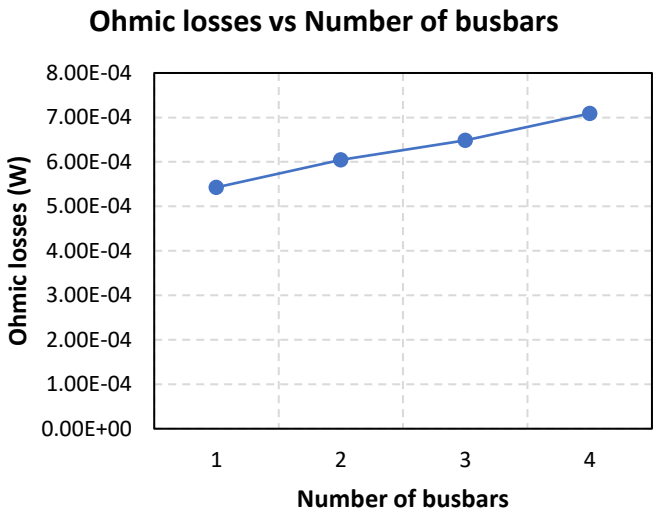

(A)

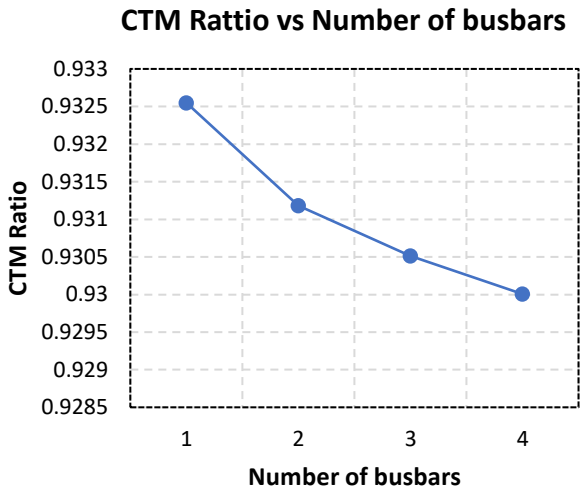

(B)

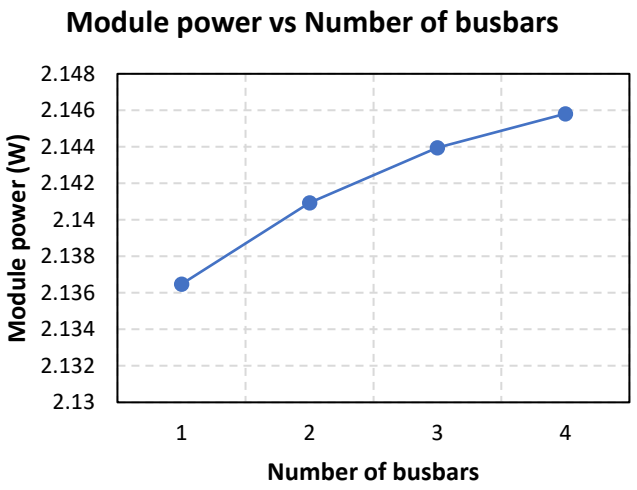

(C)

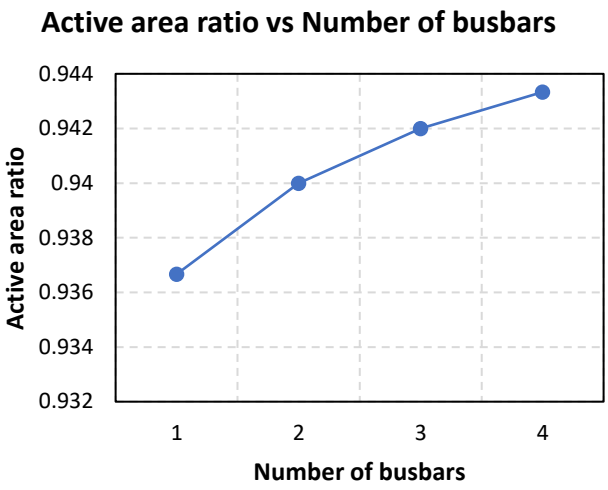

(D)

Figure 32 (A-D) Summary of varying performance trends with increasing number of busbars (increasing active area ratio) for test module with black backsheet

Therefore, from the results presented, it can be concluded that the most optimum number of busbars to include during the cell laser cutting process is 1. This holds true for both white and black backsheet test module. However, if cells are directly fabricated and it is possible to integrate more busbars, then multibusbar design is more performance compliant. Moreover, it should be noted that with higher number of busbars the Bill of Materials (BoM) can increase and the simulation results from this work can be utilized to make the most optimum design choice regarding the number of busbars.

4.1.3 Effect of cell metallization in an embedded environment

The tool provides with means to estimate the effect of cell top metallization in a module embedded environment. Without the embedding of the cell within the module, when the cells are placed in air, the loss fraction due to top metallization on the photocurrent generation can be estimated by determining the contact covered area and dividing it by total cell surface area [31], i.e. the active area ratio, as defined in equation 11. However, when the cells are placed in an embedded environment, as that of a module, the reflected light from these metallization on cell top can be redirected to the active area and contribute to the indirect optical gains.

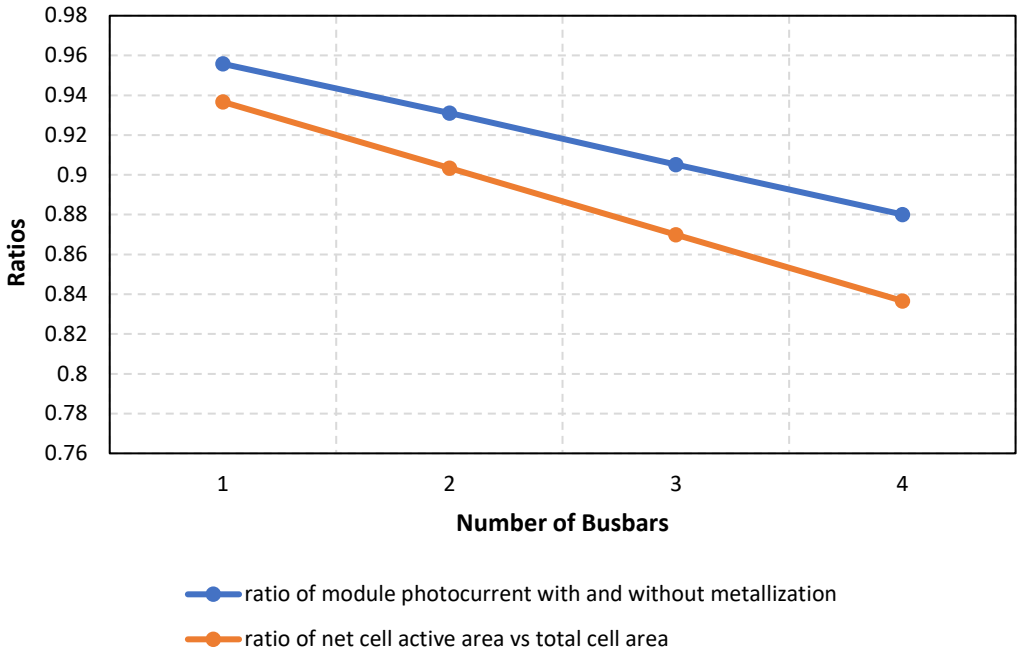

Figure 33 comparison of active area ratio and ratio of module photocurrent with vs without metallization for test module with white backsheet

From Figure 33, it is seen that the active area ratio (in 'orange') is changing with an increasing number of busbars. In an non-embedded environment, the ratio of module photocurrent with and without metallization (in 'blue') would have followed the 'orange' line. However, due to the presence of indirect optical gains, it is observed that the module photocurrent ratio of with and without metallization is always above the 'orange' curve.

Another observation, made from Figure 33, is that the difference between the two lines ('orange' and 'blue') is increasing as the number of busbars is increasing. This observation can be explained by the fact that as the top metallization increases, the amount of light rays getting reflected by them also increases. And therefore as a consequence of the embedded environment of the module, a larger number of light rays can be redirected to the active area of the cells.

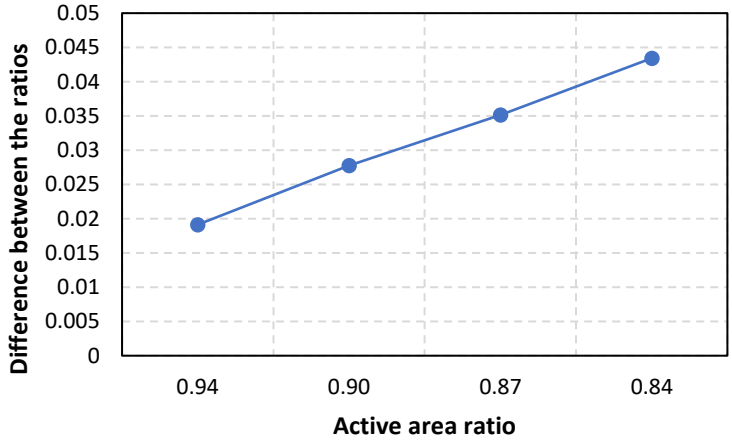

Figure 34 Difference between the ratios ('orange' and 'blue') vs the active area ratio

As is evident form Figure 34, the difference between the 'orange' and 'blue' lines, as shown in Figure 33, linearly increases with decreasing active area ratio. The tool can build a linear first degree polynomial model from the data in Figure 34. For the test module with white backsheet the following first degree polynomial model has been built (equation 12)-

$$f(x) = p1\,(x) + p2 \tag{12}$$

where for a function *f(x)*, *p1* and *p2* are the slope and ordinate intercept respectively.
Using the above coefficients, the following empirical equation can be formed-

$$p1 = -0.2408 \quad p2 = 0.2449 \tag{13}$$

$$R_P = A_C + (-0.2408 \times A_C + 0.2449) \tag{14}$$

Where, R_P is the Ratio of module photocurrent with to without metallization in an embedded environment. A_C is the ratio of net active top cell area vs total cell top area.

Therefore, using equation 14, one can predict the effect of metallization on the module photocurrent in an embedded environment. It must be noted that the above equation is only valid for module architecture of the test module. However, depending on the need, such an equation can be generated using the tool for other module architecture as well. This feature of the tool comes in handy for applications of the tool on tailored PV modules wherein creation and modelling the cell top metallization can be challenging. In such cases, with the help of such an equation for a similar module architecture helps to make the estimation of the effect of cell metallization on the photocurrent, even without actually including the metallization structure in the module model.

4.1.4 Optical balance of the module

The tool provides with means to evaluate the optical balance of the module structure. This information is useful as it gives an estimate of where the light rays are getting utilized in the module. Using this estimation one can easily identify the particular elements in the module structure which are hindering more performance output from the module and therefore focus the direction of research in optimizing that particular element in the module structure.

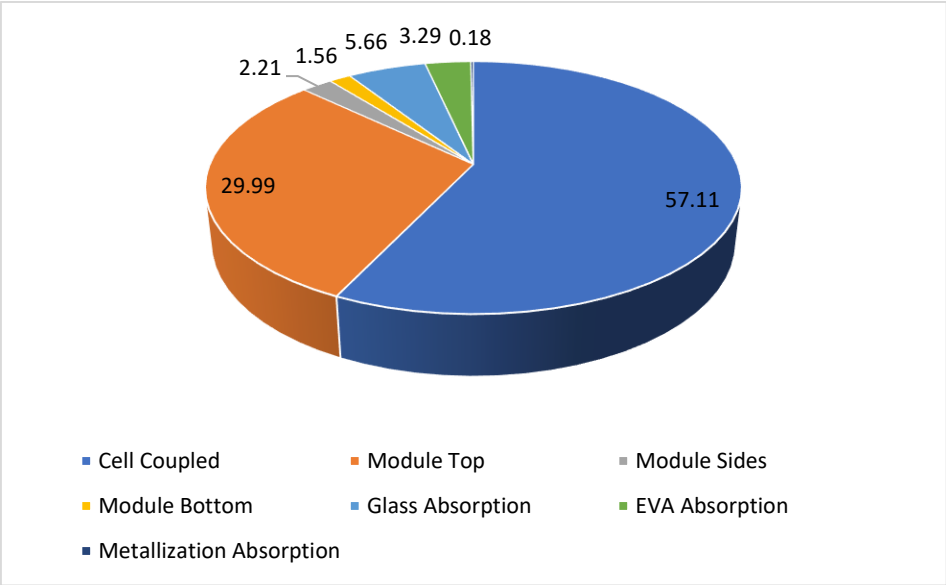

Figure 35 optical balance (%) for the test module with white backsheet

Figure 35, gives the details of the optical balance of the test module with white backsheet and, as evident, only 57.11 % of the incident light rays are coupled for photocurrent generation by the active areas of the cell. Furthermore, the plot also provides an estimation for the percentage of light rays lost from the module top, bottom and sides. The absorption of the incident rays by other module structure elements like the glass, EVA and metallization is also presented.

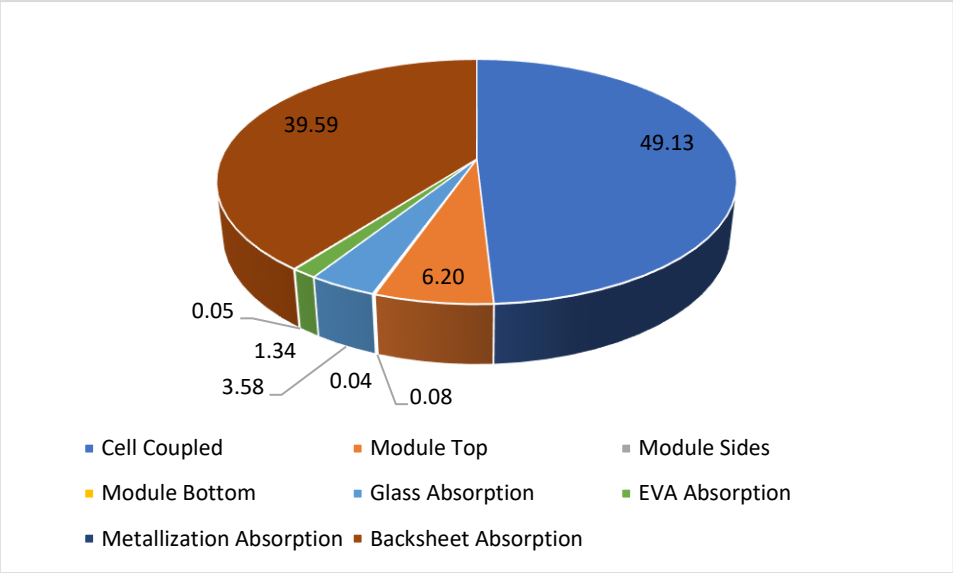

Figure 36 Optical balance (%) fort the test module with black backsheet

As is evident from Figure 36, in the black backsheet module the coupling of light rays is 49.13 % which is considerably lower than that of the white backsheet module. This can be attributed to the high absorption (39.59 %) and absence of redirection of light by the black backsheet.

4.2. Full cell vs half cut cell modules

Half cut cell modules are gaining an increasing share in the market due to their superior performance benefits as compared to their full cell counterpart.

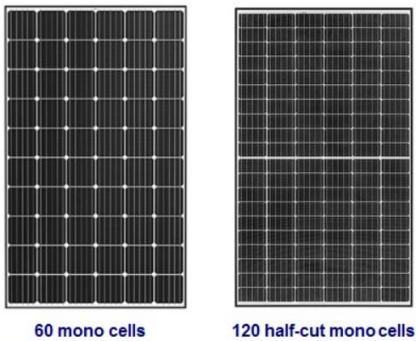

Figure 37 Schematic of half cut cells modules vs full cell modules [32]

Figure 37 illustrates a sample 60 cell mono-facial module and its 120 half cut cell counterpart. The lower current flowing in the series connected cells as well as the benefit due to the lower operating conditions result in better performance of half cut cell modules. Furthermore, these modules provide better resistance to partial shading [33].

The tool provides a platform to measure and quantify the performance gains one could expect by considering to switch to a half cut cell design methodology. To demonstrate this feature of the tool, initially a 60 cell module of cell size 15.6 cm × 15.6 cm is considered wherein number of cells in series is 10 in each string and strings in parallel is 6. The backsheet used is perfect white. Other parameters are identical to the test module earlier used. The tool is used to simulate the module with these parameters and the results are recorded. Next, we consider a half cut cell module of 120 cells with cells of size 15.6 cm × 7.8 cm. The number of cells in series of each string now is 10 and the number of strings in parallel is 12.

Now the tool is again used to perform simulation on the half cut cell module structure and the results are recorded. The tool can then present a comparison of the performance difference between the two module architectures.

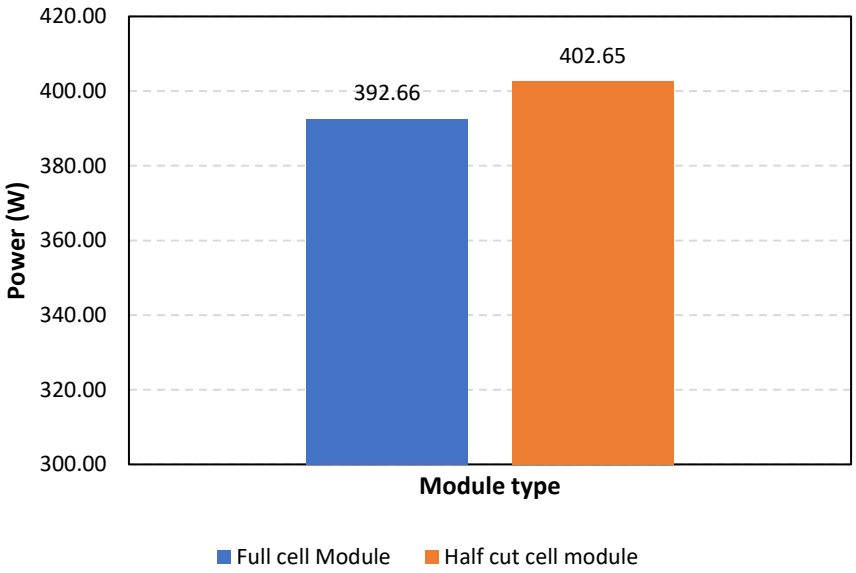

Figure 38 Module power comparison for full cell and half cut cell modules

It is evident from Figure 38 that by using a half cut cell module architecture, a power gain of around 2.5 % is achievable. This power gain can be attributed to various factors as described hereunder.

Firstly, ohmic losses in both the modules is considered.

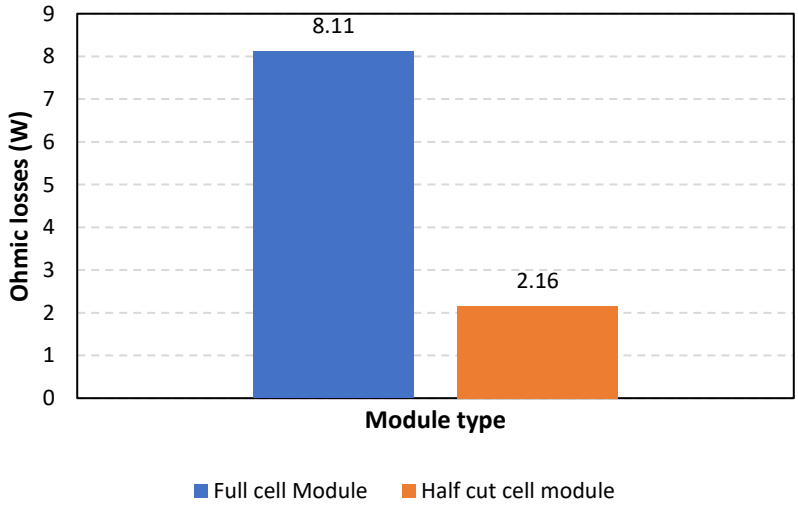

Figure 39 Ohmic losses comparison for full cell and half cut cell modules

It is evident from Figure 39, by switching to the half cut cell structure, the ohmic losses are reduced from 8.11 W to 2.16 W. This reduction is due to the reduce current production from the individual cells which results in a lower ohmic loss dissipation in the series interconnecting tabs.

Furthermore, existing literature [34] suggests that, in half cut cell modules, a larger cell gap area is present to accommodate the extra cells and therefore the module size marginally increases. This increase in the cell gap area aids the light redirection from the backsheet and therefore also increases the indirect optical gains. This is reflected in the photocurrent densities of the two modules as shown in Figure 40.

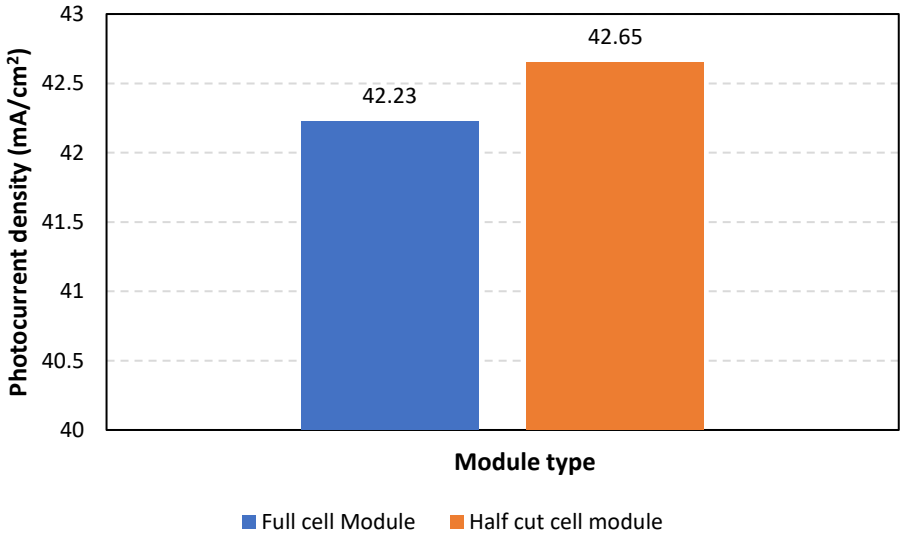

Figure 40 Photocurrent density comparison for full cell and half cut cell modules

It must be noted that the photocurrent density, mentioned in the Figure 40, is defined with respect to the total cell area in the module.

Finally the CTM can be compared for the two module structures as shown in Figure 41.

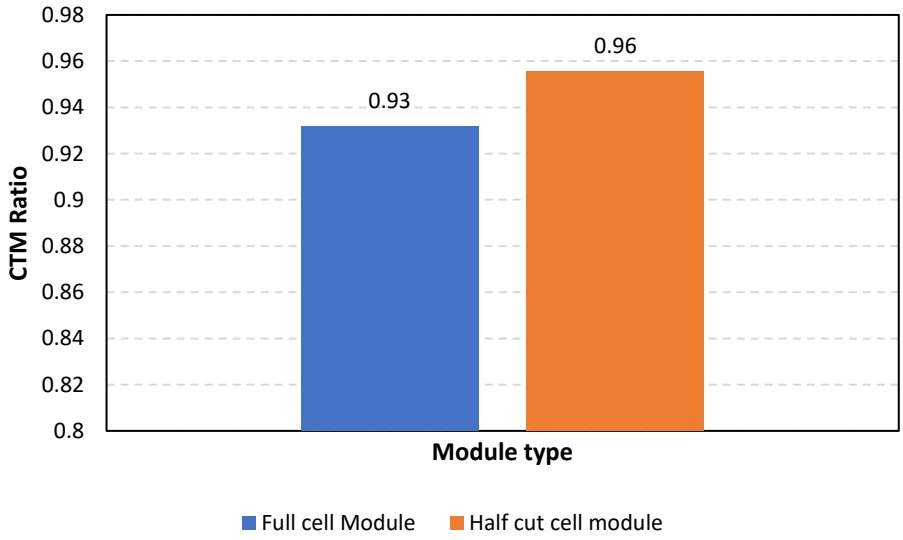

Figure 41 CTM ratio comparison for full cell and half cut cell modules

From Figure 41 it is evident that a CTM gain of 3.23 % is achieved by switching to the half-cell module structure owing to the reduced ohmic losses and the increased indirect optical gains caused by redirection of light by the backsheet.

4.3. Glass-Glass modules

In the recent years double glass modules have shown to be a market competitor owing to features such as superior weather resistance and aesthetic appeal [35]. Furthermore, their ability to transmit light through them enables their application in Building Integrated Photovoltaics (BIPV) as they can aid in natural indoor illumination when used as a façade.

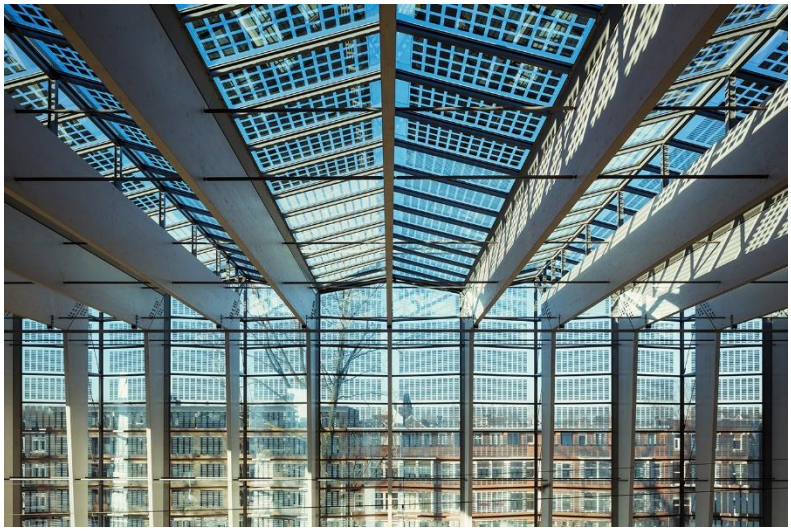

Figure 42 Rotterdam central station equipped with glass-glass modules [36]

Figure 42 shows the solar roof used at the Rotterdam central station. These roofs implement glass-glass modules as they enable light transmission which can be used for natural illumination. The tool developed in this work is also equipped to perform analysis on such modules and thereby helping to make better design decisions for these modules.

The test glass-glass module used for demonstrating the efficacy of the tool is identical and comprises of mono-facial cells, as described in the previous sections, with the exception that instead of the backsheet a glass layer of 4 mm, as shown in Figure 43, is used.

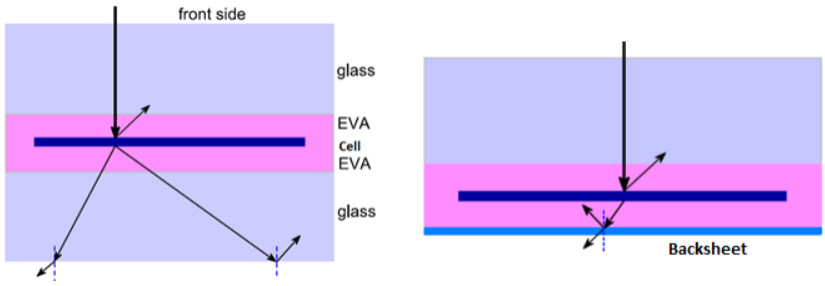

Figure 43 Module with glass vs backsheet as bottom layer [37]

The backsheet acts as a scattering media and much of the light gets redirected towards the cell. In case of glass-glass modules, some light is reflected back towards the cells and the rest is transmitted through the module structure.

4.3.1 Cell-cell and edge-cell spacing

As already explained in the previous section of PV mini modules, in the current section the effect of varying cell to cell and edge spacing on the performance of the glass-glass module is demonstrated.

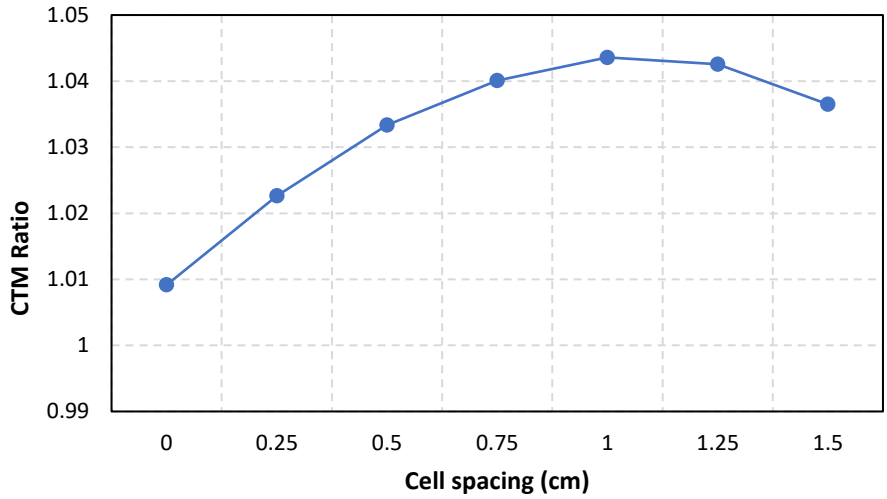

Figure 44 CTM ratio v s cell spacing for the test glass-glass module

As shown in Figure 44, the trend in the CTM ratio with a decreasing edge-cell spacing and simultaneously increasing cell-cell spacing is similar to that of the test module with white backsheet. The noticeable difference between the two being the amount of variation in the CTM ratio. In the test glass-glass module, the CTM ratio is varying only by 3.3% as compared to the 5.53 % variation in the test module with white backsheet. This can be explained by the limited redirection of light by a glass base as compared to a widespread redirection achieved by a white backsheet. Therefore, there is only a limited amount of redirected light that can be coupled by varying the cell and edge spacing to the cell active area for photocurrent generation.

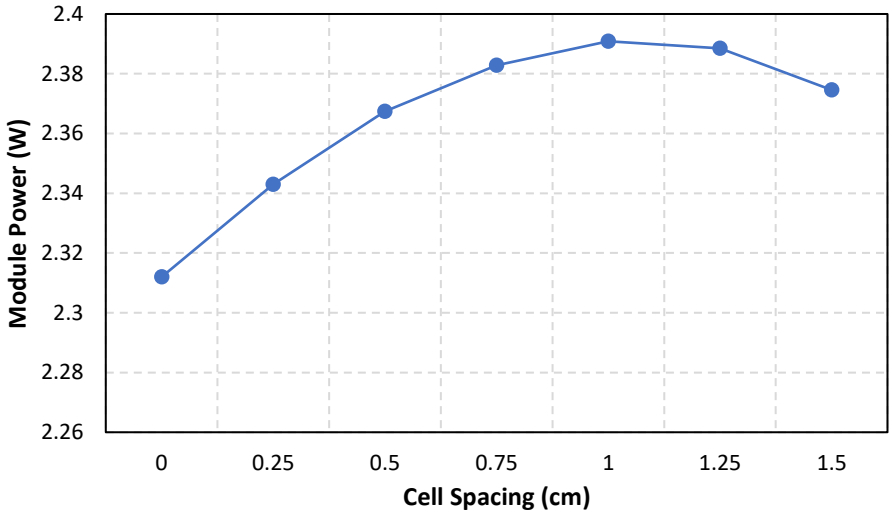

Figure 45 Module power vs cell spacing for test glass-glass module

Figure 45 illustrates the variation of module power with varying cell spacing. As is evident, the module power follows the CTM ratio trend as shown in Figure 44. The saturation point, as discussed earlier, is reached at around 1 cm, resulting in it being the most optimum cell spacing parameter. Corresponding edge-

cell distance is 0.5 cm. Furthermore, the maximum power generation for the test glass-glass module is 2.39 W as compared to 2.48 W of the white backsheet module. This is again due to the lower indirect optical gains arising due to the glass base.

4.3.2 Light transmittance

With glass-glass modules, another important consideration is the light transmittance through the module which might be helpful for purposes like natural illumination. The tool provides the framework for performing simulations to find the same. Firstly, the transmittance, defined here as the percentage of light passing through the module layers and emerging out of the module at the rear end, variation with reference to the cell spacing is recorded.

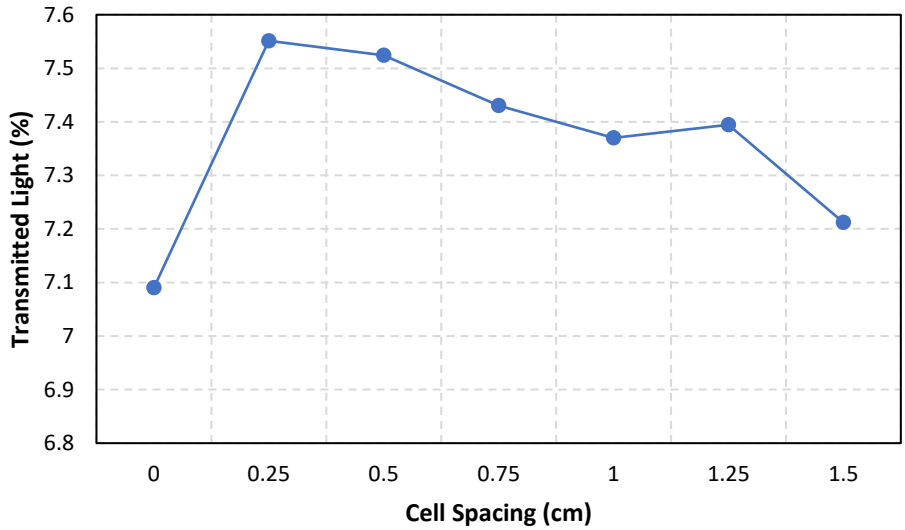

Figure 46 Transmission (%) of light for the test glass-glass module

As seen in Figure 46, as the cell spacing starts increasing (simultaneous decrease of edge-cell spacing), initially the transmitted light increases. This is due to the fact that amount of light which can now go through the inter cell spacing increases and overcompensates for the reduction of light passing through the edges. But after a point (around 0.25 cm), the decrease in the transmitted light through the edges due to reducing edge-spacing becomes dominating and cannot be compensated with any further increase in the cell-cell spacing.

Therefore, as indicated by the simulation results, for the most power producing module design choice, the optimum cell spacing is around 1 cm. However, a trade-off can be made in the power production by selecting a different cell spacing if marginal boost in transmittance is required.

Often, in building architecture designing, a fixed value of light is required to be transmitted by a façade for the purpose of better natural illumination. Using the tool, the module size required to achieve a target transmission (%) value can be attained.

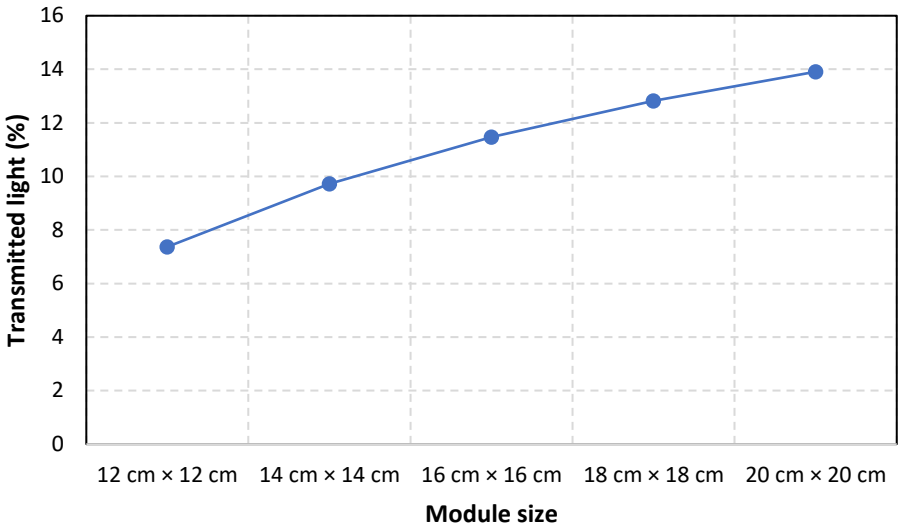

Figure 47 Transmitted light (%) vs module size for the test glass-glass module

Figure 47 shows the increase in the transmitted light trough the module with the increase in the module dimensions. In the given simulation the desired target transmission of light was 14% and the results show that, for the test module, an increase in the dimensions to 20 cm × 20 cm is required to achieve it. It would again be a trade-off between whether to increase the module dimensions and keep cell number and cell dimensions the same to achieve the target transmission or rather let go of the target transmittance and maximize the power output of the module by incorporating more cells.

However, there is also some performance gain when the module size is increased to meet the target transmission of light.

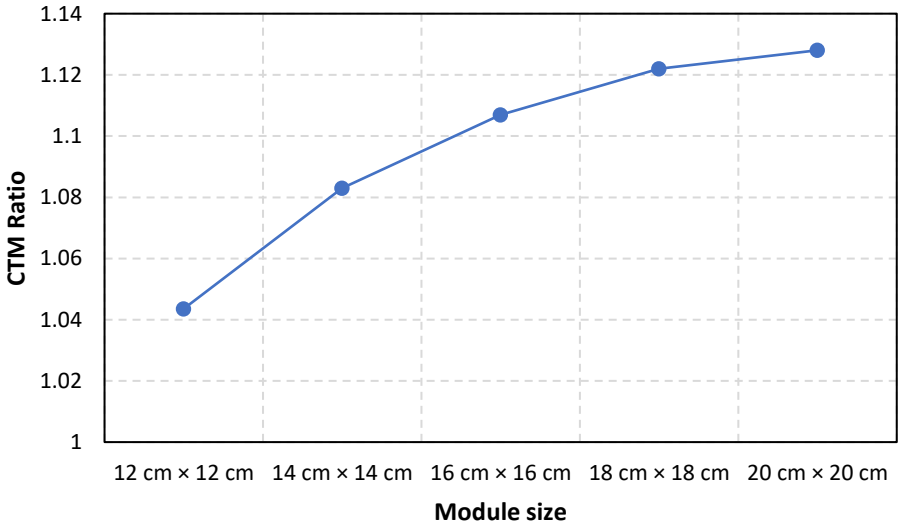

Figure 48 CTM ratio vs module size for the test glass-glass module

As can be observed in Figure 48, by increasing the module size we obtain a gain in the CTM ratio. This is due to the fact that the indirect gains arising due to the redirection of light to the active area increases by using a larger bottom glass layer. However, the trend is seen to be approaching saturation and after a certain point, not much gain be derived despite increasing the module size.
It must be noted, that for each increasing module size, again an optimization for cell and edge spacing can be performed using the tool to derive at the most optimum tuning for the module.

4.4. Triangular (tailored) PV module

One of the primary objectives of this thesis work is to develop a tool for CTM ratio estimation and optimization for tailored PV modules. As per Arturo's work mentioned in [10], conventional CTM ratio estimation algorithms are not much suitable for estimation of CTM ratio of tailored PV modules and therefore a different algorithm needs to be developed for higher accuracy. This tool provides such an algorithm as has been explained in the previous chapters.

Tailored PV modules have been gaining importance in the urban PV share due to its better integrability and aesthetics [38]. In this section, the efficacy of the tool to model and simulate triangular modules as an example for tailored PV modules is demonstrated. Triangular modules have been chosen as they provide high modularity in developing other module shapes using them. For example, consider a complex shape as shown in Figure 49.

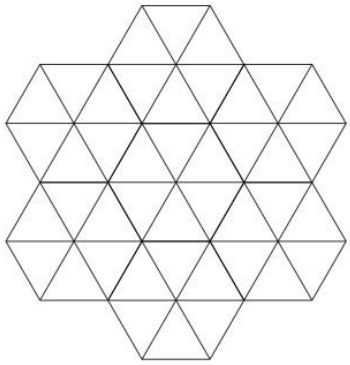

Figure 49 Complex shapes made using triangular blocks [39]

It is evident from Figure 49 that triangular modules can be clubbed to form a variety of other shapes to suit the desired application. Therefore, the developed tool is used and customarily modified to automatically model and simulate triangular modules of desired characteristics. The modified code is attached in the Appendix for reference. It must be noted that depending upon the application the tool can also be modified to enable such automatic modelling and simulation of other module shapes as well.

For demonstrating the tool's application for triangular modules, the same test module as the previous cases is used. However, now in the shape of a triangle as shown in Figure 14. The following parameters, as shown in Table 5, are however different from the test module.

Sl. No.	Parameter	Value
1	Length of the equilateral module edge	10 cm
2	Number of cells in the base row of the module	5
3	Length of the equilateral triangle cell edge	3 cm

Table 5 Triangular module parameters

The simulations are run for both white and black backsheets to compare the difference in the performance.

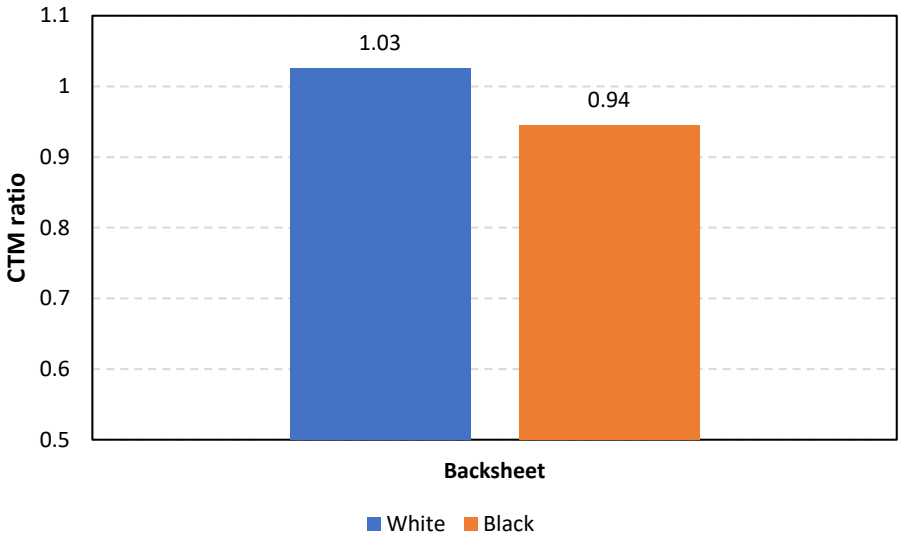

Figure 50 Comparison of performance (CTM Ratio) of triangular module with white and black backsheets

As is evident from Figure 50, the module with the white backsheet outperforms the one with a the black backsheet by around 9 % absolute. Furthermore, the tool also provides an estimate of the power production potential for the above-mentioned triangular modules.

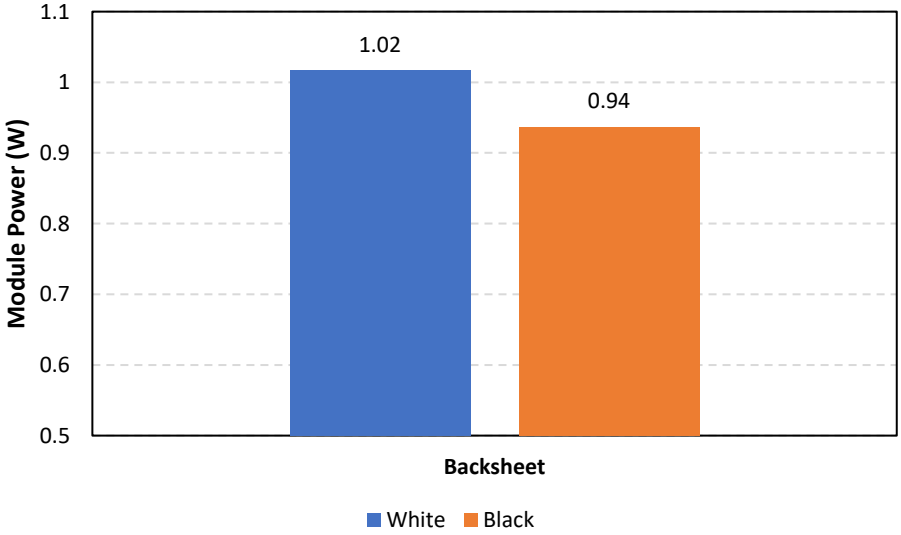

Figure 51 Comparison of performance (Module Power) of triangular module with white and black backsheets

The power production of the white backsheet triangular module is higher as compared to the black backsheet owing to the higher indirect optical gains arising from the widespread scattering caused by the white backsheet.

In this chapter the applicability of the tool for various module types namely, mini modules, half cut cell modules, glass-glass modules and triangular modules was demonstrated. Furthermore, quantification of performance of these modules was achieved. Lastly, the tool was able to identify various performance trends with varying parameters to arrive at optimized design for the different module types.

5. Conclusions and future recommendations

Through the work in this thesis, a tool, which can automatically model and simulate various module architectures and obtain the target performance metric i.e. the CTM ratio along with other performance indicators like the various losses, power production, optical balance, gains, etc., has been developed. The tool aims to help make the user take informed design choices for producing various types of modules.

The tool is based on the development of a code for automatic creation of vertices in three-dimensional space and thereafter programmed selection of the vertices to build desired module surfaces. The surfaces can further be defined with the relevant optical characteristics. Ray tracing has been successfully implemented on the developed module structure and optical performance are measured. Furthermore, an electrical loss calculation model has been developed using the differential element method. With the knowledge of the electrical losses and the optical performance of the module structure the tool successfully yielded the CTM ratio and other performance indicators. Furthermore, it is possible to optimize various parameters of the module using parameter sweeping.

As a demonstration of the developed tool's features, the tool has been to perform analysis on a test PV mini module. Thereafter, an analysis has been carried out for both white and black backsheet mini module. The target optimization parameters being cell placement within the module and number of busbars to be included during the cell cutting process.

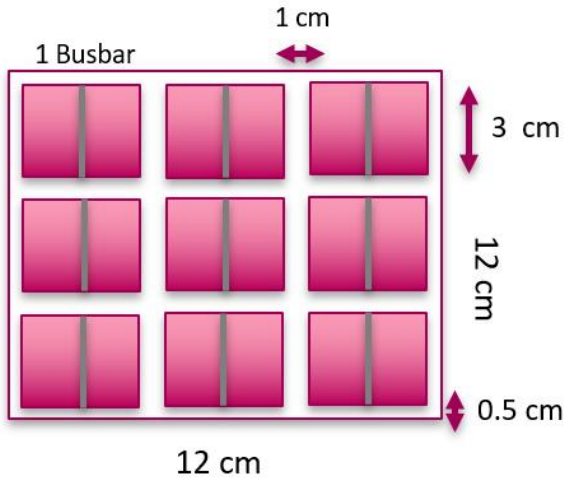

Figure 52 Optimized test mini module with white backsheet

As illustrated from Figure 52, the most optimum cell-spacing for the test module has been found to be 1 cm with corresponding edge-cell distance of 0.5 cm. Furthermore, the CTM ratio for the above shown optimized module is 1.084, thereby achieving around 5.52 % relative gain compared to the worst-case design of the above module by using the tool. The power production capacity for the optimized module is found to be 2.48 W. Furthermore, the best performance has been observed for a single busbar design. As compared to, for example, a 4-busbar design, the test module shows around 7.89 % higher power production when a single busbar is used. However, if the mini-cells are being fabricated instead of being laser cut, and there is a possibility to integrate more busbars onto it in such a way so as to increase the active area ratio upon each

bus bar added, the results are opposite. Around 0.28 % (relative) better performance is observed for the 4-busbar design as compared to a single busbar design.

A similar analysis has been performed for the test mini module with black backsheet. The final optimized module layout is shown in Figure 53.

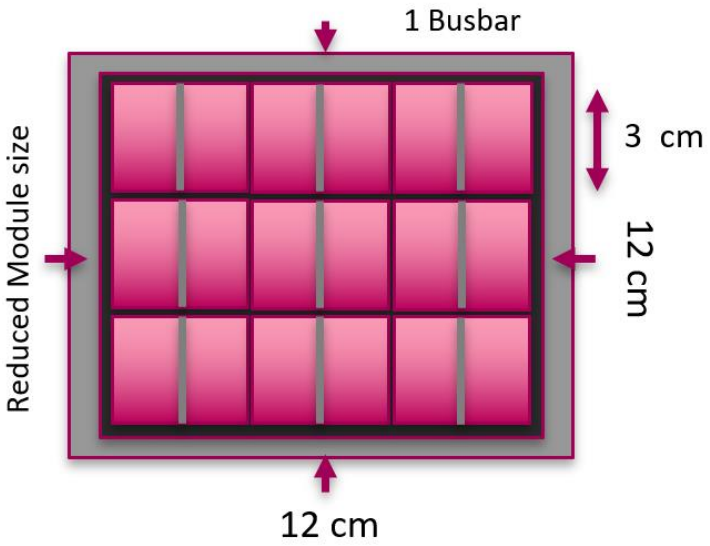

Figure 53 Optimized test mini module with black backsheet

Simulation results reveal that for the black backsheet nodule, the cell spacing should be kept as small as possible. Furthermore, it has been observed that, due to the slightly higher (around 0.12 %) light ray density around the edges, the cells must be placed as close as possible to the module edge to utilize these light rays. Therefore, as shown in Figure 53, it is recommended to reduce the module size. The CTM ratio and the power production capacity of the optimized module is found to be 0.933 and 2.14 W respectively. Similar trends as that of the white backsheet has been observed regarding the number of busbars. When mini-cells are produced by laser cutting then a single busbar design is recommended (7.96% higher power production than 4 busbar design), whereas, for mini-cells directly fabricated, a multibusbar design shows better power production performance (0.46 % higher than single busbar). Overall a black backsheet module, optimized using the tool, shows around 0.285 % increase in power production capacity.

When compared, the white backsheet module's power production capacity is found to outperform the black backsheet module by around 13.93 %. This difference is mainly attributed to the reduced indirect optical gains when using the non-scattering black backsheet.

Furthermore, the tool is also able to derive novel empirical formulas which, depending upon the module architecture, estimate the effect of the cell top metallization on the cell photocurrent generation capacity.

Secondly, the tool is used to model and simulate a standard 60 cell mono-facial module and obtain its performance metrics. Furthermore, the tool has been used to simulate the performance of a 120-half cut cell module, modelled from its 60-cell counterpart, to perform a comparative study. The power production capacity of the 60-cell module is found to be 392.66 W with a CTM ratio of 0.932. On the other hand, the corresponding half cut cell module gives a power production capacity of 402.65 W with a CTM ratio of 0.96. Therefore, the half-cut cell module proves to have a 2.48 % boost in power production capacity and 2.91 % gain in CTM ratio. Simulation results reveal that these gains are primarily caused due to the reduced ohmic losses and extra indirect optical gains owing to the increased exposure of the backsheet because of higher net cell spacing.

Thirdly, glass-glass modules are modelled and optimized based on application needs. The optimized cell spacing for the test glass-glass module is found to be 1 cm with a corresponding edge to cell distance of 0.5 cm. However, the transmission (%) of light through the module shows very little variation with the change in the cell spacing. The highest transmission (%) is found to be 7.55% at 0.25 cm cell spacing whereas the lowest transmission (%) of 7.09 % has been observed at no cell spacing. Furthermore, for achieving a target transmission (%) of 14 % the tool indicates that an increase in the module size to 20 cm × 20 cm is required. The power production capacity and the CTM ratio for the test glass-glass module is found to be 2.39 W and 1.04 respectively.

In summary, for the same test module with different backsheets, the white backsheet module is found to outperform both glass-glass and black backsheet module. The glass-glass test module, owing to higher indirect optical gains shows better performance than that of the black backsheet counterpart.

Lastly, the efficacy of the tool is demonstrated for a test tailored (triangular) PV module. The triangular module has been modelled and simulated for both white and black backsheets. The white backsheet module shows a CTM ratio of 1.03 and a power production capacity of 1.02 W. The black backsheet, however, underperforms as compared to the white backsheet by showing a CTM ratio of 0.94 and a power production capacity of 0.937 W.

The developed tool is able to successfully accomplish the objectives set forth in chapter 1 and thereafter show its efficacy upon application to various module architectures. However, there are still room for certain improvements which can be implemented to further enhance the tool's capability to be applicable in more diverse applications. These recommendations are listed hereunder-

- The tool has been designed to produce results under STC, and therefore, taking into considerations the field exposure is not possible. However, taking the work done by the authors in [6] and [40], it would be possible to take into consideration the field exposure effects on the CTM analysis. It must be noted that to undertake such considerations into the modelling, it is required to switch to the energy domain in contrast to the power domain as implemented in this work.

- The tool also finds its application for bifacial module study. Though not explored within the scope of this work, implementing bifacial module study using the developed tool is conceivable. However, due to current void in the uniformity of industry standards for characterization and testing of bifacial modules, it may be challenging to adopt the correct and suitable standard. The tool's flexibility to designate optical properties to surfaces makes it simple to convert a mono-facial cell into a bi-facial cell. Furthermore, another emitting surface at the bottom of the module can be created to take into considerations the light incident on the rear end of the module. These light sources can be programmed to take into consideration the albedo coefficients of the environment for better accuracy. Presently, most of the PV industry uses a fixed illumination source, both at the top and at the bottom of the bifacial module, for the purpose of characterizing the module. This method can also be implemented readily, using the tool, to simulate the performance of the bifacial module.

- The usage of LUX limits the tool to create the module surfaces with a minimum of three and a maximum of four vertices. Though this is sufficient for most module architectures, certain complex tailored PV modules can be better modelled without the given limitation. Modifications in the algorithm of LUX to accommodate higher number of vertices for defining a surface can effectively enhance the tools applicability in a wider assortment of tailored PV modules.

- In this work, perfect absorbers have been used as a replacement of solar cells to provide an estimation of the performance potential of a particular module design. However, if certain applications require the optical properties of actual solar cells in order to achieve the actual performance and not the performance potential, required changes in the optical properties can be made effortlessly in the tool. However, the

creation of front surface textures of the cells, though possible to create using the tool, possess limitation of impractically high computation times. To mitigate this, a viable option can be to build libraries for the textures and use them according to the application instead of creating them upon every simulation.

6. References

[1] A. Zahedi, “Solar photovoltaic (PV) energy; latest developments in the building integrated and hybrid PV systems.,” *Renewable Energy,*, vol. 31, no. 5, pp. 711-718, 2006.

[2] C. Peike, I. Hädrich, K. Weiß and I. Dürr, “Overview of PV module encapsulation materials,” *Photovoltaics International,* vol. 19, pp. 85-92, 2013.

[3] “https://blog.ibc-solar.com/,” ibc-solar, 09 2018. [Online]. Available: https://blog.ibc-solar.com/2018/09/new-module-technologies-lhs-half-cut-mbb/. [Accessed 25 04 2020].

[4] I. Haedrich, I. Surve and A. Thomson, “Cell to module (CTM) ratios for varying industrial cell types,” *Asia Pacific Solar Research Conference,* pp. 1-6, 2015.

[5] H. Schulte-Huxel, R. Witteck, H. Holst, M. Vogt, S. Blankemeyer, D. Hinken, T. Brendemühl, T. Dullweber, K. Bothe, M. Köntges and R. Brendel, “High-efficiency modules with passivated emitter and rear solar cells—an analysis of electrical and optical losses,” *IEEE Journal of Photovoltaics,* vol. 7, no. 1, pp. 25-31, 2016.

[6] I. Haedrich, D. Jordan and M. Ernst, “Methodology to predict annual yield losses and gains caused by solar module design and materials under field exposure,” *Solar Energy Materials and Solar Cells,* vol. 202, p. 110069, 2019.

[7] H. Hanifi, C. Pfau, D. Dassler, J. Schneider, S. Schindler, M. Turek and J. Bagdahn, “Investigation of cell-to-module (CTM) ratios of PV modules by analysis of loss and gain mechanisms,” *Photovolt. Int,* vol. 32, pp. 89-99, 2016.

[8] I. Haedrich, U. Eitner, M. Wiese and H. Wirth, “Unified methodology for determining CTM ratios: Systematic prediction of module power,” *Solar energy materials and solar cells,* vol. 131, pp. 14-23, 2014.

[9] O. Dupré, J. Levrat, J. Champliaud, M. Despeisse, M. Boccard and C. Ballif, “Reassessment of cell to module gains and losses: Accounting for the current boost specific to cells located on the edges,” 2018.

[10] V. A. M. Lopez, “Enhancing Solar Energy Integration with Innovative Mini-modules,” Delft University of Technology, Delft, 2019.

[11] R. Santbergen, *LUX published with MATLAB® R2013b for PVMD research group. TU Delft,* Delft.

[12] D. Amans, S. Callard, A. Gagnaire, J. Joseph, G. Ledoux and F. Huisken, “Ellipsometric study of silicon nanocrystal optical constants,” *Journal of Applied Physics,* vol. 93, no. 7, pp. 4173-4179, 2003.

[13] C. Honsberg and S. Bowden, “pveducation.org,” 2019. [Online]. Available: https://www.pveducation.org/pvcdrom/design-of-silicon-cells/surface-texturing. [Accessed 10 05 2020].

[14] NREL, “nrel.gov,” [Online]. Available: https://rredc.nrel.gov/solar//spectra/am1.5/. [Accessed 10 05 2020].

[15] S. N. Laboratories, “PV Performance Modelling Collaborative,” [Online]. Available: https://pvpmc.sandia.gov/modeling-steps/2-dc-module-iv/effective-irradiance/spectral-response/. [Accessed 11 05 2020].

[16] “Lake Photonics,” [Online]. Available: https://www.lake-photonics.com/en/materials/. [Accessed 12 05 2020].

[17] “PV Lighthouse: SunSolve™,” PV Lighthouse, [Online]. Available: https://www.pvlighthouse.com.au/sunsolve. [Accessed 12 05 2020].

[18] A. Pfreundt, M. Mittag, M. Heinrich and U. Eitner, “Rapid calculation of the backsheet coupling gain using ray groups,” in *32nd European Photovoltaic Solar Energy Conference and Exhibition (EUPVSEC)*, 2018.

[19] M. Zarmai, N. Ekere, C. Oduoza and E. Amalu, “A review of interconnection technologies for improved crystalline silicon solar cell photovoltaic module assembly,” *Applied energy ,* vol. 154, pp. 173-182, 2015.

[20] V. Gazuz and C. Buerhop, “Detection of power losses in busbar solder contacts by electroluminescence imaging of solar cells,” *Measurement Science and Technology,* vol. 22, no. 11, p. 115702, 2011.

[21] “AZO Materials-Sample Preparation and Microstructural Analysis of Solar Cells,” [Online]. Available: https://www.azom.com/article.aspx?ArticleID=5768. [Accessed 4 7 2020].

[22] “Lasergraaf NL-Wat is een fiber laser nu precies,” [Online]. Available: https://lasergraaf.nl/archief/wat-is-een-fiber-laser-nu-precies/. [Accessed 05 07 2020].

[23] S. Villa, “Colored PV modules based on Interference Filters,” *Master of Science, TU Delft ,* 2018.

[24] P. Ortega, S. Bermejo and L. Castaner, “High voltage photovoltaic mini-modules,” *Progress in Photovoltaics: Research and Applications,* vol. 16, no. 5, pp. 369-377, 2008.

[25] M. Köntges, H. Schulte-Huxel, S. Blankemeyer, M. Vogt, H. Holst and R. Reineke-Koch, “Measuring the light recovery factor of backsheets in photovoltaic modules,” *Solar Energy Materials and Solar Cells,* vol. 186, pp. 175-183, 2018.

[26] “PVEducation.com,” [Online]. Available: https://pveducation.com/solar-concepts/solar-pv-module-efficiency/. [Accessed 11 07 2020].

[27] G. Makrides, M. Theristis, J. Bratcher, J. Pratt and G. Georghiou, “Five-year performance and reliability analysis of monocrystalline photovoltaic modules with different backsheet materials,” *Solar Energy,* vol. 171, pp. 491-499, 2018.

[28] I. E. Agency, “Review of Failures of Photovoltaic Modules,” 2014.

[29] A. Qayoom, A. Qadir and Q. Ali, “The effects of metallization of busbars on the performance of PV CELL,” *J Clean Energy Technol,* vol. 7, no. 1, pp. 7-10, 2019.

[30] S. Braun, G. Hahn, R. Nissler, C. Pönisch and D. Habermann, “Multi-busbar solar cells and modules: high efficiencies and low silver consumption,” *Energy Procedia,* vol. 38, pp. 334-339, 2013.

[31] A. Mette, “New Concepts for Front Side Metallization of Industrial Silicon Solar Cells-Fraunhofer-Institut für Solare Energiesysteme,” 2007.

[32] J. Svarc, “cleanenergyreviews,” 12 February 2020. [Online]. Available: https://www.cleanenergyreviews.info/blog/2017/9/11/best-solar-panels-top-modules-review. [Accessed 21 07 2020].

[33] J. Qian, A. Thomson, A. Blakers and M. Ernst, “Comparison of half-cell and full-cell module hotspot-induced temperature by simulation,” *IEEE Journal of Photovoltaics,* vol. 8, no. 3, pp. 834-839, 2018.

[34] M. Mittag, A. Pfreundt, J. Shahid, N. Wöhrle and D. Neuhaus, “Techno-Economic Analysis of Half Cell Modules: The Impact of Half Cells on Module Power and Costs,” in *36th European Photovoltaic Solar Energy Conference and Exhibition (EU PVSEC),* 2019.

[35] J. Tang, C. Ju, R. Lv, J. Chen, X. Zeng, D. Fu, J. Jaubert and T. Xu, “The performance of double glass photovoltaic modules under composite test conditions.,” *Energy Procedia,* vol. 130, pp. 87-93, 2017.

[36] mvsa-architects, [Online]. Available: https://mvsa-architects.com/project/projects-rotterdam-central-station-transportation-logistics/. [Accessed 23 07 2020].

[37] J. Singh, S. Guo, I. Peters, A. Aberle and T. Walsh, “Comparison of glass/glass and glass/backsheet PV modules using bifacial silicon solar cells,” *IEEE Journal of Photovoltaics,* vol. 5, no. 3, pp. 783-791, 2015.

[38] N. Adamovic, A. Zimmermann, A. Caviasca, R. Harboe and F. Ibanez, “Custom designed photovoltaic modules for PIPV and BIPV applications,” *Journal of Renewable and Sustainable Energy,* vol. 9, no. 2, p. 021202, 2017.

[39] “illustrativemathematics,” [Online]. Available: https://tasks.illustrativemathematics.org/content-standards/tasks/1125. [Accessed 26 07 2020].

[40] A. Smets, K. Jäger, O. Isabella, R. Swaaij and M. Zeman, Solar energy: The physics and engineering of photovoltaic conversion, technologies and systems, 2015.

Appendix

A1 Matlab code for the developed tool for square/rectangular modules

```
%%%%% Developed tool code %%%%%%%%%

clear all

%%%%% Input Parameters %%%%%%%%%

% r_m       Rows of cells in the module
% c_m       Columns of cells in the module
% l         Cell Length (edge to edge along y axis)
% b         Cell breadth  (edge to edge along x axis)
% l_m       Length of the module (edge to edge along y axis)
% b_m       Breadth of the module (edge to edge along x axis)
% t_c       Cell thickness (edge to edge along z axis)
% s_c       Spacing between cells( end edge of one cell to starting edge of adjacent cell)
% t_bc      Thickness of the back contact below the cell (edge to edge along z axis)
% t_eva_ac  Thickness of EVA layer above the cell front surface. Make sure to specify the height taking into consideration the height of the front metallization (edge to edge along z axis)
% t_eva_bc  Thickness of EVA layer below the cell back contact layer (edge to edge along z axis)
% t_bs      Thickness of the Back Sheet below the EVA Layer (edge to edge along z axis)
% t_fg      Thickness of the front glass above the EVA Layer (edge to edge along z axis)
% t_enc     Thickness of the enclosure above the glass and below the backsheet for emitting and collecting rays (edge to edge along z axis)
% t_enc_s   Width of the enclosure side of the module edge for collecting rays (edge to edge along x axis)
% n_bb      Number of busbars placed along the y axis on each cell
% w_bb      Width of each busbar (edge to edge along x axis)
% t_bb      Thickness of each busbar (edge to edge along z axis)
% t_bb_t    Thickness of busbar tabs (edge to edge along z axis)
% d_bb      Distance between the starting edge of one busbar and the starting edge of next busbar (edge to edge along z axis)
% d_s_bb    Distance of the starting edge of the first busbar from the edge of the solar cell (edge to edge along x axis)
% d_fi      Distance between the fingers starting edge and the next fingers starting edge placed horizontally along the y axis (edge to edge along y axis)
% t_fi      Thickness of the fingers (edge to edge along z axis)
% w_fi      Width of the fingers (edge to edge along y axis)
% wl        Wavelengths used for integration to compute the cell photocurrent density
% v_oc      Open circuit voltage of a single solar cell in Volts. Enter 0.65 if unknown
% res_fi    Resistivity of cell finger material in ohm um
```

```
% res_bb    Resistivity of busbar material in ohm um
% res_bc    Resistivity of Backcontact material in ohm um
% res_int   Resistivity of interconnection material in ohm um
% n_c_ser   Number of cells in series in a string
% n_s_par   Number of strings in parallel in a string (1 if no strings in parallel)
% t_par     Thickness of the cable after joining of strings to carry parallel current
% w_par     Width of the cable after joining of strings to carry parallel current

% all dimensions in um


r_m=3;
c_m=3;
l = 30000;
b = 30000;
l_m= 200000;
b_m= 200000;
t_c = 180;
s_c= 10000;
t_bc=1000;
t_eva_ac=1000;
t_eva_bc=1000;
t_fg= 4000;
t_enc=10;
t_enc_s=10;
t_bs=4000;  %%% 0 for single layer backsheet
n_bb=1;
w_bb=1000;
t_bb_t=800;
t_bb=15;
d_bb=0;
d_s_bb=15000;
d_fi=1568;
t_fi=15;
w_fi=45;
v_oc=0.65;
res_fi=1.638495*1e-2;
res_bb=1.638495*1e-2;
res_bc=1.638495*1e-2;
res_int=1.638495*1e-2;
n_c_ser=3;
n_s_par=3;
t_par=800;
w_par=5000;
wl =0.3:0.1:1.2;


%%%% Calculation of cell to edge spacing for centralization of the cells in the module %%%%
```

```
s_c_m=((b_m)-(b*c_m))/(c_m-1);
s_e_b=(b_m-((c_m*b)+((c_m-1)*s_c)))/2; %calculation of the cell to edge spacing horizontally (along x axis)
s_e_l=(l_m-((r_m*l)+((r_m-1)*s_c)))/2; %calculation of the cell to edge spacing vertically (along y axis)

 %%%%%%%%%%%%%%%%%  Solar Cell %%%%%%%%%%%%%%%%%

%VERTEX MATRIX FOR SOLAR CELLS (vertex xyz-coordinates [um])

a=1;
x=0;
y=0;
z=0;
for j=1:1:r_m
   for i=1:1:c_m
      if i==1
         x=x+s_e_b;
         y=y+s_e_l;
      else
         x=x+s_c;
      end
      V(a:a+7,:)=[ x+b  y  z;
         x+b y+l z;
         x  y+l z;
         x   y  z;
         x+b  y  z+t_c;
         x+b y+l z+t_c;
         x  y+l z+t_c;
         x   y  z+t_c;
         ];
      a=a+8;
      x=x+b;
   end
   x=0;
   y=y-s_e_l+l+s_c;
end
[e_solarcells,~]=size(V);
% Lux(V); return


%FACET MATRIX FOR SOLAR CELLS (vertex numbers)
i=1;
r=1;
for a=1:1:(r_m*c_m)
   F(r:r+5,:)=[ i+3  i+2 i+1 i;
      i+4 i+5 i+6 i+7;
      i  i+1 i+5 i+4;
      i+1 i+2 i+6 i+5;
```

```
      i+2 i+3 i+7 i+6;
      i+3  i  i+4 i+7;];
   i=i+8;
   r=r+6;
end
[fn_solarcells_e,~]=size(F);
% Lux(V,F); return


%%%%% Solar Cell Top Metallization and Interconnection %%%%%%%%%%%

%VERTEX MATRIX FOR SOLAR CELL TOP METALLIZATION GRID AND
INTERRCONNECTION(vertex xyz-coordinates [um])

i=1;
c_i=0;
a=e_solarcells+1;
while (i<=e_solarcells)
   x_s=V(i+2,1);
   y_e=V(i+1,2);
   y_s=V(i+3,2);

   for i1=1:1:n_bb

      if i<=(r_m-1)*c_m*8
         V(a:a+7,:)=[   x_s+d_s_bb  y_s  t_c;
            x_s+d_s_bb+w_bb  y_s t_c;
            x_s+d_s_bb  y_e+s_c  t_c;
            x_s+d_s_bb+w_bb  y_e+s_c  t_c;

            x_s+d_s_bb  y_s  t_c+t_bb;
            x_s+d_s_bb+w_bb y_s t_c+t_bb;
            x_s+d_s_bb  y_e+s_c  t_c+t_bb;
            x_s+d_s_bb+w_bb  y_e+s_c  t_c+t_bb;
            ];
         x_s=x_s+d_bb;
         a=a+8;
               else                          %TO remove interconnection- remove the else part and the if
                                             statement. Next remove the added s_c from y_e in the V matrix
         V(a:a+7,:)=[   x_s+d_s_bb  y_s  t_c;
            x_s+d_s_bb+w_bb  y_s t_c;
            x_s+d_s_bb  y_e  t_c;
            x_s+d_s_bb+w_bb  y_e  t_c;

            x_s+d_s_bb  y_s  t_c+t_bb;
            x_s+d_s_bb+w_bb y_s t_c+t_bb;
            x_s+d_s_bb  y_e  t_c+t_bb;
            x_s+d_s_bb+w_bb  y_e  t_c+t_bb;
            ];
         x_s=x_s+d_bb;
```

```
        a=a+8;
      end
    end
    x_e=V(i,1);
    x_s=V(i+2,1);
    y_e=V(i+1,2);
    y_s=V(i+3,2);
    counter=0;
    n_fi=zeros;
    while( y_s<y_e)
      counter=counter+1;
      V(a:a+7,:)=[ x_s  y_s  t_c;
        x_e  y_s  t_c;
        x_s  y_s+w_fi t_c;
        x_e  y_s+w_fi  t_c;

        x_s  y_s  t_c+t_fi;
        x_e  y_s  t_c+t_fi;
        x_s  y_s+w_fi t_c+t_fi;
        x_e  y_s+w_fi  t_c+t_fi;
        ];
      y_s=y_s+d_fi;
      a=a+8;
    end
    i=i+8;
end
% Lux(V); return

%FACET MATRIX FOR SOLAR CELLS TOP METALLIZATION GRID AND
INTERRCONNECTION (vertex numbers)
[fn_met_s,~]=size(F);
r=fn_met_s+1;

for i1=1:1:r_m
    for i2=1:1:c_m
      for a=1:1:(n_bb)
        F(r:r+4,:)=[ i+4  i+5 i+7 i+6;
          i i+4 i+6 i+2;
          i  i+1 i+5 i+4;
          i+1 i+3 i+7 i+5;
          i+6 i+7 i+3 i+2;
          ];
        i=i+8;
        r=r+5;
      end
      [r,~]=size(F);
      r=r+1;
      for a=1:1:counter
```

```
            F(r:r+4,:)=[ i+4  i+5 i+7 i+6;
                i i+4 i+6 i+2;
                i  i+1 i+5 i+4;
                i+1 i+3 i+7 i+5;
                i+6 i+7 i+3 i+2;
                ];
            i=i+8;
            r=r+5;

        end
    end
end

[fn_met_e,~]=size(F);
% Lux(V,F); return


%%%%%%%%%%%%%Solar Cell Back Contacts %%%%%%%%%%%%%

%VERTEX MATRIX FOR BACK CONTACT(vertex xyz-coordinates [um])
[s_bc_s,~]=size(V);
a=s_bc_s+1;
x=0;
y=0;
z=0;
for j=1:1:r_m
    for i=1:1:c_m
        if i==1
            x=x+s_e_b;
            y=y+s_e_l;
        else
            x=x+s_c;
        end
        V(a:a+3,:)=[
            x+b  y  z-t_bc;
            x+b y+l z-t_bc;
            x  y+l z-t_bc;
            x   y  z-t_bc;
            ];
        a=a+4;
        x=x+b;
    end
    x=0;
    y=y-s_e_l+l+s_c;
end
% Lux(V); return


% %%%%FACET MATRIX FOR BACK CONTACTS (vertex numbers)
```

```
sc_fbc=(1:e_solarcells);
[fn_bc_s,~]=size(F);
i=s_bc_s+1;
r=fn_bc_s+1;
a1=1;
for a=1:1:(r_m*c_m)

   F(r:r+4,:)=[ i+3  i+2 i+1 i;
      i+3 sc_fbc(a1+3) sc_fbc(a1+2) i+2;
      i+3 i sc_fbc(a1) sc_fbc(a1+3);
      i i+1 sc_fbc(a1+1) sc_fbc(a1);
      i+1 i+2 sc_fbc(a1+2) sc_fbc(a1+1);];
   i=i+4;
   r=r+5;
   a1=a1+8;
end
[fn_bc_e,~]=size(F);

% Lux(V,F); return


%%%%%%%%%%%%Encapsulation %%%%%%%%%%%%

%VERTEX MATRIX FOR ENCAPSULATION(vertex xyz-coordinates [um])
[s_eva_s,~]=size(V);
x=0;
y=0;
z=0;
V(i:i+7,:)= [ x+b_m          y              z-(t_eva_bc+t_bc);
   x+b_m   y+l_m  z-(t_eva_bc+t_bc);
   x             y+l_m  z-(t_eva_bc+t_bc)  ;
   x                    y             z-(t_eva_bc+t_bc);
   x+b_m          y             z+t_c+(t_eva_ac);
   x+b_m   y+l_m  z+t_c+(t_eva_ac);
   x             y+l_m  z+t_c+(t_eva_ac);
   x                    y             z+t_c+(t_eva_ac);
   ];
[s_eva_e,~]=size(V);
% Lux(V); return

%%%%FACET MATRIX FOR ENCAPSULATION (vertex numbers)
[fn_eva_s,~]=size(F);
F(r:r+5,:)=[ i+3  i+2 i+1 i;
   i+4 i+5 i+6 i+7;
   i+3 i+7 i+6 i+2;
   i+3 i i+4 i+7;
   i i+1 i+5 i+4;
   i+1 i+2 i+6 i+5;];
```

```
[fn_eva_e,~]=size(F);
eva_fbc=(s_eva_s+1:s_eva_e);
% Lux(V,F); return

 %%%%%%%%%%%% Front Glass %%%%%%%%%%%%

%VERTEX MATRIX FOR FRONT GLASS(vertex xyz-coordinates [um])
x=0;
y=0;
z=0;
[i,~] =size(V);
i=i+1;
V(i:i+3,:)= [

x+b_m          y              z+t_c+(t_eva_ac)+t_fg;
x+b_m   y+l_m  z+t_c+(t_eva_ac)+t_fg;
x              y+l_m  z+t_c+(t_eva_ac)+t_fg;
x                     y             z+t_c+(t_eva_ac)+t_fg;
];
% Lux(V); return

%%%%%FACET MATRIX FOR FRONT GLASS(vertex numbers)
[r,~] =size(F);
[fn_frontglass_s,~]=size(F);
r=r+1;
F(r:r+4,:)=[ i  i+1 i+2 i+3;

eva_fbc(5) eva_fbc(6) i+1 i;
eva_fbc(6) eva_fbc(7) i+2 i+1;
eva_fbc(7) eva_fbc(8) i+3 i+2;
eva_fbc(8) eva_fbc(5) i i+3;

];
[fn_frontglass_e,~]=size(F);
% Lux(V,F); return


%%%%%%%%%%%% Backsheet %%%%%%%%%%%%


%VERTEX MATRIX FOR BACKSHEET(vertex xyz-coordinates [um])
[i,~]=size(V);
i=i+1;
x=0;
y=0;
z=0;
V(i:i+3,:)= [ x+b_m          y              z-(t_eva_bc+t_bc+t_bs);
   x+b_m   y+l_m  z-(t_eva_bc+t_bc+t_bs);
   x              y+l_m  z-(t_eva_bc+t_bc+t_bs)  ;
   x                     y             z-(t_eva_bc+t_bc+t_bs);
```

```
    ];
% Lux(V); return


%%%%%FACET MATRIX FOR BACKSHEET (vertex numbers)
[fn_bs_s,~]=size(F);
r=fn_bc_s+1;
F(r:r+4,:)=[ i+3  i+2 i+1 i;

i i+1 eva_fbc(2) eva_fbc(1);
i+1 i+2 eva_fbc(3) eva_fbc(2);
i+2 i+3 eva_fbc(4) eva_fbc(3);
i+3 i eva_fbc(1) eva_fbc(4);
];

[fn_bs_e,~]=size(F);
% Lux(V,F); return


%In order use a single sheet layer for backsheet comment this section out and use Encapsulation
bottom layer as backsheet in the optical properties section


%%%%%%%%%% Enclosure %%%%%%%%%%%%%%%

%VERTEX MATRIX FOR ENCLOSURE(vertex xyz-coordinates [um])
x=0;
y=0;
z=0;
[i,~] =size(V);
i=i+1;
V(i:i+7,:)= [ x+b_m+t_enc_s          y-t_enc_s              z+t_c+(t_eva_ac)+t_fg+t_enc;
   x+b_m+t_enc_s    y+l_m+t_enc_s   z+t_c+(t_eva_ac)+t_fg+t_enc;
   x-t_enc_s             y+l_m+t_enc_s   z+t_c+(t_eva_ac)+t_fg+t_enc  ;
   x-t_enc_s                    y-t_enc_s              z+t_c+(t_eva_ac)+t_fg+t_enc;
   x+b_m+t_enc_s          y-t_enc_s              z-t_bc-(t_eva_bc)-t_bs-t_enc;
   x+b_m+t_enc_s    y+l_m+t_enc_s   z-t_bc-(t_eva_bc)-t_bs-t_enc;
   x-t_enc_s             y+l_m+t_enc_s   z-t_bc-(t_eva_bc)-t_bs-t_enc;
   x-t_enc_s                    y-t_enc_s              z-t_bc-(t_eva_bc)-t_bs-t_enc;
   ];

% Make t_bs=0 if using a single layer backsheet
% Lux(V); return

%%%%%FACET MATRIX FOR ENCLOSURE(vertex numbers)
[r,~] =size(F);
[fn_enc,~] =size(F);
r=r+1;
F(r:r+5,:)=[ i+3  i+2 i+1 i;
   i+4 i+5 i+6 i+7;
```

```
    i  i+1 i+5 i+4;
    i+1 i+2 i+6 i+5;
    i+2 i+3 i+7 i+6;
    i+3  i  i+4 i+7;];

%  Lux(V,F); return


%%%%%%%%%% Optical Properties %%%%%%%%%%%%

%SURFACE TYPE STRUCTURE
clear Type

Type(1).RT      = {0 0 'Ceiling'};        % Top absorber surface of the enclosure used for emitting
rays
Type(1).Plot    = {[0.3 0.3 0.3] 0.3};
Type(1).Emit    = {50000 0 0};              % Increase the number of rays for higher accuracy
Type(1).Facet   =  fn_enc+1;

Type(2).RT      = {0 0 'Floor'};          % Bottom absorber surface of the enclosure
Type(2).Plot    = {[0.3 0.3 0.3] 0.3};
Type(2).Facet   = fn_enc+2;

Type(3).RT      = {0 0 'Wall'};           % Side absorber walls of the enclosure
Type(3).Plot    = {[0.3 0.3 0.3] 0.3};
Type(3).Facet   = fn_enc+3:fn_enc+6;

Type(4).RT      = {'air' 'glass'};        % Air/Glass interface
Type(4).Plot    = {[0 0 1] 0.1};
Type(4).Facet   = fn_frontglass_s+1;

Type(5).RT      = {'air' 'glass'};        % Air/Glass side walls interface
Type(5).Plot    = {[0 0 1] 0.1};
Type(5).Facet   = fn_frontglass_s+2:fn_frontglass_s+5;

Type(6).RT      = {'glass' 'EVA(G)'};     % Glass/Encapsulation interface
Type(6).Plot    = {[0 0 1] 0.2};
Type(6).Facet   = fn_eva_s+2;

Type(7).RT      = {'air' 'EVA(G)'};       % Air/Encapsulation side walls interface
Type(7).Plot    = {[0.6 0.6 0.6] 0.6};
Type(7).Facet   = fn_eva_s+3:fn_eva_e;

Type(8).RT      = {0 0 'cell'};           % Cell absorber surfaces
Type(8).Plot    = {[1 0 0] 0.5};
Type(8).Facet   = 1:fn_solarcells_e;

Type(9).RT      = {'EVA(G)' 'Ag'};        % Encapsulation/front metallization interface
Type(9).Plot    = {[0.5 0.5 0.5] 1};
Type(9).Facet   = fn_met_s+1:fn_met_e;
```

```
Type(9).Scat    = {1,1};

Type(10).RT     = {'EVA(G)' 'Ag'};        % Encapsulation/Backcontact interface
Type(10).Plot   = {[0 0 0] 0.9};
Type(10).Facet  = fn_bc_s+1:fn_bc_e;
Type(10).Scat   = {1,1};

Type(11).RT     = {'glass' 'EVA(G)'};     % Encapsulation/Backsheet top surface interface
% Type(11).RT     = {1 0 'Backsheet'};       %Uncomment this statement along with comment mentioned in Backsheet section to use single layer backsheet
Type(11).Plot   = {[0 0 1] 0.1};
Type(11).Facet  = fn_eva_s+1;
% Type(11).Scat   = {1,1};                % Haze and Phong exponent (for Lambertian scatterer use 1 for both. Comment out this line if using a glass-glass module)

Type(12).RT     = { 'air' 'glass'};       % Air/Backsheet bottom and side surfaces interface ( Along with the comment in the backsheet section, remove this Type structure if a single backsheet surface is required)
Type(12).Plot   = {[0 0 1] 0.1};
Type(12).Facet  = fn_bs_s+1:fn_bs_e;

% Lux(V,F,Type);  return
CTM_M = Lux(V,F,Type,wl);                 % Start ray-tracing

%%%%%%%%%%%% Net Module Active Area Analysis %%%%%%%%%%%
cell_top_area=(l*b*r_m*c_m*1e-8);
metallization_area_top=(w_bb*l*n_bb*r_m*c_m*1e-8)+(counter*w_fi*b*r_m*c_m*1e-8);
net_active_area_top=(cell_top_area-metallization_area_top);
active_area_ratio= net_active_area_top/cell_top_area;

%%%%%%%%%%%% Module Electrical Loss Analysis %%%%%%%%%%%

cell_photocurrent_density = (CTM_M(10).Current*(((l_m+(2*t_enc_s))*(b_m+(2*t_enc_s))*1e-8)/((l*b*r_m*c_m*1e-8)))); %Cell photo current density with respect to the cell top active area. Ensure x in CTM_(x) in this statement is for the cell as in CTM_M structure.
single_cell_current= (cell_photocurrent_density*1e-3)*(l*b*1e-8);

if (n_bb==1)

    %power loss in cell fingers
    current_single_busbar_single_cell= single_cell_current/n_bb;

    current_single_finger_left= (current_single_busbar_single_cell*(d_s_bb/b)/counter);
    current_single_finger_right= (current_single_busbar_single_cell*(1-((d_s_bb)/b))/counter);

    current_density_left_fi=(current_single_finger_left/(d_s_bb));
    current_density_right_fi=(current_single_finger_right/((b-d_s_bb-w_bb)));

    powerloss_left_fi=((current_density_left_fi^2)*(res_fi)*(d_s_bb)/(3*t_fi*w_fi));
    powerloss_right_fi=((current_density_right_fi^2)*(res_fi)*((b-d_s_bb-w_bb))/(3*t_fi*w_fi));
```

```
    total_power_loss_fingers_cell=(powerloss_left_fi+powerloss_right_fi)*counter;

    %power loss in busbar
    current_density_busbar=current_single_busbar_single_cell/(l);
    powerloss_bb=(current_density_busbar^2)*(res_bb)*(l)/(3*t_bb*w_bb);

    %power loss in backcontact
    current_density_backcontact=single_cell_current/(l);
    powerloss_backcontact=(current_density_backcontact^2)*(res_bc)*(l)/(3*t_bc*b);

    %total ohmic power loss in cell
    tot_ohmic_cell=total_power_loss_fingers_cell+powerloss_bb+powerloss_backcontact;

    %total ohmic power loss in series interconnection string

powerloss_ser_inter=(current_single_busbar_single_cell^2)*(res_int*((s_c+l)/(t_bb_t*w_bb)))*(n
_c_ser-1)*n_s_par;  %assuming same geometrical properties of the interconnection as in the cell
busbars and length of interconnection tabs equal to cell space

    %total ohmic power loss in parallel interconnection string

powerloss_par_inter=((single_cell_current*n_s_par)^2)*(res_int*((t_eva_bc+t_bs)/(t_par*w_par))
)*2; %Assuming all the strings are connected at a point and the length of the cable used for
carrying the current after the point is equal to length of the module

    %total ohmic power loss
    tot_power_loss_ohmic=(tot_ohmic_cell*r_m*c_m)+powerloss_ser_inter+powerloss_par_inter;

elseif (n_bb==2)

    %power loss in cell finger
    current_single_busbar_1= (cell_photocurrent_density*1e-3)*(l*(d_s_bb+(d_bb/2))*1e-8);
    current_single_busbar_2= (cell_photocurrent_density*1e-3)*(l*(b-(d_s_bb+(d_bb/2)))*1e-8);

    current_single_finger_left_1= (current_single_busbar_1*(d_s_bb/(d_s_bb+(d_bb/2)))/counter);
    current_single_finger_right_1= (current_single_busbar_1*(1-
(d_s_bb/(d_s_bb+(d_bb/2))))/counter);
    current_single_finger_left_2= (current_single_busbar_2*((d_bb/2)/((d_bb/2)+w_bb+(b-d_s_bb-
d_bb-w_bb)))/counter);
    current_single_finger_right_2= (current_single_busbar_2*(1-((d_bb/2)/((d_bb/2)+w_bb+(b-
d_s_bb-d_bb-w_bb))))/counter);

    current_density_left_fi_1=(current_single_finger_left_1/(d_s_bb));
    current_density_right_fi_1=(current_single_finger_right_1/(((d_bb/2)-w_bb)));
    current_density_left_fi_2=(current_single_finger_left_2/(((d_bb/2)-w_bb)));
    current_density_right_fi_2=(current_single_finger_right_2/((b-d_s_bb-d_bb-w_bb)));

    powerloss_left_fi_1=((current_density_left_fi_1^2)*(res_fi)*(d_s_bb)/(3*t_fi*w_fi));
    powerloss_right_fi_1=((current_density_right_fi_1^2)*(res_fi)*((d_bb/2))/(3*t_fi*w_fi));
```

```
    powerloss_left_fi_2=((current_density_left_fi_2^2)*(res_fi)*((d_bb/2))/(3*t_fi*w_fi));
    powerloss_right_fi_2=((current_density_right_fi_2^2)*(res_fi)*((b-d_s_bb-w_bb-
d_bb))/(3*t_fi*w_fi));


total_power_loss_fingers_cell=(powerloss_left_fi_1+powerloss_right_fi_1+powerloss_left_fi_2+p
owerloss_right_fi_2)*counter;

    %power loss in busbar
    current_density_busbar_1=current_single_busbar_1/(l);
    powerloss_bb_1=(current_density_busbar_1^2)*(res_bb)*(l)/(3*t_bb*w_bb);

    current_density_busbar_2=current_single_busbar_2/(l);
    powerloss_bb_2=(current_density_busbar_2^2)*(res_bb)*(l)/(3*t_bb*w_bb);

    powerloss_bb=powerloss_bb_1+powerloss_bb_2;

    %power loss in backcontact
    current_density_backcontact=single_cell_current/(l);
    powerloss_backcontact=(current_density_backcontact^2)*(res_bc)*(l)/(3*t_bc*b);

    %total ohmic power loss in cell
    tot_ohmic_cell=total_power_loss_fingers_cell+powerloss_bb+powerloss_backcontact;


    %total ohmic power loss in series interconnection string

powerloss_ser_inter=(current_single_busbar_1^2+current_single_busbar_2^2)*((res_int*((s_c+l)/(
t_bb_t*w_bb)))*(n_c_ser-1)*n_s_par);  %assuming same width of the interconnection tabs as in
the cell busbars and length of interconnection tabs equal to cell space

    %total ohmic power loss in parallel interconnection string

powerloss_par_inter=((single_cell_current*n_s_par)^2)*(res_int*((t_eva_bc+t_bs)/(t_par*w_par))
)*2; %Assuming all the strings are connected at a point and the length of the cable used for
carrying the current after the point is equal to length of the module

    %total ohmic power loss
    tot_power_loss_ohmic=(tot_ohmic_cell*r_m*c_m)+powerloss_ser_inter+powerloss_par_inter;

elseif (n_bb==3)

    %power loss in cell finger
    current_single_busbar_1= (cell_photocurrent_density*1e-3)*(l*(d_s_bb+(d_bb/2))*1e-8);
    current_single_busbar_2= (cell_photocurrent_density*1e-3)*(l*d_bb*1e-8);
    current_single_busbar_3= (cell_photocurrent_density*1e-3)*(l*(b-
(d_s_bb+d_bb+(d_bb/2)))*1e-8);

    current_single_finger_left_1= (current_single_busbar_1*(d_s_bb/(d_s_bb+(d_bb/2)))/counter);
```

```
    current_single_finger_right_1= (current_single_busbar_1*(1-
(d_s_bb/(d_s_bb+(d_bb/2))))/counter);
    current_single_finger_left_2=
(current_single_busbar_2*((d_bb/2)/((d_bb/2)+w_bb+(d_bb/2)))/counter);
    current_single_finger_right_2= (current_single_busbar_2*(1-
((d_bb/2)/((d_bb/2)+w_bb+(d_bb/2))))/counter);
    current_single_finger_left_3= (current_single_busbar_3*((d_bb/2)/((d_bb/2)+w_bb+(b-d_s_bb-
d_bb-d_bb)))/counter);
    current_single_finger_right_3= (current_single_busbar_3*(1-((d_bb/2)/((d_bb/2)+w_bb+(b-
d_s_bb-d_bb-d_bb))))/counter);


    current_density_left_fi_1=(current_single_finger_left_1/(d_s_bb));
    current_density_right_fi_1=(current_single_finger_right_1/(((d_bb/2)-w_bb)));
    current_density_left_fi_2=(current_single_finger_left_2/(((d_bb/2)-w_bb)));
    current_density_right_fi_2=(current_single_finger_right_2/(((d_bb/2)-w_bb)));
    current_density_left_fi_3=(current_single_finger_left_3/(((d_bb/2)-w_bb)));
    current_density_right_fi_3=(current_single_finger_right_3/((b-d_s_bb-d_bb-d_bb-w_bb)));

    powerloss_left_fi_1=((current_density_left_fi_1^2)*(res_fi)*(d_s_bb)/(3*t_fi*w_fi));
    powerloss_right_fi_1=((current_density_right_fi_1^2)*(res_fi)*(((d_bb/2)-
w_bb))/(3*t_fi*w_fi));
    powerloss_left_fi_2=((current_density_left_fi_2^2)*(res_fi)*(((d_bb/2)-w_bb))/(3*t_fi*w_fi));
    powerloss_right_fi_2=((current_density_right_fi_2^2)*(res_fi)*(((d_bb/2)-
w_bb))/(3*t_fi*w_fi));
    powerloss_left_fi_3=((current_density_left_fi_3^2)*(res_fi)*(((d_bb/2)-w_bb))/(3*t_fi*w_fi));
    powerloss_right_fi_3=((current_density_right_fi_3^2)*(res_fi)*((b-d_s_bb-d_bb-w_bb-
d_bb))/(3*t_fi*w_fi));


total_power_loss_fingers_cell=(powerloss_left_fi_1+powerloss_right_fi_1+powerloss_left_fi_2+p
owerloss_right_fi_2+powerloss_left_fi_3+powerloss_right_fi_3)*counter;

    %power loss in busbar
    current_density_busbar_1=current_single_busbar_1/(l);
    powerloss_bb_1=(current_density_busbar_1^2)*(res_bb)*(l)/(3*t_bb*w_bb);


    current_density_busbar_2=current_single_busbar_2/(l);
    powerloss_bb_2=(current_density_busbar_2^2)*(res_bb)*(l)/(3*t_bb*w_bb);

    current_density_busbar_3=current_single_busbar_3/(l);
    powerloss_bb_3=(current_density_busbar_3^2)*(res_bb)*(l)/(3*t_bb*w_bb);

    powerloss_bb=powerloss_bb_1+powerloss_bb_2+powerloss_bb_3;

    %power loss in backcontact
    current_density_backcontact=single_cell_current/(l);
    powerloss_backcontact=(current_density_backcontact^2)*(res_bc)*(l)/(3*t_bc*b);
```

```
    %total ohmic power loss in cell
    tot_ohmic_cell=total_power_loss_fingers_cell+powerloss_bb+powerloss_backcontact;


    %total ohmic power loss in series interconnection string

powerloss_ser_inter=(current_single_busbar_1^2+current_single_busbar_2^2+current_single_bus
bar_3^2)*((res_int*((s_c+l)/(t_bb_t*w_bb)))*(n_c_ser-1)*n_s_par);  %assuming same width of
the interconnection as in the cell busbars and length of interconnection tabs equal to cell space

    %total ohmic power loss in parallel interconnection string

powerloss_par_inter=((single_cell_current*n_s_par)^2)*(res_int*((t_eva_bc+t_bs)/(t_par*w_par))
)*2; %Assuming all the strings are connected at a point and the length of the cable used for
carrying the current after the point is equal to length of the module

    %total ohmic power loss
    tot_power_loss_ohmic=(tot_ohmic_cell*r_m*c_m)+powerloss_ser_inter+powerloss_par_inter;

elseif (n_bb==4)

    %power loss in cell finger
    current_single_busbar_1= (cell_photocurrent_density*1e-3)*(l*(d_s_bb+(d_bb/2))*1e-8);
    current_single_busbar_2= (cell_photocurrent_density*1e-3)*(l*d_bb*1e-8);
    current_single_busbar_3= (cell_photocurrent_density*1e-3)*(l*d_bb*1e-8);
    current_single_busbar_4= (cell_photocurrent_density*1e-3)*(l*(b-
(d_s_bb+d_bb+d_bb+(d_bb/2)))*1e-8);

    current_single_finger_left_1= (current_single_busbar_1*(d_s_bb/(d_s_bb+(d_bb/2)))/counter);
    current_single_finger_right_1= (current_single_busbar_1*(1-
(d_s_bb/(d_s_bb+(d_bb/2))))/counter);
    current_single_finger_left_2=
(current_single_busbar_2*((d_bb/2)/((d_bb/2)+w_bb+(d_bb/2)))/counter);
    current_single_finger_right_2= (current_single_busbar_2*(1-
((d_bb/2)/((d_bb/2)+w_bb+(d_bb/2))))/counter);
    current_single_finger_left_3=
(current_single_busbar_3*((d_bb/2)/((d_bb/2)+w_bb+(d_bb/2)))/counter);
    current_single_finger_right_3= (current_single_busbar_3*(1-
((d_bb/2)/((d_bb/2)+w_bb+(d_bb/2))))/counter);
    current_single_finger_left_4= (current_single_busbar_4*((d_bb/2)/((d_bb/2)+w_bb+(b-d_s_bb-
d_bb-d_bb-d_bb)))/counter);
    current_single_finger_right_4= (current_single_busbar_4*(1-((d_bb/2)/((d_bb/2)+w_bb+(b-
d_s_bb-d_bb-d_bb-d_bb))))/counter);


    current_density_left_fi_1=(current_single_finger_left_1/(d_s_bb));
    current_density_right_fi_1=(current_single_finger_right_1/(((d_bb/2)-w_bb)));
    current_density_left_fi_2=(current_single_finger_left_2/(((d_bb/2)-w_bb)));
    current_density_right_fi_2=(current_single_finger_right_2/(((d_bb/2)-w_bb)));
    current_density_left_fi_3=(current_single_finger_left_3/(((d_bb/2)-w_bb)));
```

```
    current_density_right_fi_3=(current_single_finger_right_3/(((d_bb/2)-w_bb)));
    current_density_left_fi_4=(current_single_finger_left_4/(((d_bb/2)-w_bb)));
    current_density_right_fi_4=(current_single_finger_right_4/((b-d_s_bb-d_bb-d_bb-d_bb-
w_bb)));

    powerloss_left_fi_1=((current_density_left_fi_1^2)*(res_fi)*(d_s_bb)/(3*t_fi*w_fi));
    powerloss_right_fi_1=((current_density_right_fi_1^2)*(res_fi)*(((d_bb/2)-
w_bb))/(3*t_fi*w_fi));
    powerloss_left_fi_2=((current_density_left_fi_2^2)*(res_fi)*(((d_bb/2)-w_bb))/(3*t_fi*w_fi));
    powerloss_right_fi_2=((current_density_right_fi_2^2)*(res_fi)*(((d_bb/2)-
w_bb))/(3*t_fi*w_fi));
    powerloss_left_fi_3=((current_density_left_fi_3^2)*(res_fi)*(((d_bb/2)-w_bb))/(3*t_fi*w_fi));
    powerloss_right_fi_3=((current_density_right_fi_3^2)*(res_fi)*(((d_bb/2)-
w_bb))/(3*t_fi*w_fi));
    powerloss_left_fi_4=((current_density_left_fi_4^2)*(res_fi)*(((d_bb/2)-w_bb))/(3*t_fi*w_fi));
    powerloss_right_fi_4=((current_density_right_fi_4^2)*(res_fi)*((b-d_s_bb-d_bb-d_bb-d_bb-
w_bb))/(3*t_fi*w_fi));


total_power_loss_fingers_cell=(powerloss_left_fi_1+powerloss_right_fi_1+powerloss_left_fi_2+p
owerloss_right_fi_2+powerloss_left_fi_3+powerloss_right_fi_3+powerloss_left_fi_4+powerloss_r
ight_fi_4)*counter;


    %power loss in busbar
    current_density_busbar_1=current_single_busbar_1/(l);
    powerloss_bb_1=(current_density_busbar_1^2)*(res_bb)*(l)/(3*t_bb*w_bb);


    current_density_busbar_2=current_single_busbar_2/(l);
    powerloss_bb_2=(current_density_busbar_2^2)*(res_bb)*(l)/(3*t_bb*w_bb);

    current_density_busbar_3=current_single_busbar_3/(l);
    powerloss_bb_3=(current_density_busbar_3^2)*(res_bb)*(l)/(3*t_bb*w_bb);

    current_density_busbar_4=current_single_busbar_4/(l);
    powerloss_bb_4=(current_density_busbar_4^2)*(res_bb)*(l)/(3*t_bb*w_bb);

    powerloss_bb=powerloss_bb_1+powerloss_bb_2+powerloss_bb_3+powerloss_bb_4;


    %power loss in Backcontact
    current_density_backcontact=single_cell_current/(l);
    powerloss_backcontact=(current_density_backcontact^2)*(res_bc)*(l)/(3*t_bc*b);

    %total ohmic power loss in cell
    tot_ohmic_cell=total_power_loss_fingers_cell+powerloss_bb+powerloss_backcontact;


    %total ohmic power loss in series interconnection string
```

```
powerloss_ser_inter=(current_single_busbar_1^2+current_single_busbar_2^2+current_single_bus
bar_3^2+current_single_busbar_4^2)*((res_int*((s_c+l)/(t_bb_t*w_bb)))*(n_c_ser-1)*n_s_par);
%assuming same width of the interconnection tab as in the cell busbars and length of
interconnection tabs equal to cell space

    %total ohmic power loss in parallel interconnection string

powerloss_par_inter=((single_cell_current*n_s_par)^2)*(res_int*((t_eva_bc+t_bs)/(t_par*w_par))
)*2; %Assuming all the strings are connected at a point and the length of the cable used for
carrying the current after the point is equal to length of the module

    %total ohmic power loss
    tot_power_loss_ohmic=(tot_ohmic_cell*r_m*c_m)+powerloss_ser_inter+powerloss_par_inter;

end

%%%%%%%%%% Module Power Analysis %%%%%%%%%%

module_power=(((cell_photocurrent_density*1e-3)*(l*b*r_m*c_m*1e-8))*v_oc)-
tot_power_loss_ohmic;

%%%%%%%% Single Cell Power Analysis %%%%%%%%%

cell_photocurrent_density_abs=46.456;
cell_photocurrent_density_abs_metal=cell_photocurrent_density_abs*active_area_ratio;
single_cell_current_abs=(cell_photocurrent_density_abs_metal*1e-3)*(l*b*1e-8);



if (n_bb==1)

    %power loss in cell fingers
    current_single_busbar_single_cell_abs= single_cell_current_abs/n_bb;

    current_single_finger_left_abs= (current_single_busbar_single_cell_abs*(d_s_bb/b)/counter);
    current_single_finger_right_abs= (current_single_busbar_single_cell_abs*(1-
((d_s_bb)/b))/counter);

    current_density_left_fi_abs=(current_single_finger_left_abs/(d_s_bb));
    current_density_right_fi_abs=(current_single_finger_right_abs/((b-d_s_bb-w_bb)));

    powerloss_left_fi_abs=((current_density_left_fi_abs^2)*(res_fi)*(d_s_bb)/(3*t_fi*w_fi));
    powerloss_right_fi_abs=((current_density_right_fi_abs^2)*(res_fi)*((b-d_s_bb-
w_bb))/(3*t_fi*w_fi));

    total_power_loss_fingers_cell_abs=(powerloss_left_fi_abs+powerloss_right_fi_abs)*counter;

    %power loss in busbar
    current_density_busbar_abs=current_single_busbar_single_cell_abs/(l);
```

```
    powerloss_bb_abs=(current_density_busbar_abs^2)*(res_bb)*(l)/(3*t_bb*w_bb);

    %power loss in Backcontact
    current_density_backcontact_abs=single_cell_current_abs/(l);
    powerloss_backcontact_abs=(current_density_backcontact_abs^2)*(res_bc)*(l)/(3*t_bc*b);

    %total ohmic power loss in cell

tot_ohmic_cell_abs=total_power_loss_fingers_cell_abs+powerloss_bb_abs+powerloss_backcontact_abs;

elseif (n_bb==2)

    %power loss in cell finger
    current_single_busbar_1_abs= (cell_photocurrent_density_abs_metal*1e-3)*(l*(d_s_bb+(d_bb/2))*1e-8);
    current_single_busbar_2_abs= (cell_photocurrent_density_abs_metal*1e-3)*(l*(b-(d_s_bb+(d_bb/2)))*1e-8);

    current_single_finger_left_1_abs= (current_single_busbar_1_abs*(d_s_bb/(d_s_bb+(d_bb/2)))/counter);
    current_single_finger_right_1_abs= (current_single_busbar_1_abs*(1-(d_s_bb/(d_s_bb+(d_bb/2))))/counter);
    current_single_finger_left_2_abs= (current_single_busbar_2_abs*((d_bb/2)/((d_bb/2)+w_bb+(b-d_s_bb-d_bb-w_bb)))/counter);
    current_single_finger_right_2_abs= (current_single_busbar_2_abs*(1-((d_bb/2)/((d_bb/2)+w_bb+(b-d_s_bb-d_bb-w_bb))))/counter);

    current_density_left_fi_1_abs=(current_single_finger_left_1_abs/(d_s_bb));
    current_density_right_fi_1_abs=(current_single_finger_right_1_abs/(((d_bb/2)-w_bb)));
    current_density_left_fi_2_abs=(current_single_finger_left_2_abs/(((d_bb/2)-w_bb)));
    current_density_right_fi_2_abs=(current_single_finger_right_2_abs/((b-d_s_bb-d_bb-w_bb)));

    powerloss_left_fi_1_abs=((current_density_left_fi_1_abs^2)*(res_fi)*(d_s_bb)/(3*t_fi*w_fi));

powerloss_right_fi_1_abs=((current_density_right_fi_1_abs^2)*(res_fi)*((d_bb/2))/(3*t_fi*w_fi));
    powerloss_left_fi_2_abs=((current_density_left_fi_2_abs^2)*(res_fi)*((d_bb/2))/(3*t_fi*w_fi));
    powerloss_right_fi_2_abs=((current_density_right_fi_2_abs^2)*(res_fi)*((b-d_s_bb-w_bb-d_bb))/(3*t_fi*w_fi));


total_power_loss_fingers_cell_abs=(powerloss_left_fi_1_abs+powerloss_right_fi_1_abs+powerloss_left_fi_2_abs+powerloss_right_fi_2_abs)*counter;

    %power loss in busbar
    current_density_busbar_1_abs=current_single_busbar_1_abs/(l);
    powerloss_bb_1_abs=(current_density_busbar_1_abs^2)*(res_bb)*(l)/(3*t_bb*w_bb);

    current_density_busbar_2_abs=current_single_busbar_2_abs/(l);
```

```
    powerloss_bb_2_abs=(current_density_busbar_2_abs^2)*(res_bb)*(l)/(3*t_bb*w_bb);

    powerloss_bb_abs=powerloss_bb_1_abs+powerloss_bb_2_abs;

    %power loss in Backcontact
    current_density_backcontact_abs=single_cell_current_abs/(l);
    powerloss_backcontact_abs=(current_density_backcontact_abs^2)*(res_bc)*(l)/(3*t_bc*b);

    %total ohmic power loss in cell

tot_ohmic_cell_abs=total_power_loss_fingers_cell_abs+powerloss_bb_abs+powerloss_backconta
ct_abs;

elseif (n_bb==3)

    %power loss in cell finger
    current_single_busbar_1_abs= (cell_photocurrent_density_abs_metal*1e-
3)*(l*(d_s_bb+(d_bb/2))*1e-8);
    current_single_busbar_2_abs= (cell_photocurrent_density_abs_metal*1e-3)*(l*d_bb*1e-8);
    current_single_busbar_3_abs= (cell_photocurrent_density_abs_metal*1e-3)*(l*(b-
(d_s_bb+d_bb+(d_bb/2)))*1e-8);

    current_single_finger_left_1_abs=
(current_single_busbar_1_abs*(d_s_bb/(d_s_bb+(d_bb/2)))/counter);
    current_single_finger_right_1_abs= (current_single_busbar_1_abs*(1-
(d_s_bb/(d_s_bb+(d_bb/2))))/counter);
    current_single_finger_left_2_abs=
(current_single_busbar_2_abs*((d_bb/2)/((d_bb/2)+w_bb+(d_bb/2)))/counter);
    current_single_finger_right_2_abs= (current_single_busbar_2_abs*(1-
((d_bb/2)/((d_bb/2)+w_bb+(d_bb/2))))/counter);
    current_single_finger_left_3_abs=
(current_single_busbar_3_abs*((d_bb/2)/((d_bb/2)+w_bb+(b-d_s_bb-d_bb-d_bb)))/counter);
    current_single_finger_right_3_abs= (current_single_busbar_3_abs*(1-
((d_bb/2)/((d_bb/2)+w_bb+(b-d_s_bb-d_bb-d_bb))))/counter);


    current_density_left_fi_1_abs=(current_single_finger_left_1_abs/(d_s_bb));
    current_density_right_fi_1_abs=(current_single_finger_right_1_abs/(((d_bb/2)-w_bb)));
    current_density_left_fi_2_abs=(current_single_finger_left_2_abs/(((d_bb/2)-w_bb)));
    current_density_right_fi_2_abs=(current_single_finger_right_2_abs/(((d_bb/2)-w_bb)));
    current_density_left_fi_3_abs=(current_single_finger_left_3_abs/(((d_bb/2)-w_bb)));
    current_density_right_fi_3_abs=(current_single_finger_right_3_abs/((b-d_s_bb-d_bb-d_bb-
w_bb)));

    powerloss_left_fi_1_abs=((current_density_left_fi_1_abs^2)*(res_fi)*(d_s_bb)/(3*t_fi*w_fi));
    powerloss_right_fi_1_abs=((current_density_right_fi_1_abs^2)*(res_fi)*(((d_bb/2)-
w_bb))/(3*t_fi*w_fi));
    powerloss_left_fi_2_abs=((current_density_left_fi_2_abs^2)*(res_fi)*(((d_bb/2)-
w_bb))/(3*t_fi*w_fi));
```

```
    powerloss_right_fi_2_abs=((current_density_right_fi_2_abs^2)*(res_fi)*(((d_bb/2)-
w_bb))/(3*t_fi*w_fi));
    powerloss_left_fi_3_abs=((current_density_left_fi_3_abs^2)*(res_fi)*(((d_bb/2)-
w_bb))/(3*t_fi*w_fi));
    powerloss_right_fi_3_abs=((current_density_right_fi_3_abs^2)*(res_fi)*((b-d_s_bb-d_bb-
w_bb-d_bb))/(3*t_fi*w_fi));


total_power_loss_fingers_cell_abs=(powerloss_left_fi_1_abs+powerloss_right_fi_1_abs+powerlo
ss_left_fi_2_abs+powerloss_right_fi_2_abs+powerloss_left_fi_3_abs+powerloss_right_fi_3_abs)*
counter;

    %power loss in busbar
    current_density_busbar_1_abs=current_single_busbar_1_abs/(l);
    powerloss_bb_1_abs=(current_density_busbar_1_abs^2)*(res_bb)*(l)/(3*t_bb*w_bb);


    current_density_busbar_2_abs=current_single_busbar_2_abs/(l);
    powerloss_bb_2_abs=(current_density_busbar_2_abs^2)*(res_bb)*(l)/(3*t_bb*w_bb);

    current_density_busbar_3_abs=current_single_busbar_3_abs/(l);
    powerloss_bb_3_abs=(current_density_busbar_3_abs^2)*(res_bb)*(l)/(3*t_bb*w_bb);

    powerloss_bb_abs=powerloss_bb_1_abs+powerloss_bb_2_abs+powerloss_bb_3_abs;

    %power loss in Backcontact
    current_density_backcontact_abs=single_cell_current_abs/(l);
    powerloss_backcontact_abs=(current_density_backcontact_abs^2)*(res_bc)*(l)/(3*t_bc*b);

    %total ohmic power loss in cell

tot_ohmic_cell_abs=total_power_loss_fingers_cell_abs+powerloss_bb_abs+powerloss_backconta
ct_abs;

elseif (n_bb==4)

    %power loss in cell finger
    current_single_busbar_1_abs= (cell_photocurrent_density_abs_metal*1e-
3)*(l*(d_s_bb+(d_bb/2))*1e-8);
    current_single_busbar_2_abs= (cell_photocurrent_density_abs_metal*1e-3)*(l*d_bb*1e-8);
    current_single_busbar_3_abs= (cell_photocurrent_density_abs_metal*1e-3)*(l*d_bb*1e-8);
    current_single_busbar_4_abs= (cell_photocurrent_density_abs_metal*1e-3)*(l*(b-
(d_s_bb+d_bb+d_bb+(d_bb/2)))*1e-8);

    current_single_finger_left_1_abs=
(current_single_busbar_1_abs*(d_s_bb/(d_s_bb+(d_bb/2)))/counter);
    current_single_finger_right_1_abs= (current_single_busbar_1_abs*(1-
(d_s_bb/(d_s_bb+(d_bb/2))))/counter);
    current_single_finger_left_2_abs=
(current_single_busbar_2_abs*((d_bb/2)/((d_bb/2)+w_bb+(d_bb/2)))/counter);
```

```
    current_single_finger_right_2_abs= (current_single_busbar_2_abs*(1-
((d_bb/2)/((d_bb/2)+w_bb+(d_bb/2))))/counter);
    current_single_finger_left_3_abs=
(current_single_busbar_3_abs*((d_bb/2)/((d_bb/2)+w_bb+(d_bb/2)))/counter);
    current_single_finger_right_3_abs= (current_single_busbar_3_abs*(1-
((d_bb/2)/((d_bb/2)+w_bb+(d_bb/2))))/counter);
    current_single_finger_left_4_abs=
(current_single_busbar_4_abs*((d_bb/2)/((d_bb/2)+w_bb+(b-d_s_bb-d_bb-d_bb-d_bb)))/counter);
    current_single_finger_right_4_abs= (current_single_busbar_4_abs*(1-
((d_bb/2)/((d_bb/2)+w_bb+(b-d_s_bb-d_bb-d_bb-d_bb))))/counter);


    current_density_left_fi_1_abs=(current_single_finger_left_1_abs/(d_s_bb));
    current_density_right_fi_1_abs=(current_single_finger_right_1_abs/(((d_bb/2)-w_bb)));
    current_density_left_fi_2_abs=(current_single_finger_left_2_abs/(((d_bb/2)-w_bb)));
    current_density_right_fi_2_abs=(current_single_finger_right_2_abs/(((d_bb/2)-w_bb)));
    current_density_left_fi_3_abs=(current_single_finger_left_3_abs/(((d_bb/2)-w_bb)));
    current_density_right_fi_3_abs=(current_single_finger_right_3_abs/(((d_bb/2)-w_bb)));
    current_density_left_fi_4_abs=(current_single_finger_left_4_abs/(((d_bb/2)-w_bb)));
    current_density_right_fi_4_abs=(current_single_finger_right_4_abs/((b-d_s_bb-d_bb-d_bb-
d_bb-w_bb)));

    powerloss_left_fi_1_abs=((current_density_left_fi_1_abs^2)*(res_fi)*(d_s_bb)/(3*t_fi*w_fi));
    powerloss_right_fi_1_abs=((current_density_right_fi_1_abs^2)*(res_fi)*(((d_bb/2)-
w_bb))/(3*t_fi*w_fi));
    powerloss_left_fi_2_abs=((current_density_left_fi_2_abs^2)*(res_fi)*(((d_bb/2)-
w_bb))/(3*t_fi*w_fi));
    powerloss_right_fi_2_abs=((current_density_right_fi_2_abs^2)*(res_fi)*(((d_bb/2)-
w_bb))/(3*t_fi*w_fi));
    powerloss_left_fi_3_abs=((current_density_left_fi_3_abs^2)*(res_fi)*(((d_bb/2)-
w_bb))/(3*t_fi*w_fi));
    powerloss_right_fi_3_abs=((current_density_right_fi_3_abs^2)*(res_fi)*(((d_bb/2)-
w_bb))/(3*t_fi*w_fi));
    powerloss_left_fi_4_abs=((current_density_left_fi_4_abs^2)*(res_fi)*(((d_bb/2)-
w_bb))/(3*t_fi*w_fi));
    powerloss_right_fi_4_abs=((current_density_right_fi_4_abs^2)*(res_fi)*((b-d_s_bb-d_bb-
d_bb-d_bb-w_bb))/(3*t_fi*w_fi));


total_power_loss_fingers_cell_abs=(powerloss_left_fi_1_abs+powerloss_right_fi_1_abs+powerlo
ss_left_fi_2_abs+powerloss_right_fi_2_abs+powerloss_left_fi_3_abs+powerloss_right_fi_3_abs+
powerloss_left_fi_4_abs+powerloss_right_fi_4_abs)*counter;


    %power loss in busbar
    current_density_busbar_1_abs=current_single_busbar_1_abs/(l);
    powerloss_bb_1_abs=(current_density_busbar_1_abs^2)*(res_bb)*(l)/(3*t_bb*w_bb);


    current_density_busbar_2_abs=current_single_busbar_2_abs/(l);
```

```
    powerloss_bb_2_abs=(current_density_busbar_2_abs^2)*(res_bb)*(l)/(3*t_bb*w_bb);

    current_density_busbar_3_abs=current_single_busbar_3_abs/(l);
    powerloss_bb_3_abs=(current_density_busbar_3_abs^2)*(res_bb)*(l)/(3*t_bb*w_bb);

    current_density_busbar_4_abs=current_single_busbar_4_abs/(l);
    powerloss_bb_4_abs=(current_density_busbar_4_abs^2)*(res_bb)*(l)/(3*t_bb*w_bb);


powerloss_bb_abs=powerloss_bb_1_abs+powerloss_bb_2_abs+powerloss_bb_3_abs+powerloss_
bb_4_abs;


    %power loss in Backcontact
    current_density_backcontact_abs=single_cell_current_abs/(l);
    powerloss_backcontact_abs=(current_density_backcontact_abs^2)*(res_bc)*(l)/(3*t_bc*b);

    %total ohmic power loss in cell

tot_ohmic_cell_abs=total_power_loss_fingers_cell_abs+powerloss_bb_abs+powerloss_backconta
ct_abs;

end

cell_power_abs=(single_cell_current_abs*v_oc)-tot_ohmic_cell_abs;

 %%%%%%%%%% CTM Analysis %%%%%%%%%%

CTM_RATIO=module_power/(cell_power_abs*r_m*c_m);
sum_tot_photocurrent=0;

for i=1:1:11
    sum_tot_photocurrent=sum_tot_photocurrent+CTM_M(i).Current;
end

 for i=1:1:11
    Lost(i).Label=CTM_M(i).label;
    Lost(i).Percentage_loss=(CTM_M(i).Current/sum_tot_photocurrent)*100;

End
```

A2 Matlab code for the developed tool for triangular modules

```
%%%%%%%%%% Developed tool code (Triangular Module) %%%%%%%%%%%%
clear all

%%%%%%%%%Input Parameters %%%%%%%%%

% r_m       Rows of cells in the module
% c_m       Columns of cells in the module
% l         Cell Length (edge to edge along y axis)
% b         Cell breadth  (edge to edge along x axis)
% l_m       Length of the module (edge to edge along y axis)
% b_m       Breadth of the module (edge to edge along x axis)
% t_c       Cell thickness (edge to edge along z axis)
% s_c       Spacing between cells( end edge of one cell to starting edge of adjacent cell)
% t_bc      Thickness of the back contact below the cell (edge to edge along z axis)
% t_eva_ac  Thickness of EVA layer above the cell front surface. Make sure to specify the height taking into consideration the height of the front metallization (edge to edge along z axis)
% t_eva_bc  Thickness of EVA layer below the cell back contact layer (edge to edge along z axis)
% t_bs      Thickness of the Back Sheet below the EVA Layer (edge to edge along z axis)
% t_fg      Thickness of the front glass above the EVA Layer (edge to edge along z axis)
% t_enc     Thickness of the enclosure above the glass and below the backsheet for emitting and collecting rays (edge to edge along z axis)
% t_enc_s   Width of the enclosure side of the module edge for collecting rays (edge to edge along x axis)
% n_bb      Number of busbars placed along the y axis on each cell
% w_bb      Width of each busbar (edge to edge along x axis)
% t_bb      Thickness of each busbar (edge to edge along z axis)
% t_bb_t    Thickness of busbar tabs (edge to edge along z axis)
% d_bb      Distance between the starting edge of one busbar and the starting edge of next busbar (edge to edge along z axis)
% d_s_bb    Distance of the starting edge of the first busbar from the edge of the solar cell (edge to edge along x axis)
% d_fi      Distance between the fingers starting edge and the next fingers starting edge placed horizontally along the y axis (edge to edge along y axis)
% t_fi      Thickness of the fingers (edge to edge along z axis)
% w_fi      Width of the fingers (edge to edge along y axis)
% wl        Wavelengths used for integration to compute the cell photocurrent density
% v_oc      Open circuit voltage of a single solar cell in Volts. Enter 0.65 if unknown
% res_fi    Resistivity of cell finger material in ohm um
% res_bb    Resistivity of busbar material in ohm um
% res_bc    Resistivity of Backcontact material in ohm um
% res_int   Resistivity of interconnection material in ohm um
% n_c_ser   Number of cells in series in a string
% n_s_par   Number of strings in parallel in a string (1 if no strings in parallel)
% t_par     Thickness of the cable after joining of strings to carry parallel current
% w_par     Width of the cable after joining of strings to carry parallel current
```

```
% all dimensions in um
m_e=100000;
c_m_b=5;
c_e = 30000;
t_c = 1800;
s_c= 1500;
t_bc=1000;
t_eva_ac=1000;
t_eva_bc=1000;
t_fg= 4000;
t_enc=10;
t_enc_s=10;
t_bs=0;
n_bb=1;
w_bb=1000;
t_bb_t=800;
t_bb=15;
d_bb=0;
d_s_bb=15000;
d_fi=1568;
t_fi=15;
w_fi=15;
v_oc=0.65;
res_fi=1.638495*1e-2;
res_bb=1.638495*1e-2;
res_bc=1.638495*1e-2;
res_int=1.638495*1e-2;
n_c_ser=3;
n_s_par=3;
t_par=800;
w_par=5000;
wl =0.3:0.1:1.2;



%%%%%%%% Calculation of total cells in the module %%%%%%%%%%
totalcells=0;
for i=1:2:c_m_b
   totalcells=totalcells+i;
end

%%%%%%%%%%%%%%% Solar Cell %%%%%%%%%%%%%%%

%VERTEX MATRIX FOR SOLAR CELLS (vertex xyz-coordinates [um])
cmb_x=c_m_b;
a=1;
x=0;
y=0;
```

```
z=0;
count=1;
while(cmb_x>=1)

   for i=1:1:cmb_x

      if(rem(i,2)~=0)
         V(a:a+5,:)=[ x y z;
            x+c_e y z;
            x+(c_e/2) y+(0.5*sqrt(3)*c_e) z;

            x y z+t_c;
            x+c_e y z+t_c;
            x+(c_e/2) y+(0.5*sqrt(3)*c_e) z+t_c;
            ];
         a=a+6;
         x=x+c_e+s_c;
      else
         V(a:a+5,:)=[ x y z;
            x-(c_e/2) y+(0.5*sqrt(3)*c_e) z;
            x+(c_e/2) y+(0.5*sqrt(3)*c_e) z;

            x y z+t_c;
            x-(c_e/2) y+(0.5*sqrt(3)*c_e) z+t_c;
            x+(c_e/2) y+(0.5*sqrt(3)*c_e) z+t_c;
            ];
         a=a+6;
         x=x+s_c;
      end

   end
   if(count==1)
      x=(c_e/2)+s_c;
   else
      x=(count)*((c_e/2)+s_c);
   end
   y=y+(0.5*sqrt(3)*c_e)+s_c;
   cmb_x=cmb_x-2;
   count=count+1;
end

[e_solarcells,~]=size(V);
% Lux(V); return


%FACET MATRIX FOR SOLAR CELLS (vertex numbers)
i=1;
r=1;
for a=1:1:(totalcells)
   F(r:r+4,:)=[ i  i+2 i+1 NaN;
```

```
        i+3 i+4 i+5 NaN;
        i+1  i+2 i+5 i+4;
        i+2 i i+3 i+5;
        i i+1 i+4 i+3;
        ];
    i=i+6;
    r=r+5;
end
[fn_solarcells_e,~]=size(F);
% Lux(V,F); return

%%%%%%%%%%%%% Solar Cell Back Contacts %%%%%%%%%%%%%

%VERTEX MATRIX FOR BACK CONTACT (vertex xyz-coordinates [um])
[s_bc_s,~]=size(V);
cmb_x1=c_m_b;
a=s_bc_s+1;
x=0;
y=0;
z=0;
count=1;
while(cmb_x1>=1)

    for i=1:1:cmb_x1

        if(rem(i,2)~=0)
            V(a:a+2,:)=[

            x y z-t_bc;
            x+c_e y z-t_bc;
            x+(c_e/2) y+(0.5*sqrt(3)*c_e) z-t_bc;
            ];
        a=a+3;
        x=x+c_e+s_c;
        else
            V(a:a+2,:)=[

            x y z-t_bc;
            x-(c_e/2) y+(0.5*sqrt(3)*c_e) z-t_bc;
            x+(c_e/2) y+(0.5*sqrt(3)*c_e) z-t_bc;
            ];
        a=a+3;
        x=x+s_c;
        end

    end
    if(count==1)
        x=(c_e/2)+s_c;
    else
```

```
        x=(count)*((c_e/2)+s_c);
    end
    y=y+(0.5*sqrt(3)*c_e)+s_c;
    cmb_x1=cmb_x1-2;
    count=count+1;
end

%  Lux(V); return

% % % %%%%FACET MATRIX FOR BACK CONTACTS (vertex numbers)

%FACET MATRIX FOR SOLAR CELLS (vertex numbers)
sc_fbc=(1:e_solarcells);
[fn_bc_s,~]=size(F);
i=s_bc_s+1;
r=fn_bc_s+1;
a1=1;

for a=1:1:(totalcells)
    F(r:r+3,:)=[ i  i+2 i+1 NaN;
        i+2 i sc_fbc(a1) sc_fbc(a1+2);
        i  i+1 sc_fbc(a1+1) sc_fbc(a1);
        i+1 i+2 sc_fbc(a1+2) sc_fbc(a1+1);

        ];
    i=i+3;
    r=r+4;
    a1=a1+6;
end

[fn_bc_e,~]=size(F);

% Lux(V,F); return

% % %%%%%%%%%%% Encapsulation %%%%%%%%%%%%%

% % %VERTEX MATRIX FOR ENCAPSULATION(vertex xyz-coordinates [um])

m_h=0.5*sqrt(3)*m_e;

c_r_b=round(c_m_b/2);

me_h= (m_h-(0.5*sqrt(3)*c_e*(count-1))-(s_c*(count-2)))/2;
me_e= (m_e-(c_e*(c_r_b))-(s_c*(count)))/2;

if(me_e<0)
    error('Cells are lying outside the module borders');
end

[s_eva_s,~]=size(V);
```

```
x=0;
y=0;
z=0;

V(i:i+5,:)= [ x-me_e                    y-me_e              z-(t_eva_bc+t_bc);
   x+(c_e*c_r_b)+(s_c*(count))+me_e   y-me_e          z-(t_eva_bc+t_bc);
   (x+(c_e*(c_r_b))+(s_c*(count)))/2    y+(0.5*sqrt(3)*c_e*(count-1))+(s_c*(count-2))+me_h  z-
(t_eva_bc+t_bc);



    x-me_e                    y-me_e              z+t_c+(t_eva_ac);
   x+(c_e*c_r_b)+(s_c*(count))+me_e   y-me_e          z+t_c+(t_eva_ac);
   (x+(c_e*(c_r_b))+(s_c*(count)))/2    y+(0.5*sqrt(3)*c_e*(count-1))+(s_c*(count-2))+me_h
z+t_c+(t_eva_ac);



];

[s_eva_e,~]=size(V);

%  Lux(V); return

% % %%%%%FACET MATRIX FOR ENCAPSULATION (vertex numbers)

[fn_eva_s,~]=size(F);

F(r:r+4,:)=[ i  i+2 i+1 NaN;
   i+3 i+4 i+5 NaN;
   i+5 i+2 i i+3;
   i i+1 i+4 i+3;
   i+1 i+2 i+5 i+4;];

[fn_eva_e,~]=size(F);
eva_fbc=(s_eva_s+1:s_eva_e);
% Lux(V,F); return


% % %%%%%%% Front Glass %%%%%%%%%%%%

% % %VERTEX MATRIX FOR FRONT GLASS(vertex xyz-coordinates [um])
x=0;
y=0;
z=0;
[i,~] =size(V);
i=i+1;
V(i:i+2,:)= [ x-me_e                    y-me_e              z+t_c+(t_eva_ac)+t_fg;
   x+(c_e*c_r_b)+(s_c*(count))+me_e   y-me_e          z+t_c+(t_eva_ac)+t_fg;
```

```
   (x+(c_e*(c_r_b))+(s_c*(count)))/2    y+(0.5*sqrt(3)*c_e*(count-1))+(s_c*(count-2))+me_h
z+t_c+(t_eva_ac)+t_fg;

];
% Lux(V); return

% % %%%%%FACET MATRIX FOR FRONT GLASS(vertex numbers)
[r,~] =size(F);
[fn_frontglass_s,~]=size(F);
r=r+1;
F(r:r+3,:)=[ i  i+1 i+2 NaN;
i i+2  eva_fbc(6) eva_fbc(4);
eva_fbc(4) eva_fbc(5) i+1 i;
eva_fbc(5) eva_fbc(6) i+2 i+1;

];
[fn_frontglass_e,~]=size(F);
% Lux(V,F); return


% % %%%%%%%%% Backsheet %%%%%%%%%%%

% % % % %VERTEX MATRIX FOR BACKSHEET(vertex xyz-coordinates [um])
% [i,~]=size(V);
% i=i+1;
% x=0;
% y=0;
% z=0;
% V(i:i+2,:)= [ x-me_e                    y-me_e              z-(t_eva_bc+t_bs);
%     x+(c_e*c_r_b)+(s_c*(count))+me_e   y-me_e          z-(t_eva_bc+t_bs);
%     (x+(c_e*(c_r_b))+(s_c*(count)))/2    y+(0.5*sqrt(3)*c_e*(count-1))+(s_c*(count-2))+me_h
z-(t_eva_bc+t_bs);
%
%     ];
% % Lux(V); return
%
%
% % % % %%%%%FACET MATRIX FOR BACKSHEET (vertex numbers)
% [fn_bs_s,~]=size(F);
% r=fn_bc_s+1;
% F(r:r+3,:)=[ i  i+2 i+1 NaN;
% i+2 i eva_fbc(1) eva_fbc(2);
% i i+1 eva_fbc(2) eva_fbc(1);
% i+1 i+2 eva_fbc(3) eva_fbc(2);
%
% ];
%
% [fn_bs_e,~]=size(F);
% % Lux(V,F); return
```

```
%In order use a single sheet layer for backsheet comment this section out and use Encapsulation
bottom layer as backsheet in the optical properties section


%% %%%%%%%%%% Enclosure %%%%%%%%%%%%

% % %VERTEX MATRIX FOR ENCLOSURE(vertex xyz-coordinates [um])
x=0;
y=0;
z=0;
[i,~] =size(V);
i=i+1;
V(i:i+5,:)= [ x-me_e-t_enc_s                    y-me_e-t_enc_s
z+t_c+(t_eva_ac)+t_fg+t_enc;
   x+(c_e*c_r_b)+(s_c*(count))+me_e+t_enc_s   y-me_e-t_enc_s
z+t_c+(t_eva_ac)+t_fg+t_enc;
   (x+(c_e*(c_r_b))+(s_c*(count)))/2    y+(0.5*sqrt(3)*c_e*(count-1))+(s_c*(count-
2))+me_h+t_enc_s  z+t_c+(t_eva_ac)+t_fg+t_enc;

x-me_e-t_enc_s                    y-me_e-t_enc_s                z-t_bc-(t_eva_bc)-t_bs-t_enc;
   x+(c_e*c_r_b)+(s_c*(count))+me_e+t_enc_s   y-me_e-t_enc_s           z-t_bc-(t_eva_bc)-t_bs-
t_enc;
   (x+(c_e*(c_r_b))+(s_c*(count)))/2    y+(0.5*sqrt(3)*c_e*(count-1))+(s_c*(count-
2))+me_h+t_enc_s   z-t_bc-(t_eva_bc)-t_bs-t_enc;

   ];

% Lux(V); return

% % %%%%%FACET MATRIX FOR ENCLOSURE(vertex numbers)
[r,~] =size(F);
[fn_enc,~] =size(F);
r=r+1;
F(r:r+4,:)=[ i  i+2 i+1 NaN;
   i+3 i+4 i+5 NaN;
   i+3  i+5 i+2 i;
   i+4 i+3 i i+1;
   i+1 i+2 i+5 i+4;
  ];
% Make t_bs=0 if using a single layer backshee
%  Lux(V,F); return


% % %%%%%%%% Optical Properties %%%%%%%%%%%%

% SURFACE TYPE STRUCTURE
clear Type
```

```
Type(1).RT      = {0 0 'Ceiling'};        % Top absorber surface of the enclosure used for emitting rays
Type(1).Plot    = {[0.3 0.3 0.3] 0.3};
Type(1).Emit    = {100000 0 0};             % Increase the number of rays for higher accuracy
Type(1).Facet   =  fn_enc+1;

Type(2).RT      = {0 0 'Floor'};          % Bottom absorber surface of the enclosure
Type(2).Plot    = {[0.3 0.3 0.3] 0.3};
Type(2).Facet   = fn_enc+2;

Type(3).RT      = {0 0 'Wall'};           % Side absorber walls of the enclosure
Type(3).Plot    = {[0.3 0.3 0.3] 0.3};
Type(3).Facet   = fn_enc+3:fn_enc+5;

Type(4).RT      = {'air' 'glass'};        % Air/Glass interface
Type(4).Plot    = {[0 0 1] 0.1};
Type(4).Facet   = fn_frontglass_s+1;

Type(5).RT      = {'air' 'glass'};        % Air/Glass side walls interface
Type(5).Plot    = {[0 0 1] 0.1};
Type(5).Facet   = fn_frontglass_s+2:fn_frontglass_s+4;

Type(6).RT      = {'glass' 'EVA(G)'};     % Glass/Encapsulation interface
Type(6).Plot    = {[0 0 1] 0.2};
Type(6).Facet   = fn_eva_s+2;

Type(7).RT      = {'air' 'EVA(G)'};       % Air/Encapsulation side walls interface
Type(7).Plot    = {[0.6 0.6 0.6] 0.6};
Type(7).Facet   = fn_eva_s+3:fn_eva_e;

Type(8).RT      = {0 0 'cell'};           % Cell absorber surfaces
Type(8).Plot    = {[0 0 0] 0.5};
Type(8).Facet   = 1:fn_solarcells_e;


Type(9).RT     = {'EVA(G)' 'Ag'};         % Encapsulation/Backcontact interface
Type(9).Plot   = {[0 0 0] 0.9};
Type(9).Facet  = fn_bc_s+1:fn_bc_e;
Type(9).Scat   = {1,1};

% Type(10).RT     = {'glass' 'EVA(G)'};     % Encapsulation/Backsheet top surface interface
Type(10).RT     = {0 0 'Backsheet'};       %Uncomment this statement along with comment mentioned in Backsheet section to use single layer backsheet
Type(10).Plot   = {[0 0 1] 0.1};
Type(10).Facet  = fn_eva_s+1;
Type(10).Scat   = {1,1};              % Haze and Phong exponent (for Lambertian scatterer use 1 for both. Comment out this line if using a glass-glass module)
```

```
% Type(11).RT      = { 'air' 'glass'};        % Air/Backsheet bottom and side surfaces interface (
Along with the comment in the backsheet section, remove this Type structure if a single backsheet
surface is required)
% Type(11).Plot    = {[0 0 1] 0.1};
% Type(11).Facet   = fn_bs_s+1:fn_bs_e;

% Lux(V,F,Type);  return
CTM_M = Lux(V,F,Type,wl);                  % Start ray-tracing



% % %%%%%%%%% Net Module Active Area Analysis %%%%%%%%%

%%%%% finding rows of fingers %%%%%%%
c_h=0.5*sqrt(3)*c_e;
y_fi=0;
counter=0;
while(y_fi<c_h)
   counter=counter+1;
   y_fi=y_fi+d_fi;
end

%%%% finding equivalent square cell %%
l=sqrt((sqrt(3)/4)*c_e*c_e);
b=l;

%%%% finding active area ratio %%%%%
cell_top_area_s=(l*b*1e-8);
metallization_area_top_s=(w_bb*l*n_bb*1e-8)+(counter*w_fi*b*1e-8);
net_active_area_top_s=(cell_top_area_s-metallization_area_top_s);
active_area_ratio= net_active_area_top_s/cell_top_area_s;


% %%%%%%%%% Module photocurrent Analysis %%%%%%%%%%

cell_top_area=((sqrt(3)/4)*c_e*c_e*1e-8);
total_cell_top_area=((sqrt(3)/4)*c_e*c_e*totalcells*1e-8);
cell_photocurrent_density_wom =
(CTM_M(10).Current*((sqrt(3)/4)*(m_e+t_enc_s)*(m_e+t_enc_s))*1e-
8)/(((sqrt(3)/4)*c_e*c_e)*totalcells*1e-8); %Cell photo current density with respect to the cell top
active area. Ensure x in CTM_(x) in this statement is for the cell as in CTM_M structure.
current_density_ratio_white=(active_area_ratio) + (-0.2408 * active_area_ratio + 0.2449);
%insert values for p1 and p2 obtained from simulation of nearest square/rectangle module
cell_photocurrent_density_wm=cell_photocurrent_density_wom*current_density_ratio_white;


%%%%%%%%%Module Electrical Analysis %%%%%%%%%%%%

single_cell_current= (cell_photocurrent_density_wm*1e-3*cell_top_area);
```

```
if (n_bb==1)

    %power loss in cell fingers
    current_single_busbar_single_cell= single_cell_current/n_bb;

    current_single_finger_left= (current_single_busbar_single_cell*(d_s_bb/b)/counter);
    current_single_finger_right= (current_single_busbar_single_cell*(1-((d_s_bb)/b))/counter);

    current_density_left_fi=(current_single_finger_left/(d_s_bb));
    current_density_right_fi=(current_single_finger_right/((b-d_s_bb-w_bb)));

    powerloss_left_fi=((current_density_left_fi^2)*(res_fi)*(d_s_bb)/(3*t_fi*w_fi));
    powerloss_right_fi=((current_density_right_fi^2)*(res_fi)*((b-d_s_bb-w_bb))/(3*t_fi*w_fi));

    total_power_loss_fingers_cell=(powerloss_left_fi+powerloss_right_fi)*counter;

    %power loss in busbar
    current_density_busbar=current_single_busbar_single_cell/(l);
    powerloss_bb=(current_density_busbar^2)*(res_bb)*(l)/(3*t_bb*w_bb);

    %power loss in Backcontact
    current_density_backcontact=single_cell_current/(l);
    powerloss_backcontact=(current_density_backcontact^2)*(res_bc)*(l)/(3*t_bc*b);

    %total ohmic power loss in cell
    tot_ohmic_cell=total_power_loss_fingers_cell+powerloss_bb+powerloss_backcontact;

    %total ohmic power loss in series interconnection string

powerloss_ser_inter=(current_single_busbar_single_cell^2)*(res_int*((s_c+l)/(t_bb_t*w_bb)))*(n
_c_ser-1)*n_s_par;  %assuming same geometrical properties of the interconnection as in the cell
busbars and length of interconnection tabs equal to cell space

    %total ohmic power loss in parallel interconnection string

powerloss_par_inter=((single_cell_current*n_s_par)^2)*(res_int*((t_eva_bc+t_bs)/(t_par*w_par))
)*2; %Assuming all the strings are connected at a point and the length of the cable used for
carrying the current after the point is equal to length of the module

    %total ohmic power loss
    tot_power_loss_ohmic=(tot_ohmic_cell*totalcells)+powerloss_ser_inter+powerloss_par_inter;

elseif (n_bb==2)

    %power loss in cell finger
    current_single_busbar_1= (cell_photocurrent_density_wm*1e-3)*(l*(d_s_bb+(d_bb/2))*1e-8);
    current_single_busbar_2= (cell_photocurrent_density_wm*1e-3)*(l*(b-(d_s_bb+(d_bb/2)))*1e-
8);
```

```
    current_single_finger_left_1= (current_single_busbar_1*(d_s_bb/(d_s_bb+(d_bb/2)))/counter);
    current_single_finger_right_1= (current_single_busbar_1*(1-
(d_s_bb/(d_s_bb+(d_bb/2))))/counter);
    current_single_finger_left_2= (current_single_busbar_2*((d_bb/2)/((d_bb/2)+w_bb+(b-d_s_bb-
d_bb-w_bb)))/counter);
    current_single_finger_right_2= (current_single_busbar_2*(1-((d_bb/2)/((d_bb/2)+w_bb+(b-
d_s_bb-d_bb-w_bb))))/counter);

    current_density_left_fi_1=(current_single_finger_left_1/(d_s_bb));
    current_density_right_fi_1=(current_single_finger_right_1/(((d_bb/2)-w_bb)));
    current_density_left_fi_2=(current_single_finger_left_2/(((d_bb/2)-w_bb)));
    current_density_right_fi_2=(current_single_finger_right_2/((b-d_s_bb-d_bb-w_bb)));

    powerloss_left_fi_1=((current_density_left_fi_1^2)*(res_fi)*(d_s_bb)/(3*t_fi*w_fi));
    powerloss_right_fi_1=((current_density_right_fi_1^2)*(res_fi)*((d_bb/2))/(3*t_fi*w_fi));
    powerloss_left_fi_2=((current_density_left_fi_2^2)*(res_fi)*((d_bb/2))/(3*t_fi*w_fi));
    powerloss_right_fi_2=((current_density_right_fi_2^2)*(res_fi)*((b-d_s_bb-w_bb-
d_bb))/(3*t_fi*w_fi));


total_power_loss_fingers_cell=(powerloss_left_fi_1+powerloss_right_fi_1+powerloss_left_fi_2+p
owerloss_right_fi_2)*counter;

    %power loss in busbar
    current_density_busbar_1=current_single_busbar_1/(l);
    powerloss_bb_1=(current_density_busbar_1^2)*(res_bb)*(l)/(3*t_bb*w_bb);

    current_density_busbar_2=current_single_busbar_2/(l);
    powerloss_bb_2=(current_density_busbar_2^2)*(res_bb)*(l)/(3*t_bb*w_bb);

    powerloss_bb=powerloss_bb_1+powerloss_bb_2;

    %power loss in Backcontact
    current_density_backcontact=single_cell_current/(l);
    powerloss_backcontact=(current_density_backcontact^2)*(res_bc)*(l)/(3*t_bc*b);

    %total ohmic power loss in cell
    tot_ohmic_cell=total_power_loss_fingers_cell+powerloss_bb+powerloss_backcontact;


    %total ohmic power loss in series interconnection string

powerloss_ser_inter=(current_single_busbar_1^2+current_single_busbar_2^2)*((res_int*((s_c+l)/(
t_bb_t*w_bb)))*(n_c_ser-1)*n_s_par);  %assuming same width of the interconnection tabs as in
the cell busbars and length of interconnection tabs equal to cell space

    %total ohmic power loss in parallel interconnection string

powerloss_par_inter=((single_cell_current*n_s_par)^2)*(res_int*((t_eva_bc+t_bs)/(t_par*w_par))
```

```
)*2; %Assuming all the strings are connected at a point and the length of the cable used for carrying the current after the point is equal to length of the module

    %total ohmic power loss
    tot_power_loss_ohmic=(tot_ohmic_cell*totalcells)+powerloss_ser_inter+powerloss_par_inter;

elseif (n_bb==3)

    %power loss in cell finger
    current_single_busbar_1= (cell_photocurrent_density_wm*1e-3)*(l*(d_s_bb+(d_bb/2))*1e-8);
    current_single_busbar_2= (cell_photocurrent_density_wm*1e-3)*(l*d_bb*1e-8);
    current_single_busbar_3= (cell_photocurrent_density_wm*1e-3)*(l*(b-
(d_s_bb+d_bb+(d_bb/2)))*1e-8);

    current_single_finger_left_1= (current_single_busbar_1*(d_s_bb/(d_s_bb+(d_bb/2)))/counter);
    current_single_finger_right_1= (current_single_busbar_1*(1-
(d_s_bb/(d_s_bb+(d_bb/2))))/counter);
    current_single_finger_left_2=
(current_single_busbar_2*((d_bb/2)/((d_bb/2)+w_bb+(d_bb/2)))/counter);
    current_single_finger_right_2= (current_single_busbar_2*(1-
((d_bb/2)/((d_bb/2)+w_bb+(d_bb/2))))/counter);
    current_single_finger_left_3= (current_single_busbar_3*((d_bb/2)/((d_bb/2)+w_bb+(b-d_s_bb-
d_bb-d_bb)))/counter);
    current_single_finger_right_3= (current_single_busbar_3*(1-((d_bb/2)/((d_bb/2)+w_bb+(b-
d_s_bb-d_bb-d_bb))))/counter);


    current_density_left_fi_1=(current_single_finger_left_1/(d_s_bb));
    current_density_right_fi_1=(current_single_finger_right_1/(((d_bb/2)-w_bb)));
    current_density_left_fi_2=(current_single_finger_left_2/(((d_bb/2)-w_bb)));
    current_density_right_fi_2=(current_single_finger_right_2/(((d_bb/2)-w_bb)));
    current_density_left_fi_3=(current_single_finger_left_3/(((d_bb/2)-w_bb)));
    current_density_right_fi_3=(current_single_finger_right_3/((b-d_s_bb-d_bb-d_bb-w_bb)));

    powerloss_left_fi_1=((current_density_left_fi_1^2)*(res_fi)*(d_s_bb)/(3*t_fi*w_fi));
    powerloss_right_fi_1=((current_density_right_fi_1^2)*(res_fi)*(((d_bb/2)-
w_bb))/(3*t_fi*w_fi));
    powerloss_left_fi_2=((current_density_left_fi_2^2)*(res_fi)*(((d_bb/2)-w_bb))/(3*t_fi*w_fi));
    powerloss_right_fi_2=((current_density_right_fi_2^2)*(res_fi)*(((d_bb/2)-
w_bb))/(3*t_fi*w_fi));
    powerloss_left_fi_3=((current_density_left_fi_3^2)*(res_fi)*(((d_bb/2)-w_bb))/(3*t_fi*w_fi));
    powerloss_right_fi_3=((current_density_right_fi_3^2)*(res_fi)*((b-d_s_bb-d_bb-w_bb-
d_bb))/(3*t_fi*w_fi));


total_power_loss_fingers_cell=(powerloss_left_fi_1+powerloss_right_fi_1+powerloss_left_fi_2+p
owerloss_right_fi_2+powerloss_left_fi_3+powerloss_right_fi_3)*counter;

    %power loss in busbar
    current_density_busbar_1=current_single_busbar_1/(l);
```

```
    powerloss_bb_1=(current_density_busbar_1^2)*(res_bb)*(l)/(3*t_bb*w_bb);


    current_density_busbar_2=current_single_busbar_2/(l);
    powerloss_bb_2=(current_density_busbar_2^2)*(res_bb)*(l)/(3*t_bb*w_bb);

    current_density_busbar_3=current_single_busbar_3/(l);
    powerloss_bb_3=(current_density_busbar_3^2)*(res_bb)*(l)/(3*t_bb*w_bb);

    powerloss_bb=powerloss_bb_1+powerloss_bb_2+powerloss_bb_3;

    %power loss in Backcontact
    current_density_backcontact=single_cell_current/(l);
    powerloss_backcontact=(current_density_backcontact^2)*(res_bc)*(l)/(3*t_bc*b);

    %total ohmic power loss in cell
    tot_ohmic_cell=total_power_loss_fingers_cell+powerloss_bb+powerloss_backcontact;


    %total ohmic power loss in series interconnection string

powerloss_ser_inter=(current_single_busbar_1^2+current_single_busbar_2^2+current_single_bus
bar_3^2)*((res_int*((s_c+l)/(t_bb_t*w_bb)))*(n_c_ser-1)*n_s_par);  %assuming same width of
the interconnection as in the cell busbars and length of interconnection tabs equal to cell space

    %total ohmic power loss in parallel interconnection string

powerloss_par_inter=((single_cell_current*n_s_par)^2)*(res_int*((t_eva_bc+t_bs)/(t_par*w_par))
)*2; %Assuming all the strings are connected at a point and the length of the cable used for
carrying the current after the point is equal to length of the module

    %total ohmic power loss
    tot_power_loss_ohmic=(tot_ohmic_cell*totalcells)+powerloss_ser_inter+powerloss_par_inter;

elseif (n_bb==4)

    %power loss in cell finger
    current_single_busbar_1= (cell_photocurrent_density_wm*1e-3)*(l*(d_s_bb+(d_bb/2))*1e-8);
    current_single_busbar_2= (cell_photocurrent_density_wm*1e-3)*(l*d_bb*1e-8);
    current_single_busbar_3= (cell_photocurrent_density_wm*1e-3)*(l*d_bb*1e-8);
    current_single_busbar_4= (cell_photocurrent_density_wm*1e-3)*(l*(b-
(d_s_bb+d_bb+d_bb+(d_bb/2)))*1e-8);

    current_single_finger_left_1= (current_single_busbar_1*(d_s_bb/(d_s_bb+(d_bb/2)))/counter);
    current_single_finger_right_1= (current_single_busbar_1*(1-
(d_s_bb/(d_s_bb+(d_bb/2))))/counter);
    current_single_finger_left_2=
(current_single_busbar_2*((d_bb/2)/((d_bb/2)+w_bb+(d_bb/2)))/counter);
    current_single_finger_right_2= (current_single_busbar_2*(1-
((d_bb/2)/((d_bb/2)+w_bb+(d_bb/2))))/counter);
```

```
    current_single_finger_left_3=
(current_single_busbar_3*((d_bb/2)/((d_bb/2)+w_bb+(d_bb/2)))/counter);
    current_single_finger_right_3= (current_single_busbar_3*(1-
((d_bb/2)/((d_bb/2)+w_bb+(d_bb/2))))/counter);
    current_single_finger_left_4= (current_single_busbar_4*((d_bb/2)/((d_bb/2)+w_bb+(b-d_s_bb-
d_bb-d_bb-d_bb)))/counter);
    current_single_finger_right_4= (current_single_busbar_4*(1-((d_bb/2)/((d_bb/2)+w_bb+(b-
d_s_bb-d_bb-d_bb-d_bb))))/counter);


    current_density_left_fi_1=(current_single_finger_left_1/(d_s_bb));
    current_density_right_fi_1=(current_single_finger_right_1/(((d_bb/2)-w_bb)));
    current_density_left_fi_2=(current_single_finger_left_2/(((d_bb/2)-w_bb)));
    current_density_right_fi_2=(current_single_finger_right_2/(((d_bb/2)-w_bb)));
    current_density_left_fi_3=(current_single_finger_left_3/(((d_bb/2)-w_bb)));
    current_density_right_fi_3=(current_single_finger_right_3/(((d_bb/2)-w_bb)));
    current_density_left_fi_4=(current_single_finger_left_4/(((d_bb/2)-w_bb)));
    current_density_right_fi_4=(current_single_finger_right_4/((b-d_s_bb-d_bb-d_bb-d_bb-
w_bb)));

    powerloss_left_fi_1=((current_density_left_fi_1^2)*(res_fi)*(d_s_bb)/(3*t_fi*w_fi));
    powerloss_right_fi_1=((current_density_right_fi_1^2)*(res_fi)*(((d_bb/2)-
w_bb))/(3*t_fi*w_fi));
    powerloss_left_fi_2=((current_density_left_fi_2^2)*(res_fi)*(((d_bb/2)-w_bb))/(3*t_fi*w_fi));
    powerloss_right_fi_2=((current_density_right_fi_2^2)*(res_fi)*(((d_bb/2)-
w_bb))/(3*t_fi*w_fi));
    powerloss_left_fi_3=((current_density_left_fi_3^2)*(res_fi)*(((d_bb/2)-w_bb))/(3*t_fi*w_fi));
    powerloss_right_fi_3=((current_density_right_fi_3^2)*(res_fi)*(((d_bb/2)-
w_bb))/(3*t_fi*w_fi));
    powerloss_left_fi_4=((current_density_left_fi_4^2)*(res_fi)*(((d_bb/2)-w_bb))/(3*t_fi*w_fi));
    powerloss_right_fi_4=((current_density_right_fi_4^2)*(res_fi)*((b-d_s_bb-d_bb-d_bb-d_bb-
w_bb))/(3*t_fi*w_fi));


total_power_loss_fingers_cell=(powerloss_left_fi_1+powerloss_right_fi_1+powerloss_left_fi_2+p
owerloss_right_fi_2+powerloss_left_fi_3+powerloss_right_fi_3+powerloss_left_fi_4+powerloss_r
ight_fi_4)*counter;


    %power loss in busbar
    current_density_busbar_1=current_single_busbar_1/(l);
    powerloss_bb_1=(current_density_busbar_1^2)*(res_bb)*(l)/(3*t_bb*w_bb);


    current_density_busbar_2=current_single_busbar_2/(l);
    powerloss_bb_2=(current_density_busbar_2^2)*(res_bb)*(l)/(3*t_bb*w_bb);

    current_density_busbar_3=current_single_busbar_3/(l);
    powerloss_bb_3=(current_density_busbar_3^2)*(res_bb)*(l)/(3*t_bb*w_bb);
```

```
    current_density_busbar_4=current_single_busbar_4/(l);
    powerloss_bb_4=(current_density_busbar_4^2)*(res_bb)*(l)/(3*t_bb*w_bb);

    powerloss_bb=powerloss_bb_1+powerloss_bb_2+powerloss_bb_3+powerloss_bb_4;


    %power loss in Backcontact
    current_density_backcontact=single_cell_current/(l);
    powerloss_backcontact=(current_density_backcontact^2)*(res_bc)*(l)/(3*t_bc*b);

    %total ohmic power loss in cell
    tot_ohmic_cell=total_power_loss_fingers_cell+powerloss_bb+powerloss_backcontact;


    %total ohmic power loss in series interconnection string

powerloss_ser_inter=(current_single_busbar_1^2+current_single_busbar_2^2+current_single_bus
bar_3^2+current_single_busbar_4^2)*((res_int*((s_c+l)/(t_bb_t*w_bb)))*(n_c_ser-1)*n_s_par);
%assuming same width of the interconnection tab as in the cell busbars and length of
interconnection tabs equal to cell space

    %total ohmic power loss in parallel interconnection string

powerloss_par_inter=((single_cell_current*n_s_par)^2)*(res_int*((t_eva_bc+t_bs)/(t_par*w_par))
)*2; %Assuming all the strings are connected at a point and the length of the cable used for
carrying the current after the point is equal to length of the module

    %total ohmic power loss
    tot_power_loss_ohmic=(tot_ohmic_cell*totalcells)+powerloss_ser_inter+powerloss_par_inter;

end

%%%%%%%%%%%% Module Power Analysis %%%%%%%%%%%

module_power=(((cell_photocurrent_density_wm*1e-3)*(total_cell_top_area))*v_oc)-
tot_power_loss_ohmic;


%%%%%%%%%%% Single Cell Power Analysis %%%%%%%%%%%

cell_photocurrent_density_abs=46.456;
cell_photocurrent_density_abs_metal=cell_photocurrent_density_abs*active_area_ratio;
single_cell_current_abs=(cell_photocurrent_density_abs_metal*1e-3)*((sqrt(3)/4)*c_e*c_e*1e-8);


if (n_bb==1)

    %power loss in cell fingers
    current_single_busbar_single_cell_abs= single_cell_current_abs/n_bb;
```

```
    current_single_finger_left_abs= (current_single_busbar_single_cell_abs*(d_s_bb/b)/counter);
    current_single_finger_right_abs= (current_single_busbar_single_cell_abs*(1-
((d_s_bb)/b))/counter);

    current_density_left_fi_abs=(current_single_finger_left_abs/(d_s_bb));
    current_density_right_fi_abs=(current_single_finger_right_abs/((b-d_s_bb-w_bb)));

    powerloss_left_fi_abs=((current_density_left_fi_abs^2)*(res_fi)*(d_s_bb)/(3*t_fi*w_fi));
    powerloss_right_fi_abs=((current_density_right_fi_abs^2)*(res_fi)*((b-d_s_bb-
w_bb))/(3*t_fi*w_fi));

    total_power_loss_fingers_cell_abs=(powerloss_left_fi_abs+powerloss_right_fi_abs)*counter;

    %power loss in busbar
    current_density_busbar_abs=current_single_busbar_single_cell_abs/(l);
    powerloss_bb_abs=(current_density_busbar_abs^2)*(res_bb)*(l)/(3*t_bb*w_bb);

    %power loss in Backcontact
    current_density_backcontact_abs=single_cell_current_abs/(l);
    powerloss_backcontact_abs=(current_density_backcontact_abs^2)*(res_bc)*(l)/(3*t_bc*b);

    %total ohmic power loss in cell

tot_ohmic_cell_abs=total_power_loss_fingers_cell_abs+powerloss_bb_abs+powerloss_backconta
ct_abs;

elseif (n_bb==2)

    %power loss in cell finger
    current_single_busbar_1_abs= (cell_photocurrent_density_abs_metal*1e-
3)*(l*(d_s_bb+(d_bb/2))*1e-8);
    current_single_busbar_2_abs= (cell_photocurrent_density_abs_metal*1e-3)*(l*(b-
(d_s_bb+(d_bb/2)))*1e-8);

    current_single_finger_left_1_abs=
(current_single_busbar_1_abs*(d_s_bb/(d_s_bb+(d_bb/2)))/counter);
    current_single_finger_right_1_abs= (current_single_busbar_1_abs*(1-
(d_s_bb/(d_s_bb+(d_bb/2))))/counter);
    current_single_finger_left_2_abs=
(current_single_busbar_2_abs*((d_bb/2)/((d_bb/2)+w_bb+(b-d_s_bb-d_bb-w_bb)))/counter);
    current_single_finger_right_2_abs= (current_single_busbar_2_abs*(1-
((d_bb/2)/((d_bb/2)+w_bb+(b-d_s_bb-d_bb-w_bb))))/counter);

    current_density_left_fi_1_abs=(current_single_finger_left_1_abs/(d_s_bb));
    current_density_right_fi_1_abs=(current_single_finger_right_1_abs/(((d_bb/2)-w_bb)));
    current_density_left_fi_2_abs=(current_single_finger_left_2_abs/(((d_bb/2)-w_bb)));
    current_density_right_fi_2_abs=(current_single_finger_right_2_abs/((b-d_s_bb-d_bb-w_bb)));

    powerloss_left_fi_1_abs=((current_density_left_fi_1_abs^2)*(res_fi)*(d_s_bb)/(3*t_fi*w_fi));
```

```
powerloss_right_fi_1_abs=((current_density_right_fi_1_abs^2)*(res_fi)*((d_bb/2))/(3*t_fi*w_fi))
;
    powerloss_left_fi_2_abs=((current_density_left_fi_2_abs^2)*(res_fi)*((d_bb/2))/(3*t_fi*w_fi));
    powerloss_right_fi_2_abs=((current_density_right_fi_2_abs^2)*(res_fi)*((b-d_s_bb-w_bb-
d_bb))/(3*t_fi*w_fi));


total_power_loss_fingers_cell_abs=(powerloss_left_fi_1_abs+powerloss_right_fi_1_abs+powerlo
ss_left_fi_2_abs+powerloss_right_fi_2_abs)*counter;

    %power loss in busbar
    current_density_busbar_1_abs=current_single_busbar_1_abs/(l);
    powerloss_bb_1_abs=(current_density_busbar_1_abs^2)*(res_bb)*(l)/(3*t_bb*w_bb);

    current_density_busbar_2_abs=current_single_busbar_2_abs/(l);
    powerloss_bb_2_abs=(current_density_busbar_2_abs^2)*(res_bb)*(l)/(3*t_bb*w_bb);

    powerloss_bb_abs=powerloss_bb_1_abs+powerloss_bb_2_abs;

    %power loss in Backcontact
    current_density_backcontact_abs=single_cell_current_abs/(l);
    powerloss_backcontact_abs=(current_density_backcontact_abs^2)*(res_bc)*(l)/(3*t_bc*b);

    %total ohmic power loss in cell

tot_ohmic_cell_abs=total_power_loss_fingers_cell_abs+powerloss_bb_abs+powerloss_backconta
ct_abs;

elseif (n_bb==3)

    %power loss in cell finger
    current_single_busbar_1_abs= (cell_photocurrent_density_abs_metal*1e-
3)*(l*(d_s_bb+(d_bb/2))*1e-8);
    current_single_busbar_2_abs= (cell_photocurrent_density_abs_metal*1e-3)*(l*d_bb*1e-8);
    current_single_busbar_3_abs= (cell_photocurrent_density_abs_metal*1e-3)*(l*(b-
(d_s_bb+d_bb+(d_bb/2)))*1e-8);

    current_single_finger_left_1_abs=
(current_single_busbar_1_abs*(d_s_bb/(d_s_bb+(d_bb/2)))/counter);
    current_single_finger_right_1_abs= (current_single_busbar_1_abs*(1-
(d_s_bb/(d_s_bb+(d_bb/2))))/counter);
    current_single_finger_left_2_abs=
(current_single_busbar_2_abs*((d_bb/2)/((d_bb/2)+w_bb+(d_bb/2)))/counter);
    current_single_finger_right_2_abs= (current_single_busbar_2_abs*(1-
((d_bb/2)/((d_bb/2)+w_bb+(d_bb/2))))/counter);
    current_single_finger_left_3_abs=
(current_single_busbar_3_abs*((d_bb/2)/((d_bb/2)+w_bb+(b-d_s_bb-d_bb-d_bb)))/counter);
    current_single_finger_right_3_abs= (current_single_busbar_3_abs*(1-
((d_bb/2)/((d_bb/2)+w_bb+(b-d_s_bb-d_bb-d_bb))))/counter);
```

```
    current_density_left_fi_1_abs=(current_single_finger_left_1_abs/(d_s_bb));
    current_density_right_fi_1_abs=(current_single_finger_right_1_abs/(((d_bb/2)-w_bb)));
    current_density_left_fi_2_abs=(current_single_finger_left_2_abs/(((d_bb/2)-w_bb)));
    current_density_right_fi_2_abs=(current_single_finger_right_2_abs/(((d_bb/2)-w_bb)));
    current_density_left_fi_3_abs=(current_single_finger_left_3_abs/(((d_bb/2)-w_bb)));
    current_density_right_fi_3_abs=(current_single_finger_right_3_abs/((b-d_s_bb-d_bb-d_bb-
w_bb)));

    powerloss_left_fi_1_abs=((current_density_left_fi_1_abs^2)*(res_fi)*(d_s_bb)/(3*t_fi*w_fi));
    powerloss_right_fi_1_abs=((current_density_right_fi_1_abs^2)*(res_fi)*(((d_bb/2)-
w_bb))/(3*t_fi*w_fi));
    powerloss_left_fi_2_abs=((current_density_left_fi_2_abs^2)*(res_fi)*(((d_bb/2)-
w_bb))/(3*t_fi*w_fi));
    powerloss_right_fi_2_abs=((current_density_right_fi_2_abs^2)*(res_fi)*(((d_bb/2)-
w_bb))/(3*t_fi*w_fi));
    powerloss_left_fi_3_abs=((current_density_left_fi_3_abs^2)*(res_fi)*(((d_bb/2)-
w_bb))/(3*t_fi*w_fi));
    powerloss_right_fi_3_abs=((current_density_right_fi_3_abs^2)*(res_fi)*((b-d_s_bb-d_bb-
w_bb-d_bb))/(3*t_fi*w_fi));


total_power_loss_fingers_cell_abs=(powerloss_left_fi_1_abs+powerloss_right_fi_1_abs+powerlo
ss_left_fi_2_abs+powerloss_right_fi_2_abs+powerloss_left_fi_3_abs+powerloss_right_fi_3_abs)*
counter;

    %power loss in busbar
    current_density_busbar_1_abs=current_single_busbar_1_abs/(l);
    powerloss_bb_1_abs=(current_density_busbar_1_abs^2)*(res_bb)*(l)/(3*t_bb*w_bb);


    current_density_busbar_2_abs=current_single_busbar_2_abs/(l);
    powerloss_bb_2_abs=(current_density_busbar_2_abs^2)*(res_bb)*(l)/(3*t_bb*w_bb);

    current_density_busbar_3_abs=current_single_busbar_3_abs/(l);
    powerloss_bb_3_abs=(current_density_busbar_3_abs^2)*(res_bb)*(l)/(3*t_bb*w_bb);

    powerloss_bb_abs=powerloss_bb_1_abs+powerloss_bb_2_abs+powerloss_bb_3_abs;

    %power loss in Backcontact
    current_density_backcontact_abs=single_cell_current_abs/(l);
    powerloss_backcontact_abs=(current_density_backcontact_abs^2)*(res_bc)*(l)/(3*t_bc*b);

    %total ohmic power loss in cell

tot_ohmic_cell_abs=total_power_loss_fingers_cell_abs+powerloss_bb_abs+powerloss_backconta
ct_abs;

elseif (n_bb==4)
```

```
    %power loss in cell finger
    current_single_busbar_1_abs= (cell_photocurrent_density_abs_metal*1e-
3)*(l*(d_s_bb+(d_bb/2))*1e-8);
    current_single_busbar_2_abs= (cell_photocurrent_density_abs_metal*1e-3)*(l*d_bb*1e-8);
    current_single_busbar_3_abs= (cell_photocurrent_density_abs_metal*1e-3)*(l*d_bb*1e-8);
    current_single_busbar_4_abs= (cell_photocurrent_density_abs_metal*1e-3)*(l*(b-
(d_s_bb+d_bb+d_bb+(d_bb/2)))*1e-8);

    current_single_finger_left_1_abs=
(current_single_busbar_1_abs*(d_s_bb/(d_s_bb+(d_bb/2)))/counter);
    current_single_finger_right_1_abs= (current_single_busbar_1_abs*(1-
(d_s_bb/(d_s_bb+(d_bb/2))))/counter);
    current_single_finger_left_2_abs=
(current_single_busbar_2_abs*((d_bb/2)/((d_bb/2)+w_bb+(d_bb/2)))/counter);
    current_single_finger_right_2_abs= (current_single_busbar_2_abs*(1-
((d_bb/2)/((d_bb/2)+w_bb+(d_bb/2))))/counter);
    current_single_finger_left_3_abs=
(current_single_busbar_3_abs*((d_bb/2)/((d_bb/2)+w_bb+(d_bb/2)))/counter);
    current_single_finger_right_3_abs= (current_single_busbar_3_abs*(1-
((d_bb/2)/((d_bb/2)+w_bb+(d_bb/2))))/counter);
    current_single_finger_left_4_abs=
(current_single_busbar_4_abs*((d_bb/2)/((d_bb/2)+w_bb+(b-d_s_bb-d_bb-d_bb-d_bb)))/counter);
    current_single_finger_right_4_abs= (current_single_busbar_4_abs*(1-
((d_bb/2)/((d_bb/2)+w_bb+(b-d_s_bb-d_bb-d_bb-d_bb))))/counter);


    current_density_left_fi_1_abs=(current_single_finger_left_1_abs/(d_s_bb));
    current_density_right_fi_1_abs=(current_single_finger_right_1_abs/(((d_bb/2)-w_bb)));
    current_density_left_fi_2_abs=(current_single_finger_left_2_abs/(((d_bb/2)-w_bb)));
    current_density_right_fi_2_abs=(current_single_finger_right_2_abs/(((d_bb/2)-w_bb)));
    current_density_left_fi_3_abs=(current_single_finger_left_3_abs/(((d_bb/2)-w_bb)));
    current_density_right_fi_3_abs=(current_single_finger_right_3_abs/(((d_bb/2)-w_bb)));
    current_density_left_fi_4_abs=(current_single_finger_left_4_abs/(((d_bb/2)-w_bb)));
    current_density_right_fi_4_abs=(current_single_finger_right_4_abs/((b-d_s_bb-d_bb-d_bb-
d_bb-w_bb)));

    powerloss_left_fi_1_abs=((current_density_left_fi_1_abs^2)*(res_fi)*(d_s_bb)/(3*t_fi*w_fi));
    powerloss_right_fi_1_abs=((current_density_right_fi_1_abs^2)*(res_fi)*(((d_bb/2)-
w_bb))/(3*t_fi*w_fi));
    powerloss_left_fi_2_abs=((current_density_left_fi_2_abs^2)*(res_fi)*(((d_bb/2)-
w_bb))/(3*t_fi*w_fi));
    powerloss_right_fi_2_abs=((current_density_right_fi_2_abs^2)*(res_fi)*(((d_bb/2)-
w_bb))/(3*t_fi*w_fi));
    powerloss_left_fi_3_abs=((current_density_left_fi_3_abs^2)*(res_fi)*(((d_bb/2)-
w_bb))/(3*t_fi*w_fi));
    powerloss_right_fi_3_abs=((current_density_right_fi_3_abs^2)*(res_fi)*(((d_bb/2)-
w_bb))/(3*t_fi*w_fi));
```

```
    powerloss_left_fi_4_abs=((current_density_left_fi_4_abs^2)*(res_fi)*(((d_bb/2)-
w_bb))/(3*t_fi*w_fi));
    powerloss_right_fi_4_abs=((current_density_right_fi_4_abs^2)*(res_fi)*((b-d_s_bb-d_bb-
d_bb-d_bb-w_bb))/(3*t_fi*w_fi));


total_power_loss_fingers_cell_abs=(powerloss_left_fi_1_abs+powerloss_right_fi_1_abs+powerlo
ss_left_fi_2_abs+powerloss_right_fi_2_abs+powerloss_left_fi_3_abs+powerloss_right_fi_3_abs+
powerloss_left_fi_4_abs+powerloss_right_fi_4_abs)*counter;


    %power loss in busbar
    current_density_busbar_1_abs=current_single_busbar_1_abs/(l);
    powerloss_bb_1_abs=(current_density_busbar_1_abs^2)*(res_bb)*(l)/(3*t_bb*w_bb);


    current_density_busbar_2_abs=current_single_busbar_2_abs/(l);
    powerloss_bb_2_abs=(current_density_busbar_2_abs^2)*(res_bb)*(l)/(3*t_bb*w_bb);

    current_density_busbar_3_abs=current_single_busbar_3_abs/(l);
    powerloss_bb_3_abs=(current_density_busbar_3_abs^2)*(res_bb)*(l)/(3*t_bb*w_bb);

    current_density_busbar_4_abs=current_single_busbar_4_abs/(l);
    powerloss_bb_4_abs=(current_density_busbar_4_abs^2)*(res_bb)*(l)/(3*t_bb*w_bb);


powerloss_bb_abs=powerloss_bb_1_abs+powerloss_bb_2_abs+powerloss_bb_3_abs+powerloss_
bb_4_abs;


    %power loss in Backcontact
    current_density_backcontact_abs=single_cell_current_abs/(l);
    powerloss_backcontact_abs=(current_density_backcontact_abs^2)*(res_bc)*(l)/(3*t_bc*b);

    %total ohmic power loss in cell

tot_ohmic_cell_abs=total_power_loss_fingers_cell_abs+powerloss_bb_abs+powerloss_backconta
ct_abs;

end

cell_power_abs=(single_cell_current_abs*v_oc)-tot_ohmic_cell_abs;

%%%%%%%%%%CTM Analysis %%%%%%%%%%

CTM_RATIO=module_power/(cell_power_abs*totalcells);
sum_tot_photocurrent=0;

for i=1:1:12
    sum_tot_photocurrent=sum_tot_photocurrent+CTM_M(i).Current;
```

```
end

 for i=1:1:12
    Lost(i).Label=CTM_M(i).label;
    Lost(i).Percentage_loss=(CTM_M(i).Current/sum_tot_photocurrent)*100;

end
```